NASA CONTRACTOR REPORT

NASA CR-1770

STUDY OF THE CONCEPT OF INERTIALLY AIDED BAROMETRIC ALTIMETRY SYSTEM FOR SUPERSONIC AIRCRAFT

by J. Ray Ruetenik, John H. Thompson, and Kenneth R. Britting

Prepared by
KAMAN AVIDYNE
Burlington, Mass. 01803
for Electronics Research Center

NATIONAL AERONAUTICS AND SPACE ADMINISTRATION • WASHINGTON, D. C. • JUNE 1971

1. Report No.	2. Government Accession No.	3. Recipient's Catalog No.
NASA CR-1770		

4. Title and Subtitle	5. Report Date
STUDY OF THE CONCEPT OF INERTIALLY AIDED BAROMETRIC ALTIMETRY SYSTEM FOR SUPERSONIC AIRCRAFT	June 1971
	6. Performing Organization Code

7. Author(s)	8. Performing Organization Report No.
J. Ray Ruetenik, John H. Thompson, and Kenneth R. Britting	TR-65
	10. Work Unit No.

9. Performing Organization Name and Address	11. Contract or Grant No.
Kaman AviDyne A Division of Kaman Sciences Corporation 83 Second Ave., Northwest Industrial Park Burlington, Massachusetts 01803	NAS12-2132
	13. Type of Report and Period Covered
12. Sponsoring Agency Name and Address	Contractor Report
National Aeronautics and Space Administration Washington, D. C. 20546	14. Sponsoring Agency Code

15. Supplementary Notes

16. Abstract

Research needs are studied for providing a hybrid inertial-barometric altimetry system to meet vertical separation requirements of 1000 and 2000 feet for Mach-3.5 transports cruising in altitude hold at 80,000 feet. The static pressure error of the barometric subsystem must be reduced an order of magnitude from present errors for subsonic jet aircraft systems. An off-the-shelf inertial subsystem having a 3σ accuracy of 0.002 g's should be satisfactory, provided the lag of the barometric system is 10 seconds or less. The height deviations from a flight level due to turbulence, atmospheric temperature variations, and variations in isobaric surface height are estimated to be negligible for a hybrid altimeter system. The deviations near the phugoid frequency are essentially eliminated by the system. Flight tests are recommended to verify that all the important factors have been accounted for adequately.

17. Key Words (Suggested by Author(s))	18. Distribution Statement
Altimetry barometric inertial hybrid altimetry system Vertical separation Flight technical errors, system errors, errors models High altitude altimetry problems, phugoid motions Aircraft stability, equations of motions	Unclassified - Unlimited

19. Security Classif. (of this report)	20. Security Classif. (of this page)	21. No. of Pages	22. Price*
Unclassified	Unclassified	146	$3.00

*For sale by the National Technical Information Service, Springfield, Virginia 22151

FOREWORD

This research was carried out by Kaman AviDyne, Burlington, Massachusetts, for the National Aeronautics and Space Administration, Electronics Research Center, Cambridge, Massachusetts, under Contract Number NAS 12-2132. Mr. William O'Keefe of the office of Aircraft Hazard Avoidance Programs served as the technical monitor.

Dr. J. Ray Ruetenik served as Project Leader under the technical supervision of Dr. Norman P. Hobbs, Technical Director for Kaman AviDyne. Mr. Kenneth R. Britting of the Massachusetts Institute of Technology contributed significantly as a technical consultant, particularly in the areas of inertial and hybrid systems. The efforts of Mr. O'Keefe of NASA in support of the project are gratefully acknowledged.

TABLE OF CONTENTS

LIST OF ILLUSTRATIONS

LIST OF ILLUSTRATIONS (CONT.)

LIST OF TABLES

1. INTRODUCTION

Advanced supersonic aircraft, flying at Mach numbers as high as 3.5, might cruise at altitudes up to 80,000 feet. The problem of maintaining altimetry errors within the stringent requirements for 1,000- or 2,000-foot vertical separations, at these speeds and extreme altitude, requires an examination of altimetry system requirements and capability.[1]

The concern of pilots and airline operators regarding vertical separation requirements at supersonic speeds was voiced at the AIAA 6th Aerospace Science Meeting,[2] based on the inadequacies of todays altimetry systems. Aiken,[2] at the same meeting, cited the need for order of magnitude improvement in atmospheric pressure determination.

Gracey[3] evaluated 11 altitude-measuring systems for aircraft based on measurements of gravity, acceleration, atmospheric pressure and density, cosmic-ray and magnetic-field intensities, capacitance, and radio and sound-wave propagation. Each of the methods was evaluated primarily for the high-speed, high-altitude cruise condition with 1000-foot separations up to 70,000 feet. From this evaluation, it was concluded that only the most accurate of the full-range pressure-measuring instruments, the static-pressure compensator-computer system, meets the ±250-foot system accuracy requirement for these conditions.

At these altitudes, the slow response of a pressure probe could result in large height deviations for an aircraft. To meet such response requirements, a hybrid altimeter system combining an inertial system with the pressure probe could utilize the fast response capabilities of the inertial system and low frequency capabilities of the barometric system.[4-7] The potential advantages of a hybrid altimetry system are explored in the present study.

In the hybrid system that is studied, the vertical-acceleration signal from an inertial platform is combined with the barometric pressure signal from a pressure probe through a second-order filter to provide an improved estimate of barometric height. The height error for a representative supersonic airplane using a hybrid altimeter in combination with an autopilot and elevator control system is computed.

The height error depends on a number of factors, such as airplane speed, aerodynamic coefficients, distribution of mass, altimeter parameters, control parameters, and atmospheric characteristics. The present study examines the effect of pressure-probe characteristics, inertial system characteristics, hybrid logic parameters, and autopilot gains for an aircraft in representative atmospheric turbulence, temperature variations, and variation in the height of the isobaric surfaces. The hybrid system is studied for a representative supersonic jet transport weighing 388,000 lb and cruising at Mach 3.5 at an altitude of 77,800 feet.

Piggott[8] examined the effect of atmospheric turbulence on the flight technical error for jet transports having a perfect altimeter. For a supersonic airplane in cruise at Mach 2.2 and 60,000 feet, the 3σ height error was computed to be only 2.4 feet. For representative subsonic jet transports, he found the computed height error to be two orders of magnitude less than the errors measured. From the latter comparison, Piggott concluded that atmospheric turbulence, excluding such effects as waves, large updrafts, and wind shears, does not make a significant contribution to the aircraft altitude-hold error, but that the accuracy to which this contribution can be calculated is limited by the lack of adequate representation of: the pilot or autopilot, the static pressure altimeter, and components of turbulence that cannot be represented by the spectral method.

In this report, the effect of the pressure probe lag is studied along with bias and sensitivity errors in the barometric and inertial systems. In atmospheric turbulence or temperature variations, the altitude error due to probe lag is reduced two orders of magnitude by the hybrid inertial-barometric system, and it is essentially independent of the value of the hybrid logic parameter, as long as the parameter is chosen so the resulting system is stable. The 3σ height error due to probe lag is computed to be less than one foot with the hybrid altimeter system.

The predominant altimeter errors are the static error of the pressure probe and the bias and sensitivity errors of the inertial system. The probe error essentially results in a bias error in altitude. The effect of the errors of the inertial system upon the altitude error depends upon the value of the parameters of the hybrid system logic. It is shown how the parameters can be varied to minimize the resultant altitude error.

2. ALTIMETRY SYSTEM

2.1 ALTIMETRY

Maintaining an airplane at constant altitude requires both an accurate measurement of the altitude and accurate control of the aircraft longitudinal motion. The term "system error" has been used to designate the errors involved in the measurement, and the term "flight-technical error" has been employed to include the remaining errors in maintaining altitude.

Gracey[9] has defined the altimetry errors for a barometric altimetry system as follows:

> Instrument error: Statistical sum of the errors due to the mechanical imperfection of the altimeter (i.e., scale or diaphragm, hysteresis, drift, friction, temperature, instability and backlash) and the errors due to readability (altitude and barometric-setting scales).
>
> Static-pressure error: The difference between free-stream static pressure and the pressure registered by the aircraft static-pressure source (static-pressure tube or fuselage vent); for a given airplane, the statistical sum of the fixed error (the error applicable to the aircraft type) and the variable error (the probable departure of the actual error from the fixed error).
>
> Flight technical error: Random deviations of an airplane from its cruise flight level.
>
> System error: Statistical sum of the instrument error and the static-pressure error.
>
> Altimetry error: Statistical sum of the system error and the flight technical error.

σ: Standard deviation of an error.

3σ: Probable maximum value of an error or the value having a probability of 99.7%.

Figure 2.1 graphically shows the way the instrument error and the static-pressure error, which comprise the system error for a barometric system, combine with the flight technical error to give the altimetry error. These errors have been under extensive study by cognizant Government agencies in this country and abroad in order to set aircraft separation standards and maintain flight safety requirements faced with the rapidly growing air traffic. The investigation of these errors for current commercial jet aircraft has been reported by Gracey[9] and others.

Pressure altimetry has been the standard method of measuring altitude. As a consequence, the defined altitude for aircraft is the pressure altitude (flight level). Therefore, an aircraft flying in altitude-hold mode is actually flying along an isobaric surface. As noted during B-70 flights, a supersonic airplane flying isobaric surfaces at high altitudes can be climbing or diving at a significant rate in terms of "tape-line" altitude. Nevertheless, pressure altitude will probably be the air-traffic control standard for many years, so pressure altitude will be employed as the altitude navigation reference for the hybrid altimeter system studied in this report.

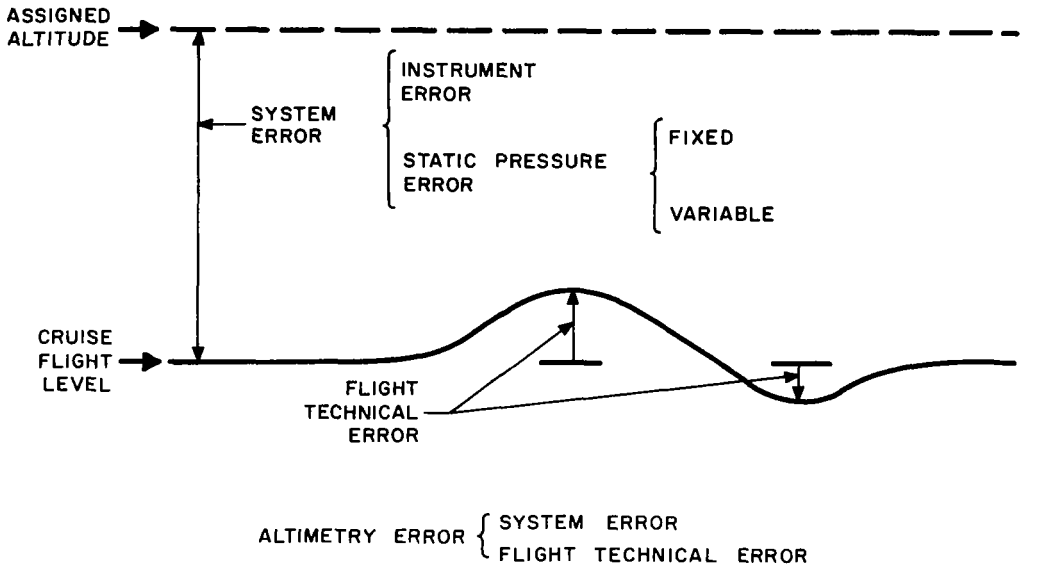

Fig. 2.1. Pressure Altimetry Errors (From Reference 9)

A hybrid altimeter is subject to the additional errors in altitude stemming from the inertial system errors and logic errors. These errors will also be included in the term "system errors." The definition that will be used for system error of the hybrid system will be:

> System error: Statistical sum of the pressure altitude measurement errors due to the barometric system, inertial system, and the logic unit.

Throughout this report the 3σ error or the 99.7% probability value will be used, unless otherwise indicated.

A pressure error δp will be interpreted in terms of height error δh using the ARDC 1959 Standard Atmosphere and assuming a linear relationship

$$\delta h = \frac{1}{\left(\frac{\partial p}{\partial h}\right)_{atmos}} \delta p \qquad (2.1)$$

where $\left(\frac{\partial p}{\partial h}\right)_{atmos}$ is obtained from the standard atmospheric tables.[10] Curves of δh for constant δp are presented in Fig. 2.2, where each curve is identified by the altitude error at 35,000 ft. For example, a pressure error of 30 ft at an altitude of 35,000 ft is a pressure error of 256-ft at 80,000 ft.

2.2 BAROMETRIC SUBSYSTEM

The estimate of errors for a barometric system on a supersonic airplane will be based in part upon error values measured

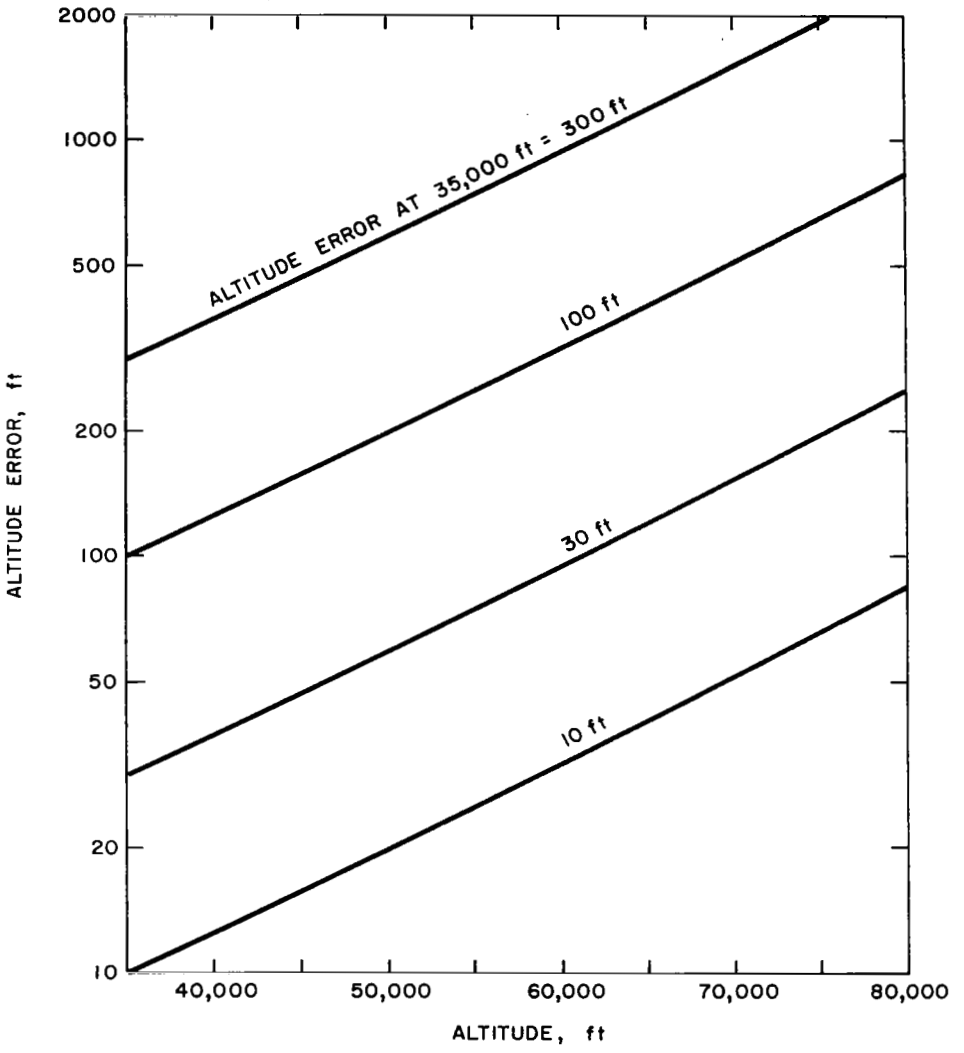

Fig. 2.2. Variation of Altitude Error With Altitude for a Barometric System

for subsonic transports. These errors are listed in the first two columns of Table 2.1.

Instrument error. In 1960, the International Air Transport Association[11] (IATA) assessed the vertical separation standards for aircraft equipped with precision altimeters or instruments with better performance. The instrument error, for an altitude of 40,000 ft, was estimated to be 249 ft. In the following year, the instrument error for precision altimeters was estimated by the International Civil Aviation Organization (ICAO) to be 132 ft at 40,000 ft.

The instrument and display error for subsonic jets with an air data computer is reported by Boeing sources[12] to be 75 ft at Mach 0.85 and 35,000 ft. This represents a reasonable improvement in technology for the intervening time period over the ICAO estimate.

If the instrument error in terms of pressure, δp_{inst}, at all altitudes remains a fixed percentage of the full-scale reading, then the instrument error δh_{inst} can readily be estimated for all altitudes using Eq. (2.1)

$$\delta h_{inst} = \frac{1}{\left(\frac{\partial p}{\partial h}\right)_{atmos}} \delta p_{inst} \qquad (2.2)$$

Extrapolation of the 75-ft error Boeing indicates for current jet aircraft would give an error for a Mach-3.5 aircraft at 77,800 ft of 565 ft. This is large.

TABLE 2.1

ALTIMETRY 3σ ERRORS (FT) FOR JET TRANSPORTS

Error	Current Subsonic Transports		Estimates for Future Supersonic Transports			
			M = 2.7/65,000 ft.		M = 3.5/80,000 ft.	
	35,000 ft.	40,000 ft.	Scaled From Col. 1 or 2	Est. by Boeing	Scaled From Col. 1 or 2	Scaled From Col. 4
Instrument error						
IATA estimate		249				
ICAO estimate (2/61)		132				
Boeing	75		310	135	565(77,800)	250(77,800)
0.010 in. Hg.	30				230(77,800)	
Static pressure error						
IATA		264				
ICAO	250					
Boeing	250		2550	335-475	4270	565-800
NASA, with corrections	116				2000	
Flight technical error						
ICAO, present objective		500 325				
NASA, autopilot		<225*			985	
Boeing, autopilot	250		795	250-350		325-455
Altimetry error						
IATA		618				
NASA (FTE added) $(\sum_i (3\sigma_i)^2)^{1/2}$		487			3205 2420	
Boeing $(\sum_i (3\sigma_i)^2)^{1/2}$	365		2700	440-605		705-960

*Non-Gaussian distribution

The Boeing source[12] has estimated that the instrument error for the Mach-2.7 SST at 65,000 ft will be 135 ft. To compare this error to the error experienced with present equipment, the 75-ft error for present equipment is extrapolated to 65,000 ft altitude, where the error would be 310 ft. This means that the instrument error for the Mach-2.7 SST is projected to be half of the present error. At the altitude of 77,800 ft, the projected Mach-2.7 SST instrument error of 135 ft extrapolates to be an error of 250 ft.

Another basis for estimating how small an instrument error might be achieved with "current technology" is to use the accuracy of calibration equipment now in use as a guide. The latter can be said to represent the current technology for fixed-base equipment, and, perhaps, serves as a reasonable criterion for the accuracy of future operational equipment. Calibration test equipment have been improved to the point where a variety of precision barometers are available that permit calibrations to be performed to an accuracy of 0.005 in. Hg., or 5 ft at sea level[11,13]. Allowing for inaccuracies between calibration points, degradation with time, etc., it seems reasonable to assume that the error in an aircraft operational unit might be 0.010 in. Hg. At 77,800 ft, this represents an error of 230 ft, or about equal to the 250-ft value extrapolated from the Boeing SST estimate.

Therefore, it is concluded that the instrument error for a Mach-3.5 SST at 77,800 ft is 565 ft for current operational instruments and is expected to be 240 ft for future operational instruments.

Static-pressure error. The IATA[11] estimated the static-pressure error for current jet aircraft at an altitude of 40,000 ft to be 264 ft. The ICAO estimated the fixed static pressure error to be 15 ft if calibration cards are applied and the variable error to be 250 ft at altitudes from 30,000 to 50,000 ft, or a combined static-pressure error of 250 ft. This is consistent with the Boeing sources[12] who indicate the static-pressure error for Mach-0.85 current jets at 35,000 ft to be 250 ft.

The error at higher altitudes and Mach numbers is estimated by assuming that the static-pressure error reflects, essentially, the error in pressure coefficient c_p. The pressure coefficient is defined by

$$c_p = \frac{p_{sp} - p}{q} \tag{2.3}$$

where p_{sp} is the pressure at the probe port, p is the free-stream pressure, and q is the dynamic pressure. The error in pressure coefficient, δc_p, is related to the static-pressure error, δp_{sp}, at a fixed Mach number by

$$\delta p_{sp} = q \delta c_p$$

In terms of airplane Mach number, M, the error due to δc_p is

$$\delta p_{sp} = 0.7pM^2 \, \delta c_p$$

In terms of altitude, the error is estimated using Eq. (2.1), giving

$$\delta h_{sp} = - \frac{1}{\left[\frac{\partial (\ln p)}{\partial h}\right]_{atmos}} \, 0.7M^2 \delta c_p$$

In the stratosphere, starting at about 36,000 ft, the temperature of the standard atmosphere is constant, so

$$\left[\frac{\partial (\ln p)}{\partial h}\right]_{atm} = - \frac{1}{20{,}800 \text{ ft}} \tag{2.4}$$

giving

$$\delta h_{sp} = 14{,}500 \, M^2 \delta c_p \tag{2.5}$$

This means that the altitude uncertainty due to the static pressure error is proportional to Mach number squared. The error of 250 ft at M = 0.85 is equivalent to $\delta c_p = 0.025$. At M = 3.5, this δc_p would give an error of 4270 ft.

Silsby and Stickle[14] of NASA measured a variable error of 105 ft for 6 military transports at 35,000 ft. The aircraft were relatively new, so this smaller error would represent what might be obtained in operation at high subsonic speeds (M = 0.85). The discussion by Gracey[9] indicates that a reasonable estimate of the fixed error is 50 ft for subsonic jet

aircraft. This gives a combined static pressure error of 116 ft. This δc_p would give an altitude error at Mach 3.5 of 2000 ft.

The Boeing source[12] has projected a static-pressure error for the Mach-2.7 SST of 335 to 475 ft. This corresponds to an error δc_p of 0.0032 to 0.0045. Chaffois[15] reported tests on a subsonic-supersonic probe designed for the Mach-2 Mirage III aircraft having a pressure coefficient less than 0.01 in the Mach-2 range. The data scatter as shown would indicate the probe might be calibrated to about $\delta c_p = 0.002$. Taking into account the errors due to aging, calibration procedures, etc., the data would appear to confirm the Boeing estimate. Extrapolated to Mach 3.5, the Boeing projected SST value would give 565 to 800 ft.

It is concluded that the static-pressure error for a Mach 3.5 SST at 77,800 ft is 2000 ft based on current operational pressure errors with subsonic jet transports and 800 ft for future operational probes. These values are tabulated in Table 2.2.

Pressure lag. Reliable data on the pressure lag for static pressure probes is difficult to obtain. The error only becomes significant at SST altitudes, so it has not been critical to this point.

The pressure lag is due in part to the acoustic time for pressure waves to traverse the tube length, but is expected to be due primarily to viscous effects as the additional air enters (leaves) the tube as the pressure rises (falls). Essentially, the viscous lag would be proportional to the tube length and inversely proportional to the atmospheric pressure. The tube diameter is an important factor, as is the chamber size at the instrument.

The pressure lag is difficult to estimate in general because it is so highly dependent upon the particular geometry of the tubing, etc. The geometry is dependent upon the

TABLE 2.2

PROJECTED BAROMETRIC SYSTEM 3σ ERRORS (FT) FOR PROJECTED MACH-3.5 SST AT 77,800 FT.

Category	Technology Status	
	Current Operational	Future Operational
Instrument error	565	240
Static-pressure error	2000	800

particular design method used to meet the stringent accuracy requirements cited above in the 860^{o}F-stagmation temperature environment at Mach 3.5.

Engineers at the NASA Flight Research Center[16] have pointed out that pressure lags at high altitude may be as great as 5 to 10 seconds where the lag at sea level is about 0.1 second.

The pressure lag has been scaled for altitude in Fig. 2.3 by assuming that lag is proportional to ambient viscosity and inversely proportional to pressure. For example, a lag of 0.2 second at sea level would be 5 seconds at 77,800 ft. Allowing for other lags in the pressure system due to instrumentation, air-data computers, etc., a nominal value of 10 seconds is probably a representative delay time at 77,800 ft. The lag is assumed to be due principally to viscous effects, so a first-order response is assumed

$$\tau \frac{dp_b}{dt} + p_b = p \tag{2.6}$$

where p_b is the measured pressure without instrument or static-pressure errors, p is the ambient pressure, and τ the time constant of the pressure lag. In terms of altitude, the pressure lag equation becomes, using Eq. (2.1)

$$\tau \frac{dh_b}{dt} + h_b = h \tag{2.7}$$

for the standard atmosphere. Here h_b does not include the instrument and static pressure errors.

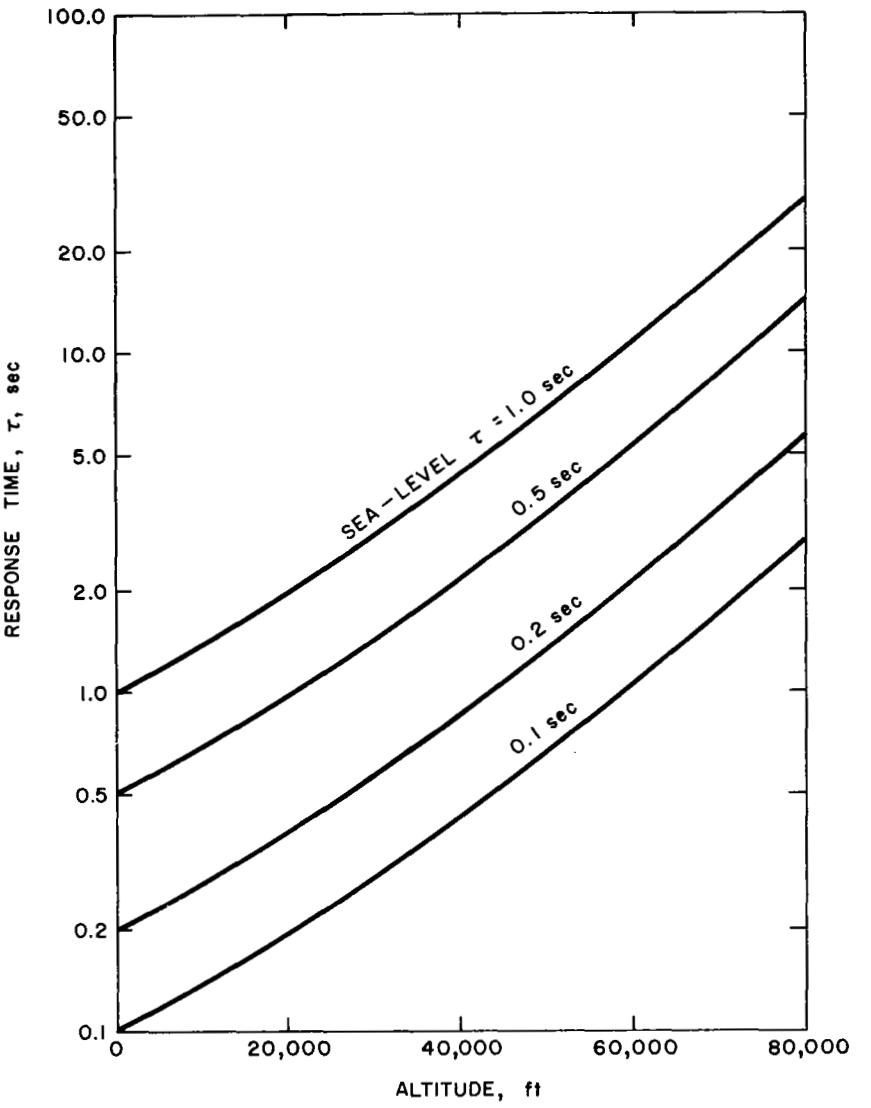

Fig. 2.3. Altitude Scaling of Pressure Lag

Isobaric surfaces. A supersonic aircraft travels so fast, that the problem of following an isobaric surfaces as it varies in tape-line altitude along the route must be considered. This will be discussed with reference to Fig. 2.4.

The airplane in Fig. 2.4 is at altitude h. It is attempting to fly in the altitude-hold mode along the isobaric surface ($p = p_o$) which is a height Δh_I above the pressure altitude h_o (given by the standard-atmosphere model for the pressure p_o). The airplane height above the isobaric surface is designated Δh. Therefore, the tape-line altitude h of the airplane is

$$h = h_o + \Delta h_I + \Delta h \tag{2.8}$$

A perfect barometer system would read the altitude h_B where

$$h_B = h_o + \Delta h \tag{2.9}$$

and it is assumed that Eq. (2.1) applies, so

$$\Delta h = \frac{1}{\left(\frac{\partial p}{\partial h}\right)_{atmos}} (p - p_o) \tag{2.10}$$

The barometric system reads h_b, which differs from h_B by pressure lag and system errors $(u)h_b$

$$\tau \frac{dh_b}{dt} + h_b = h_B + (u)h_b \tag{2.11}$$

where

$$(u)h_b = \delta h_{inst} + \delta h_{sp} \tag{2.12}$$

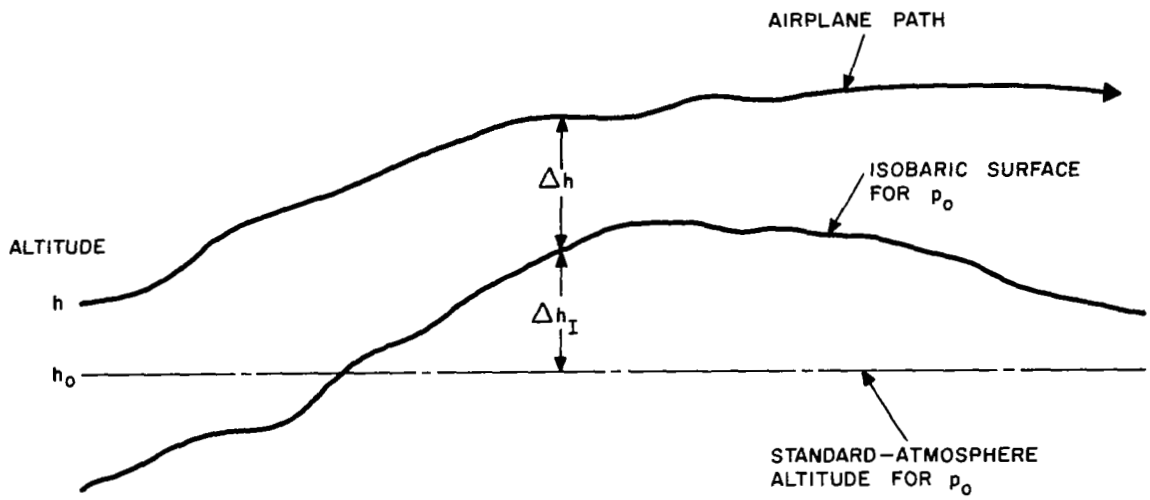

Fig. 2.4. Sketch Showing Relationship of Altitude and Barometric Altitude

Combining Eq. (2.9) and (2.11) gives

$$\tau \frac{dh_b}{dt} + h_b = h_o + \Delta h + (u)h_b \qquad (2.13)$$

A control system would try to minimize Δh. Therefore, the barometric signal Δh_b would be used where

$$\Delta h_b = h_b - h_o$$

The error in this signal, δh_b, is defined as

$$\delta h_b = \Delta h_b - \Delta h \qquad (2.14)$$

and, from Eq. (2.13) is equal to

$$\delta h_b = - \tau \frac{dh_b}{dt} + (u)h_b \qquad (2.15)$$

Eq. (2.15) gives the error in determining the altitude deviation of the aircraft from the isobaric surface using the barometric measurement.

In Sec. 2.3, the barometric measurement h_b is used to estimate the airplane tape-line altitude h. Combining Eq. (2.8) and (2.13) gives

$$\tau \frac{dh_b}{dt} + h_b = h - \Delta h_I + (u)h_b \qquad (2.16)$$

The error in this estimate of tape-line altitude is $h_b - h$, which is

$$h_b - h = - \tau \frac{dh_b}{dt} - \Delta h_I + (u)h_b \qquad (2.17)$$

2.3 INERTIAL SUBSYSTEM

In recent years, inertial navigation systems have been widely used in both commercial and military aircraft. Their application has, for the most part, been limited to the determination of the aircraft's terrestrial coordinates, latitude and longitude. This limitation arises from the well known fact that the computation of altitude in pure inertial navigation systems is divergent.[17]

There are three basic problems encountered in using a purely inertial system for altimetry purposes: (1) the specific force input (defined below) to the inertial system cannot be measured exactly, (2) undesired components of the output specific force signal from the inertial system cannot be exactly compensated and (3) the transformation from inertial to navigational coordinates cannot be precisely accomplished. When the resulting vertical acceleration signal from this imperfect system is integrated twice with respect to time to obtain change in altitude, the error in the signal produces an error in altitude determination which grows in an unbounded manner.

The following discussion treats these three problems in a simplified manner and shows the nature of error divergence or instability of a purely inertial altimetry system. Throughout the following discussion, the dynamics of the inertial system component response are assumed to be several orders of magnitude

faster than the natural response frequencies of the aircraft.[18] Consequently, these dynamical effects are neglected.

Vertical Acceleration Equation. A schematic of the basic considerations involved in obtaining a vertical acceleration signal during aircraft flight is shown in Figure 2.5. The specific force vector input to the inertial system, $\underline{f}$, is defined as the difference between inertial acceleration, $\ddot{\underline{r}}$, and gravitational mass attraction, $\underline{G}$

$$\underline{f} = \ddot{\underline{r}} - \underline{G} \tag{2.18}$$

This equation, of course, is written for an inertial reference frame. The input includes aircraft elastic motion at the location of the inertial system as well as the rigid-body acceleration of the aircraft. However, for what follows it is assumed that this excitation has been minimized by proper location of the inertial system or by some form of compensation.

The output from the inertial system $\underline{\tilde{f}}$ will be $\underline{f}$ plus some measurement error $\delta\underline{f}$ which is brought about purely by the inability to produce a perfect inertial system.

$$\underline{\tilde{f}} = \underline{f} + \delta\underline{f} \tag{2.19}$$

Note that the tilde ($\sim$) is used to denote a measured or estimate quantity. As shown in Figure 2.5, the measured specific force is transformed into geographic coordinates (north-east-down) to obtain the vertical component, $\tilde{f}_D$. Compensation for the gravitational field and centrifugal acceleration effects

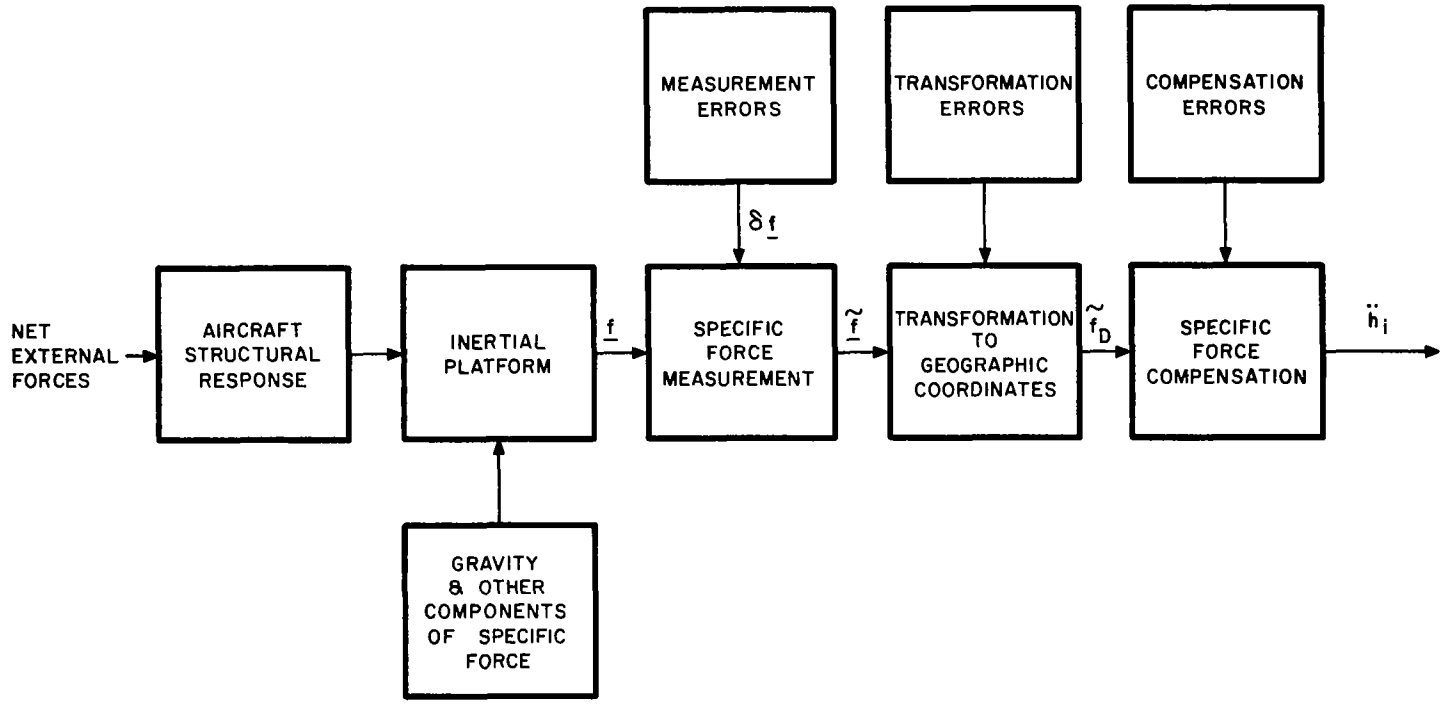

Fig. 2.5. Model of the Basic Considerations Involved in Inertial Altimetry

is then supplied to obtain the inertially measured vertical acceleration, $\ddot{h}_i$.

A detailed development of the expression for specific force in terms of geographic coordinates and other reference frames is not intended here. Such treatment may be found elsewhere[6,19,20,21] For example, an expression for the vertical component (vertical taken as being normal to the reference earth ellipsoid) of the specific force in geographic coordinates can be written in the following manner:[17,19]

$$f_D = -\ddot{h} - G_D + r_e\dot{\lambda}^2 \cos^2 L + \frac{r_L^2}{r}\dot{L}^2 \qquad (2.20)$$

where f_D = vertical component of the specific force

G_D = vertical component of the gravitational field

r_L = radius of curvature in meridian plane

r_e = radius of curvature in comeridian plane

r = geocentric position vector magnitude

L = geographic latitude

λ = celestial longitude

h = altitude above the reference ellipsoid

This is the value that would be measured by a perfect system.

Now the desired output of the inertial system, to be used for inertial altimetry, is $\ddot{h}$, the geographic altitude acceleration. To extract this from Eq. (2.20), it is necessary to determine the value of the other terms. An estimate of the vertical acceleration is thus obtained by forming the equation:

$$\ddot{h}_i = -\tilde{f}_D - \tilde{G}_D + \tilde{r}_e \dot{\tilde{\lambda}}^2 \cos^2\tilde{L} + \frac{\tilde{r}_L^2}{\tilde{r}} \dot{\tilde{L}}^2 \qquad (2.21)$$

where h_i = inertially measured vertical acceleration

and, as before, the tilde is used to denote an estimated variable.

As was mentioned previously, the vector output of the inertial system is given by Eq. (2.19). Now the assumption is made that in the operational range of the instrument the error in measurement can be approximated as a linear function of $\underline{f}$:[17]

$$\delta\underline{f} = (u)\underline{f} + \underline{A}\underline{f} \qquad (2.22)$$

where $(u)\underline{f}$ is the measurement uncertainty that is independent of the specific force and $\underline{A}$ is the diagonal scale factor uncertainty matrix. Thus Eq. (2.19) becomes

$$\tilde{\underline{f}} = (u)\underline{f} + (\underline{I} + \underline{A})\underline{f} \qquad (2.23)$$

where $\underline{I}$ is the identity matrix

The specific force measurement must be transformed from platform coordinates (platform coordinates are aircraft coordinates for the strapdown inertial system) to geographic coordinates, which introduces transformation errors. The vertical component of this transformed specific force measurement vector, $\tilde{f}_D$, is used to determine the vertical acceleration

$$\tilde{f}_D = f_D + \epsilon f_H + (u)f_D + a_D f_D \qquad (2.24)$$

where f_D = vertical component of specific force

ϵ = transformation error angle (level error)

$(u)f_D$ = uncertainty of the effective vertical accelerometer

a_D = vertical component of the effective scale factor uncertainty

f_H = horizontal specific force

It is noted that it is only in cases where the local geographic frame is instrumented by the platform that $(u)f_D$ and a_D can be associated with a single instrument. Thus, the vertical uncertainties are termed "effective" since, in general, the error contributions associated with all three instruments are lumped into a single term. In general, the errors, ϵ, a_D, and $(u)f_D$ are time varying and have random components.

The first term in Eq. (2.24) is given by Eq. (2.20) giving an expression for the measured vertical specific force $\tilde{f}_D$ in terms of the aircraft motion, gravitational field magnitude, and measurement errors

$$\tilde{f}_D = -\ddot{h} + r_\ell \dot{\lambda}^2 \cos^2 L + \frac{r_L^2}{r} \dot{L}^2 - G_D + \epsilon f_H + (u)f_D + a_D f_D \qquad (2.25)$$

Substituting Eq. (2.25) into Eq. (2.21) gives the following expression for the measured altitude acceleration

$$\ddot{h}_i = \ddot{h} + G - \tilde{G} + (u)\ddot{h}_i \qquad (2.26)$$

where

$$(u)\ddot{h}_i = \epsilon f_H + (u)f_D + a_D f_D + \Delta G + \Delta f_c \qquad (2.27)$$

and

$$\Delta f_c = -2r(\dot{\lambda}^2 \sin^2 L\, \delta L + \dot{L}\delta\dot{L} - \dot{\lambda} \cos^2 L \delta\dot{\lambda}) - (\dot{\lambda}^2 \cos^2 L + \dot{L}^2)\delta h \qquad (2.28)$$

In Eqs. (2.26), (2.27), and (2.28)

$(u)\ddot{h}_i$ = uncertainty in the inertial indication of acceleration

Δf_c = compensation error arising from the centrifugal terms in Eq. (2.21)

G = vertical component of the elliptical earth gravitational field

δL = latitude error

$\delta\lambda$ = longitude error

δh = altitude error

ΔG = gravity anamoly, which accounts for the fact that the earth is not a homogeneous ellipsoid of revolution

Because $(u)h_i$ depends on the altimetry error δh, a feedback path exists if $\ddot{h}_i$ is used to calculate $\tilde{h}$. It will be shown in the development that follows that the computation of G involves a similar dependence which is about 30 times larger than the last term in Eq. (2.28). For this reason, the dynamic variations due to δh in Eq. (2.28) will be ignored and this effect will be treated statically in the development which follows. In the derivation of Eq. (2.28), products of the error quantities and other small quantities such as the earth's ellipticity were neglected.[17] Note also that the gravity anomaly, ΔG, has been lumped in with the other uncertainty quantities in Eq. (2.27)

since the gravity anomaly, a function of aircraft position, is generally not compensated.

Table 2.3 lists the error magnitudes that are representative of a "relatively-low-cost" system, an "off-the-shelf" system, a "state of the art" system, and a system obtainable through future development. The errors are the 3σ values, in units of earth gravities. The assumed latitude and longitude 2σ errors for the four system classes were 100 nautical miles (nm), 10 nm, 1 nm, and 0.5 nm, respectively. The latitude and longitude rate errors were calculated by multiplying the circular errors by the Schuler frequency (1.25×10^{-3} rad/sec), since this is the highest frequency mode found in inertial systems. The corresponding level 2σ errors were assumed to be ϵ = 20 arc min, 10 arc min, 1 arc min, and 0.2 arc min, respectively, and f_H was assumed to have a value of 0.1 g.

It is seen in Table 2.3 that the dominant error arises from Δf_c, the inability to compensate the centrifugal acceleration terms exactly. For the low cost system, two values for Δf_c and $(u)\ddot{h}_i$ are shown, with the asterisk denoting the use of a navigation aid, such as Loran, Decca, doppler, etc., which results in an overall system which is as accurate as the off-the-shelf, pure inertial system.[17,22,23]

TABLE 2.3

INERTIAL SYSTEM 3σ UNCERTAINTIES (UNITS OF g)

Inertial System	Transformation Error ϵf_H	Unc. of Effective Vertical Accel. $(u)f_D$	Scale Error Uncert. $a_D f_D$	Gravity Anomaly ΔG	Error in Compens. of Centrif. Accel. Δf_c	Unc. of Inertial Indic. of Accel. $(u)\ddot{h}_i$
Low Cost	8.7×10^{-4}	1.5×10^{-3}	1.5×10^{-3}	8.4×10^{-5}	2×10^{-2} (2×10^{-3})*	2×10^{-2} (3×10^{-3})*
Off the Shelf	4.4×10^{-4}	1.5×10^{-4}	3×10^{-4}	8.4×10^{-5}	2×10^{-3}	2×10^{-3}
State of Art	4.4×10^{-5}	1.5×10^{-5}	1.5×10^{-4}	1.5×10^{-6}	2×10^{-4}	2.5×10^{-4}
Future	8.7×10^{-6}	1.5×10^{-6}	1.5×10^{-5}	3×10^{-6}	1.8×10^{-5}	2.4×10^{-5}

*Aided Inertial System

It is seen from the analysis in Ref. 19 which considers the specific force compensation for airborne gravimeters, that the gravitational component G_D is the most difficult term to compensate since its magnitude is approximately an order of magnitude greater than the other terms in Eq. (2.25). Complicating the compensation problem is the fact that G_D is a strong function of the actual aircraft altitude.[21] An analytical expression for the gravitational field is given by

$$G_D = \frac{E}{(r_o + h)^2} [1 - J(1 - 3 \cos 2L)] + \Delta G \qquad (2.29)$$

where E = product of the earth's mass with the universal gravitational constant

r_o = magnitude of the geocentric earth radius at the point below the aircraft

J = ellipticity constant = 0.82×10^{-3}

ΔG = gravity anomaly (2.8×10^{-5} g rms)

The gravitational field magnitude in Eq. (2.21) will be determined based on an elliptic model of the Earth; effects due to gravity anomaly compensation are included in the $(u)\ddot{h}_i$ term, as reflected in Table 2.3. Thus

$$\tilde{G} = \frac{E}{(\tilde{r}_o + \tilde{h})^2} [1 - J(1 - 3 \cos 2\tilde{L})] \qquad (2.30)$$

Substituting Eq. (2.30) into Eq. (2.26), and neglecting products of small quantities, yields

$$\ddot{h}_i = \ddot{h} + 2\omega_s^2 \, \delta h + (u)\ddot{h}_i \qquad (2.31)$$

where

$\omega_s = \sqrt{\frac{E}{r^3}}$ = Schuler frequency, rad/sec

δh = error in determining altitude

The dynamic behavior of the inertial determination of altitude is readily explored via Eq. (2.31). If, for example, the inertially derived altitude magnitude h_i is used to compute the gravitational field magnitude, Eq. (2.31) becomes

$$\ddot{h}_i = \ddot{h} + 2\omega_s^2(h_i - h) + (u)\ddot{h}_i \tag{2.32}$$

Defining the acceleration error $\delta\ddot{h}_i$ by

$$\delta\ddot{h}_i = \ddot{h}_i - \ddot{h}$$

gives

$$\delta\ddot{h}_i - 2\omega_s^2\, \delta h_i = (u)\ddot{h}_i \tag{2.33}$$

This equation shows the problem in using inertial altimetry, since δh_i would grow exponentially with time. The altitude error after a Schuler period (84 min) is on the order of the radius of the Earth for a one milli-g uncertainty, $(u)\ddot{h}_i$.

On the other hand, even if the gravitational field were computed using barometric altitude, the error growth is unsatisfactory since the computation scheme is nothing more than two open loop integrators. To demonstrate this behavior, let $h_i = h + \delta h_i$ as before, and Eq. (2.31) becomes

$$\delta\ddot{h}_i = 2\omega_s^2(h_b - h) + (u)\ddot{h}_i \qquad (2.34)$$

where $(h_b - h)$ is given by Eq. (2.17). Solution of this equation gives a parabolic error growth in time. Neglecting the first term on the right-hand side, the altitude error after a Schuler period is about 400,000 ft per milli-g uncertainty. The argument for using the barometric altitude h_b in computing the gravitational field will be further justified in Appendix B.

The important conclusion based on the above discussion is that the value of $(u)\ddot{h}_i$ together with the gravitational field compensation error $2\omega_s^2\,\delta h$ will determine the length of time an inertial system altimeter can be used in an open loop manner to measure altitude without producing unacceptably large errors. At the present time, state of the art limitations for both the measurement of specific force and the compensation of inertial system output preclude the use of inertial altimeters in an open loop manner for flight duration times of more than a few minutes.

If Eq. (2.34) is examined from a frequency domain point of view, the advantage of an inertial system aided with imperfect gravitational field information is seen. As a function of frequency, ω, Eq. (2.34) becomes

$$\delta h_i = -\frac{2\omega_s^2}{\omega^2}\,\delta h - \frac{(u)\ddot{h}_i}{\omega^2} \qquad (2.35)$$

The altitude error is thus seen to decrease with the inverse square of frequency, the altitude error sensitivity to $(u)\ddot{h}_i$ being only 0.032 ft/milli-g uncertainty at ω = 1 rad/sec. The hybrid system discussed in the next section utilizes the desirable high frequency characteristics of inertial systems, while avoiding the large steady state errors pointed out herein.

2.4 HYBRID ALTIMETER

Configuration. The motivation for using both barometric and inertial information for altitude determination is based on the desire for combining the rapid response characteristics of the inertial system with the long term stability of the barometric altimeter. Several configurations for hybrid altimeter logic have been proposed. One of these makes use of an inertial system which is "updated" every few minutes with barometric information to limit the extent of the inertial altitude error predicted by Equation (2.33).

Another configuration, widely discussed in the literature, couples the barometric input to the inertial input continuously (References 4, 5, 6, 7). This system is extensively analyzed herein. This design uses a simple second-order system to filter the two inputs to the system. The filtering limits the barometric contribution to system response during high frequency excitation of the system, and also prevents divergence of the measured altitude.

A third proposed configuration would make use of Kalman filtering of the inertial and barometric inputs in order to obtain optimum utilization of measurement information. However, for the inertial-barometric hybrid system, it is to be expected that the Kalman filter would provide only a small improvement over the second-order filter. This situation arises because the two sources of information are well separated in frequency. Thus, the Kalman filter system would not be able to reduce the steady-state altimetry error significantly below the level of the barometric altimeter bias, because the inertial signal contains very little low frequency information. Only the second-order system has been examined in this study.

A sketch of the second-order system is shown in Figure 2.6. Here the output h_i from the inertial system and the output h_b from the barometric system are inputed to the second-order filter. The only parameters of the system are the gains ω_n^2 and $2\zeta\omega_n$. The output of the system is the computed barometric altitude, $\hat{h}_b$, which is fed back and mixed with h_b.

The second-order system has been discussed frequently in the literature, and in several papers an attempt has been made to determine appropriate values of ζ and ω_n.[4,5,6,7] However, the choice of the hybrid altimeter parameters ζ and ω_n to satisfy the altimetry requirements of an SST aircraft is not a simply accomplished matter. This selection will be studied in the present work.

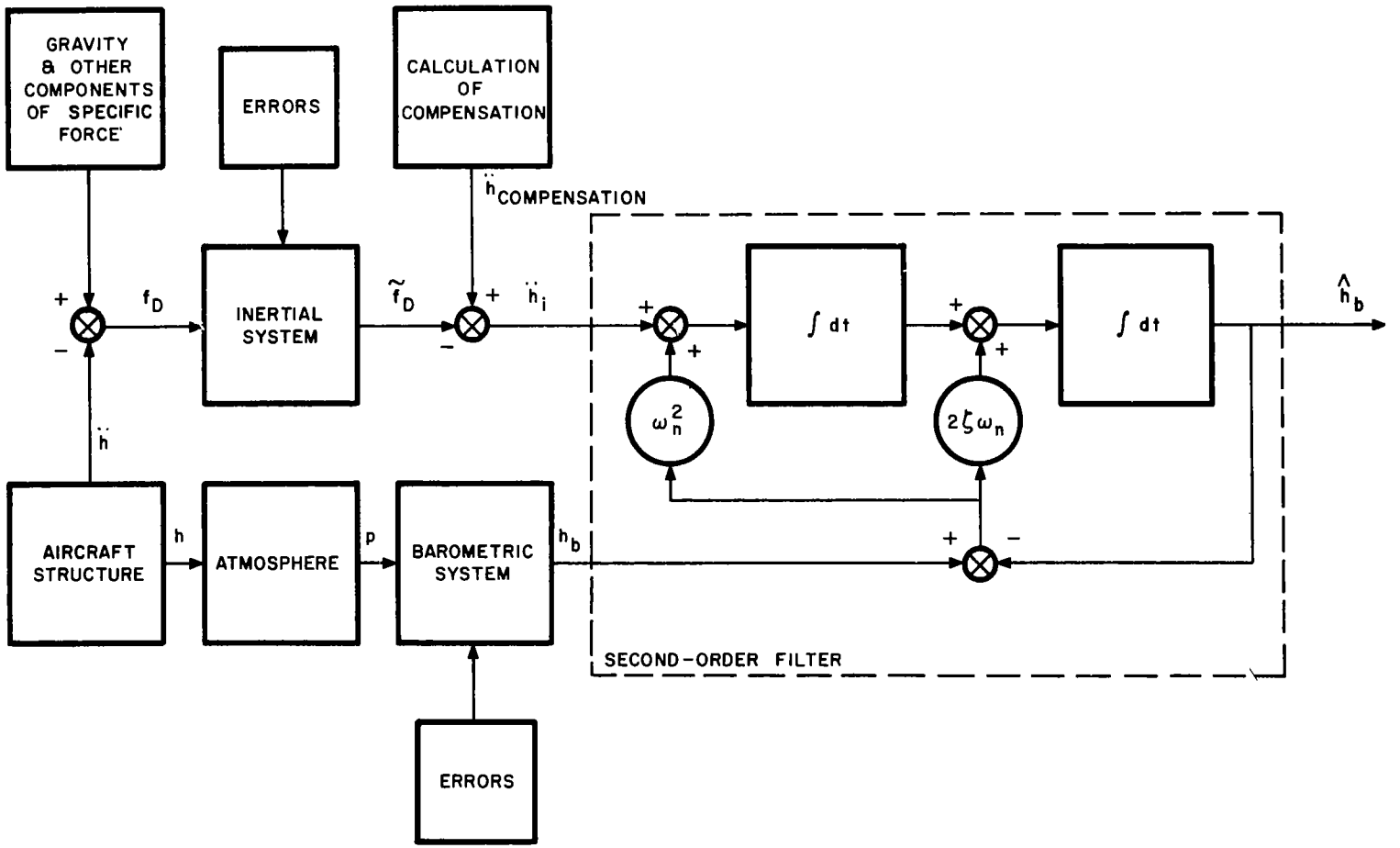

Fig. 2.6. Model of Hybrid Inertial-Barometric Altimetry System With Second-Order Filtering

A few qualitative remarks will be made about the second-order system. As mentioned, an estimate of vertical acceleration, $\ddot{h}_i$, is available from the inertial system, so two time integrations would yield a signal which is proportional to aircraft altitude, except that inertial system errors result in altitude errors which grow with the square of time. On the other hand, the barometric altimeter, while sluggish in response, possesses bounded errors. The hybrid system error is bounded by feeding back a signal which is proportional to the difference between the hybrid and barometric indications of altitude through the constant gains $2\zeta\omega_n$ and ω_n^2. It is seen that at steady-state conditions, $\hat{h}_b = h_b$. In addition, at high frequencies (zero feedback), it is seen that $\hat{h}_b = h_i$.

The signal from the inertial system is only integrated, so the noise to signal ratio is not amplified. Thus, the hybrid system does appear to combine the best aspects of the barometric and inertial systems.

Response Equations. We will now examine the response of the hybrid system. The differential equation for this hybrid system is given by

$$\ddot{\hat{h}}_b + 2\zeta\omega_n\dot{\hat{h}}_b + \omega_n^2\hat{h}_b = \ddot{h}_i + 2\zeta\omega_n\dot{h}_b + \omega_n^2 h_b \qquad (2.36)$$

with ω_n and ζ being free parameters for selection. In particular, ζ will be chosen to give a reasonable amount of transient overshoot:

$$0.5 < \zeta < 1$$

while ω_n is chosen to attenuate the inertial system error and at the same time give the desired fast response characteristics. The choice of ω_n is guided by examination of the hybrid system error differential equation, which will be carried out below.

If the barometrically derived altitude is used in the computation of the vertical component of the gravitational field, then Eq. (2.31) gives

$$\ddot{h}_i = \ddot{h} + 2\omega_s^2 (h_b - h) + (u)\ddot{h}_i \qquad (2.37)$$

Equation (2.17) is used to determine the error in tape-line altitude for the barometric measurement, so

$$\ddot{h}_i = \ddot{h} - 2\omega_s^2[\tau \dot{h}_b + \Delta h_I - (u)h_b] + (u)\ddot{h}_i$$

The barometric measurement h_b can be expressed in terms of the flight altitude by Eq. (2.13) yielding

$$\ddot{h}_i = \ddot{h} - 2\omega_s^2 \left[\frac{\tau D(\Delta h) + (u)h_b}{\tau D + 1}\right] + \Delta h_I + (u)\ddot{h}_i \qquad (2.38)$$

where the operator $D \equiv \frac{d}{dt}$ is introduced.

Substituting Eq. (2.38) into Eq. (2.36), in terms of Δh_b gives

$$(D^2 + 2\zeta\omega_n D + \omega_n^2)\ \Delta\hat{h}_b = \frac{\tau D^3 + D^2 + 2(\zeta\omega_n - \tau\omega_s^2)D + \omega_n^2}{\tau D + 1}\ \Delta h$$

$$+ (D^2 - 2\omega_s^2)\Delta h_I + \frac{2\zeta\omega_n D + 2\omega_s^2 + \omega_n^2}{\tau D + 1}\ (u)h_b + (u)\ddot{h}_i \qquad (2.39)$$

where the definition $\Delta\hat{h}_b = \hat{h}_b - h_o$ is used. This is the equation for the output of the hybrid inertial-barometric system.

Hybrid-System Error. The system can be studied by examining the error in the signal defined by the equation

$$\delta(\Delta\hat{h}_b) = \Delta\hat{h}_b - \Delta h$$

From Eq. (2.39) the error equation is

$$(D^2 + 2\zeta\omega_n D + \omega_n^2)\delta(\Delta\hat{h}_b) = -\frac{2\zeta\omega_n D + \omega_n^2 + 2\omega_s^2}{\tau D + 1}\tau D(\Delta h)$$

$$+ (D^2 - 2\omega_s^2)\Delta h_I + \frac{2\zeta\omega_n D + \omega_n^2 + 2\omega_s^2}{\tau D + 1}(u)h_b + (u)\ddot{h}_i \qquad (2.40)$$

Let us examine the error for various signal rates. To simplify the analysis, let $\Delta h_I = (u)h_b = (u)\ddot{h}_i = 0$. Then, the transfer function relating hybrid system error to altitude change is given by:

$$\frac{\delta(\Delta\hat{h}_b)}{\Delta h}(s) = \frac{-\tau s\left[\frac{2\zeta}{\omega_n}s + 1 + \frac{2\omega_s^2}{\omega_n^2}\right]}{(\tau s + 1)\left[\frac{s^2}{\omega_n^2} + \frac{2\zeta}{\omega_n}s + 1\right]} \qquad (2.41)$$

For purposes of simplification, let us first consider systems in which $\omega_n^2 >> \omega_s^2$. The transfer function is plotted in Fig.

2.7 as a function of the non-dimensional driving frequency, $\omega\tau$, for the case of $\zeta = 1$. The ordinate, then, gives the ratio of the error in the computed altitude to the amplitude of the altitude oscillation. It is desirable that this ratio be small, of course – how small it must be depends upon the complete system – autopilot, airplane, and atmospheric disturbances. But, for a "ball-park" number, if the error ratio is 10^{-1} or less, this should be acceptable.

The error ratio in large part is a function of the response time τ of the barometric system. The break frequency associated with τ is defined as the frequency where $\omega\tau = 1$. It is seen from the diagram that, if the system natural frequency, ω_n, is set at a high value compared with this break frequency, the barometric information is favored and the overall system will have poor accuracy at high frequencies. If, on the other hand, ω_n is set at a low value compared to the break frequency, the inertial information is favored and the overall system will have good high frequency accuracy.

If ω_n is set too low, however, two other problems enter. First, the error due to the inertial and barometric system uncertainties $(u)\ddot{h}_i$ and $(u)h_b$ will increase. This is seen from the following equation which is the steady-state form of the system error differential equation, Eq. (2.40)

$$\delta(\Delta\hat{h}_b)_{ss} \cong \frac{(u)\ddot{h}_i}{\omega_n^2} + \left(1 + 2\,\frac{\omega_s^2}{\omega_n^2}\right)(u)h_b - \frac{2\omega_s^2}{\omega_n^2}\,\Delta h_I \qquad (2.42)$$

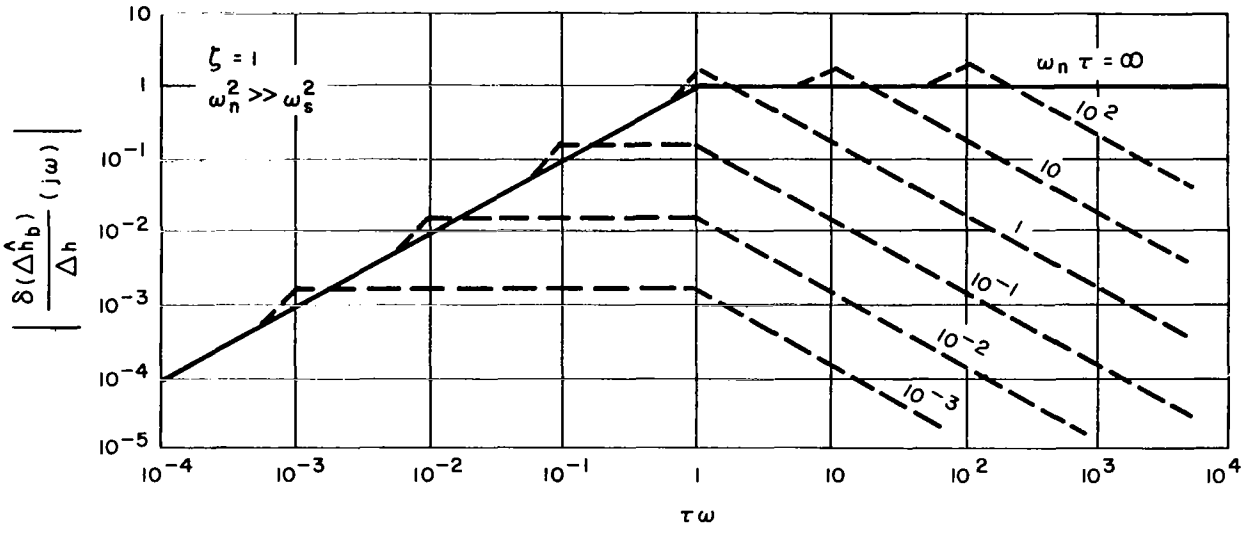

Fig. 2.7. Dynamic Altitude Measurement Error as a Function of Frequency

Here, the steady-state error due to the inertial system and the isobaric surface displacement are inversely proportional to ω_n^2. Secondly, the constant $2\omega_s^2/\omega_n^2$ in Eq.(2.42) is also inversely proportional to ω_n^2, increasing the error due to the barometric system at low values of ω_n. A plot of the steady-state altitude error as a function of ω_n is shown in Figure 2.8 for several values of inertial acceleration uncertainty $(u)\ddot{h}_i$, with $(u)h_b = \Delta h_I = 0$.

The system parameter which strongly constrains the choice of ω_n is the barometric system time constant, τ. At high altitudes, the barometric system is very sluggish and τ is quite large. Fig. 2.7 shows that the dynamic error $\delta(\Delta\hat{h}_b)$ of the hybrid system for $\tau\omega_n = 0.1$ would be about 0.17, or less, of the altitude deviation Δh. If $\omega_n\tau$ is much larger, it turns out that the aircraft response becomes unstable. At high altitudes where τ might be 10 sec, ω_n would have to be about 0.01 rad/sec, or less. Figure 2.8 shows that the altitude error for a system with $(u)\ddot{h}_i = 0.001g$ and $\omega_n = 0.01$ rad/sec would be about 320 ft.

The altitude error corresponding to the four levels of inertial system uncertainty, $(u)\ddot{h}_i$, listed in Table 2.3 are given in Table 2.4. A value of $\omega_n = 0.015$ rad/sec has been used. The error for the off-the-shelf system, for example, is 300 ft.

Eq. 2.42 indicates that the steady-state error sensitivity to barometric altimeter uncertainty is given by

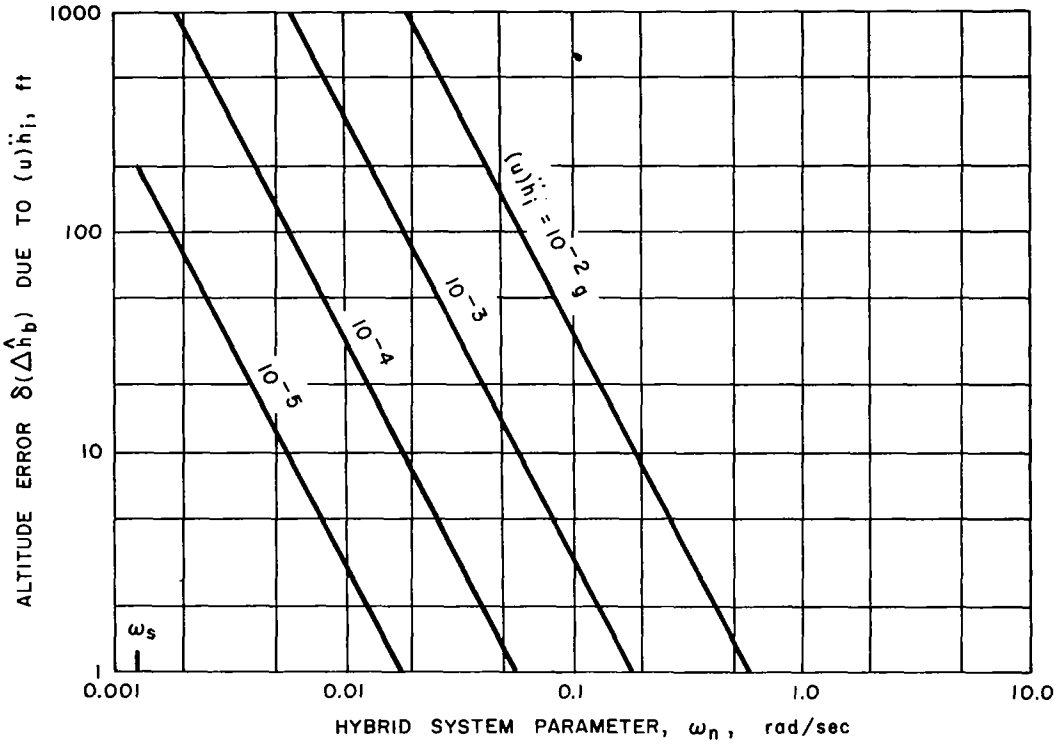

Fig. 2.8. Altitude Error of Hybrid System Due to Uncertainty of Vertical Acceleration Measurement

TABLE 2.4

STEADY STATE ALTITUDE ERRORS $\delta(\Delta\hat{h}_b)$
FOR ω_n = 0.015 RAD/SEC

Inertial System	$(u)\ddot{h}_i$, g's	$\delta(\Delta\hat{h}_b)_{ss}$, ft.
Low-Cost	2×10^{-2} (3×10^{-3})	3000 (425)*
Off-The Shelf	2×10^{-3}	300
State of the Art	2.5×10^{-4}	36
Future	2.4×10^{-5}	3

*Aided Inertial System

$$\delta(\Delta\hat{h}_b)_{ss} = 1 + \left(2\,\frac{\omega_s^2}{\omega_n^2}\right)(u)h_b$$

Thus, the sensitivity is greater than unity, depending upon the choice of ω_n. For $\omega_n = 0.015$ rad/sec, the nominal value,

$$\delta(\Delta\hat{h}_b)_{ss} = 1.007(u)h_b$$

It is seen that the sensitivity cannot be reduced to a value which is less than one. This limitation exists because the hybrid altimeter relies exclusively on the barometric altimeter for low frequency information. However, it is not difficult to keep the sensitivity very near unity.

Note that the steady-state errors due to accelerometer and barometric altimeter uncertainties result directly in flight technical errors, independent of the autopilot design. The complement of instruments must therefore be carefully chosen to keep errors of the hybrid system sufficiently small.

3. AIRCRAFT CONTROL AND RESPONSE EQUATIONS

Figure 3.1 is a block diagram of the configuration commonly used for an altitude-hold flight control system. The altitude displacement from the isobaric surface, $\Delta\hat{h}_b$, measured by the altimeter system is processed through the compensation system to yield a pitch rate command for the airplane. The compensation sets the gain and damping to the outer loop. The inner loop compares the commanded and actual pitch rates, and drives the elevator to null the error.

It is assumed that the elevator servo and actuator can be represented as a first-order system with a time lag, τ_e. In the calculations, τ_e will be taken as 0.1 sec. The rate gyro will be represented as a unity transfer function, the dynamics being ignored. The elevator control equation in the Laplace domain is

$$(\tau_e s + 1)\delta_e(s) = S_{\dot{\theta}} s[\theta(s) - \theta_c(s)] \tag{3.1}$$

The phugoid mode of the Mach-3.5 SST model has a slightly divergent oscillation when the vertical pressure gradient of the standard ARDC atmosphere is represented. The divergence rate is small, however, so the phugoid mode can be stabilized rather simply using the rate gyro in the feedback loop.

The form of the compensation equation used is

$$s\theta_c(s) = -\frac{S_h}{S_{\dot{\theta}}}(\tau_e s + 1)K_{\delta_e}(s)(\Delta h_b) \tag{3.2}$$

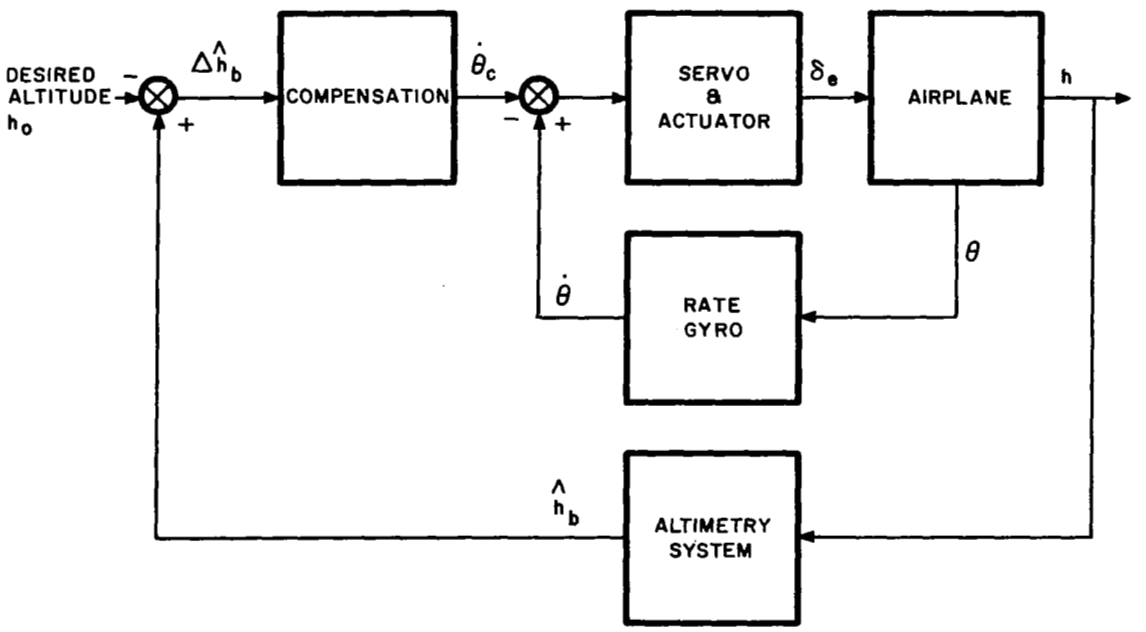

Fig. 3.1. Block Diagram of Altitude-Hold Autopilot

where

$$K_{\delta_e}(s) = \frac{(\tau_{h_2} s + 1)(\tau_{h_3} s + 1)}{(\tau_e s + 1)(\tau_{h_1} s + 1)}$$

The values of τ_{h_1}, τ_{h_2}, and τ_{h_3} are selected to provide adequate damping of the phugoid and short-period modes for the Mach-3.5 SST. The values are kept small relative to 10 seconds in order to not confuse the analysis of the effect of the barometric response time τ, which is on the order of 10 seconds. No attempt has been made to select an optimum compensation, as the chief objective of the study is to evaluate the hybrid altimeter system.

Combining the above three equations gives the elevator control equation

$$\begin{aligned}\delta_e(s) = {} & S_{\dot{\theta}} G_\theta(s)\theta(s) + S_h K_{\delta_e}(s)[H_{\Delta h}(s)\ \Delta h(s) \\ & + H_{\Delta h_I}(s)\ \Delta h_I(s) + H_{(u)h_b}(s)\ (u)h_b(s) \\ & + H_{(u)\ddot{h}_i}(s)\,(u)\ddot{h}_i(s)] \end{aligned} \tag{3.3}$$

where the expressions for G_θ and the H-functions are listed in Appendix D.

In a similar manner, the thrust control equation is derived. Thrust control is employed in this analysis to maintain a constant Mach number of the aircraft relative to the wind. Double-lead compensation is applied, so the thrust control equation is

$$\bar{T}(s) = S_T K_T(s)[\bar{u}(s) + \bar{u}_w(s) - \bar{a}(s)] \tag{3.4}$$

where $K_T(s)$

$$K_T(s) = \frac{(\tau_{T_1} s + 1)(\tau_{T_2} s + 1)}{(\tau_E s + 1)(\tau_t s + 1)}$$

and τ_E is the engine lag, τ_t is the throttle lag, S_T is the scalar gain, and τ_{T_1} and τ_{T_2} are the engine control compensation constants.

The perturbation equations of motion for the airplane in matrix notation are

$$[a(s)] \begin{Bmatrix} \bar{u}(s) \\ \bar{w}(s) \\ \theta(s) \end{Bmatrix} = [b(s)] \begin{Bmatrix} \delta_e(s) \\ \bar{T}(s) \\ \bar{u}_w(s) \\ \bar{w}_w(s) \\ \bar{p}(s) \\ \bar{a}(s) \end{Bmatrix} \tag{3.5}$$

where the elements of the matrices are derived in Appendix C. In Appendix D, the control equations, Eq. (3.3) and (3.4), are substituted into Eq. (3.5). The pressure perturbation is expressed in terms of the vertical pressure gradient and the

displacement of the isobaric surface. The aircraft response equations are obtained

$$[A(s)]\begin{Bmatrix}\bar{u}(s)\\ \bar{w}(s)\\ \bar{\theta}(s)\\ \Delta h(s)\end{Bmatrix} = [B(s)]\begin{Bmatrix}\bar{u}_w(s)\\ \bar{w}_w(s)\\ \Delta h_I(s)\\ \bar{a}(s)\\ (u)h_b(s)\\ (u)\ddot{h}_i(s)\end{Bmatrix} \qquad (3.6)$$

in terms of the atmospheric variables and the measurement uncertainties. The elements of the matrices are presented in Appendix D.

Solution of the system of equations (3.6) for transfer functions $\left[\frac{\Delta h}{\bar{u}_w}\right]$, $\left[\frac{\Delta h}{\bar{w}_w}\right]$, etc., has been accomplished using a computer program written for the IBM 360/75. The program calculates the transfer functions, obtains the impulse response time solutions, determines the roots of the characteristic equation, and gives the steady-state frequency response (phase and amplitude ratio) for sinusoidal disturbances $\bar{u}_w$, $\bar{w}_w$, etc.

4. CALCULATION OF HEIGHT ERROR

4.1 HEIGHT-ERROR EQUATION

Having the transfer functions, we can now compute the altimetry error due to atmospheric turbulence and the other factors.

Define $\Phi_i(\omega)$ to be the spectral density function of the i-th variable, $\overline{u}_w$, $\overline{w}_w$, Δh_I, $\overline{a}$, $(u)h_b$, or $(u)\ddot{h}_i$, in units of the variable squared per radian per second. The spectral density function of the height response of the airplane from the isobaric surface is then given by

$$\left|\frac{\Delta h}{(i)}(j\omega)\right|^2 \Phi_i(\omega)$$

where $\left|\frac{\Delta h}{(i)}(j\omega)\right|$ is the absolute magnitude of the appropriate transfer function. The standard deviation $\sigma_{\Delta h(i)}$ of the height response due to the i-th variable is

$$\sigma_{\Delta h(i)} = \left[\int_0^\infty \left|\frac{\Delta h}{(i)}(j\omega)\right|^2 \Phi_i(\omega)\, d\omega\right]^{1/2}, \text{ ft} \qquad (4.1)$$

Assuming that all of the i-th variables are statistically independent, we obtain for the 1σ height error $\sigma_{\Delta h}$

$$\sigma_{\Delta h} = \left[\sum_i \sigma^2_{\Delta h(i)}\right]^{1/2} \qquad (4.2)$$

We will be evaluating the component variations $\sigma_{\Delta h(i)}$, with the establishment of an error budget in mind. Also, unless indicated otherwise, the term height error will refer to the 3σ value.

The models of atmospheric turbulence, temperature variations, and isobaric surface variations for flight at 77,800 ft are presented in the remainder of this section. Very little data are available for use in formulating these models, so the data that are available have been interpreted on the high side. In this way, the aircraft response should be overestimated.

4.2 ATMOSPHERIC TURBULENCE

A general lack of experience of the response characteristics of typical supersonic transport configurations has focused attention on atmospheric turbulence effects on such aircraft. Among many overlapping areas of concern are included the turbulent structure of the atmosphere at altitudes where the SST will fly; the aerodynamic response of an SST configuration; and the effect of engine performance.[24]

Measurements of airplane response to clear-air turbulence have been obtained during supersonic flights of the XB-70 airplanes to an altitude of 74,000 ft over the Western United States. In general, the data shows that turbulence was encountered on an average of 7.2 percent of the miles between 40,000 ft and 65,000 ft and 3.3 percent of the miles above 65,000 ft. (An acceleration

threshold of ±0.06 g was used.) The XB-70 data appear to indicate that large supersonic aircraft would be expected to encounter turbulence at high altitudes more often than predicted by earlier data obtained from small subsonic aircraft.[25]

Yet no attempt was made in the 96 flights of the XB-70 aircraft to seek turbulent conditions. In fact, known areas of heavy turbulence were avoided.

The Dryden turbulence spectra, Reference 26, are employed:

Longitudinal Velocity:

$$\Phi_{u_w}(\Omega, L) = \sigma_{u_w}^2 \frac{2L}{\pi} \frac{1}{1 + (L\Omega)^2} , \frac{(ft/sec)^2}{(rad/ft)} \tag{4.3}$$

Transverse Velocity:

$$\Phi_{w_w}(\Omega, L) = \sigma_{w_w}^2 \frac{L}{\pi} \frac{1 + 3(L\Omega)^2}{[1 + (L\Omega)^2]^2} , \frac{(ft/sec)^2}{(rad/ft)} \tag{4.4}$$

where Ω is the longitudinal spatial frequency in rad/ft. The frequency relative to the airplane is

$$\omega = U_o\Omega$$

The reduced Dryden spectra are plotted in Fig. 4.1 for the Mach-3.5 SST.

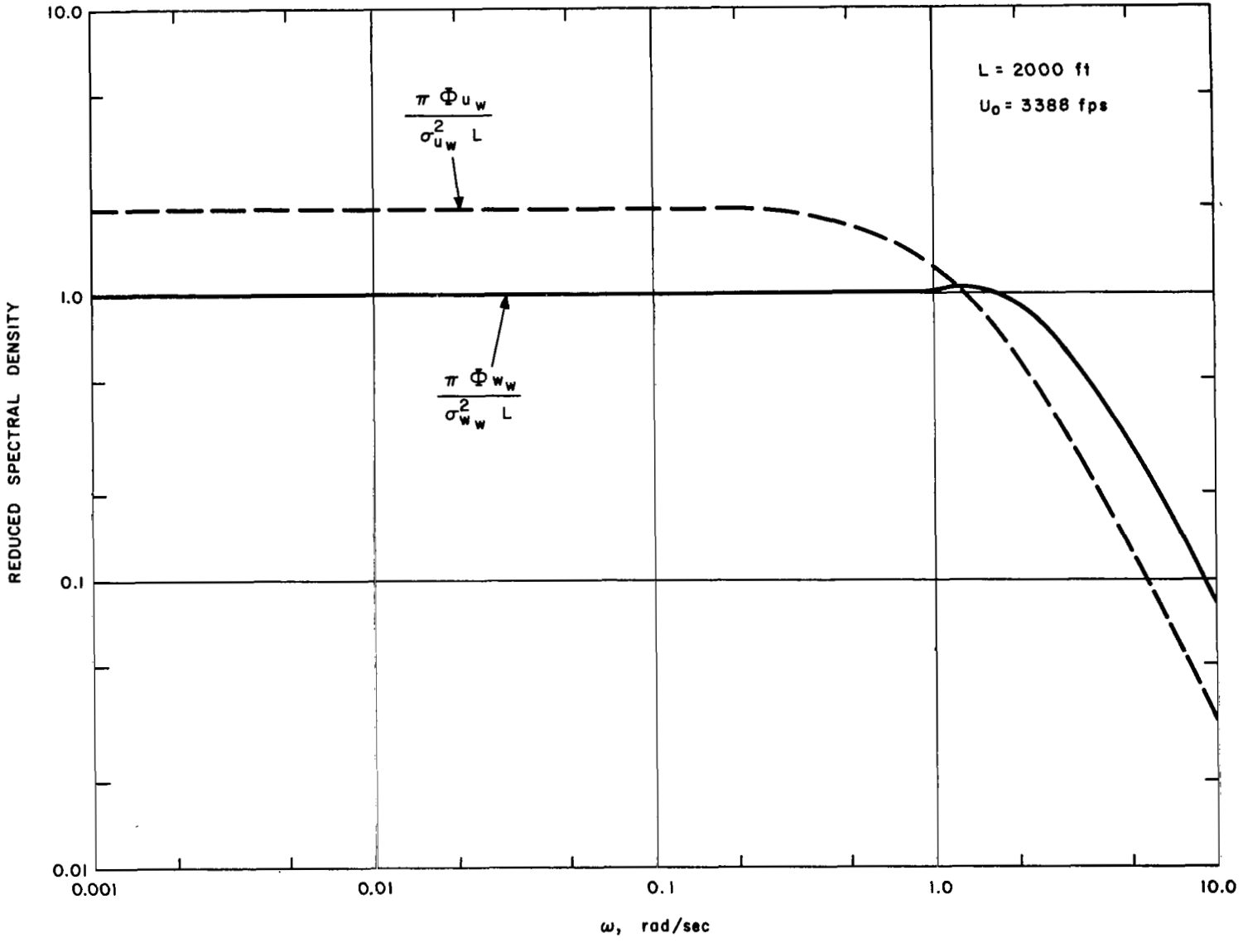

Fig. 4.1. Reduced Spectral Density of Turbulence for Dryden Model

The data of Pritchard, et al[26] on the probability density of turbulence are used. Pritchard assumes that there are separate periods of no turbulence, primary turbulence, and secondary turbulence, and that the distribution of turbulence intensity during each of the latter two periods is half-Gaussian, for example

$$p_i(\sigma_{w_w}) = \frac{1}{b_i}\sqrt{\frac{2}{\pi}} \exp\left(-\frac{\sigma_{w_w}^2}{2b_i^2}\right), \text{ (sec/ft)} \qquad (4.5)$$

where i = 0, 1, or 2 for non-turbulent, primary turbulence or secondary turbulence periods, respectively. Primary turbulence is associated with non-storm periods and secondary turbulence is associated with storms. The resultant probability p is

$$p(\sigma_{w_w}) = P_1 p_1(\sigma_{w_w}) + P_2 p_2(\sigma_{w_w}) \qquad (4.6)$$

where P_i is the proportion of total flight time spent in turbulence type i, so

$$P_o + P_1 + P_2 = 1$$

We will exclude secondary turbulence, because aircraft are controlled to avoid storms. Also, storms are essentially non-existant at 70 - 80 kilofeet. Therefore

$$P_2 = 0$$

and

$$p(\sigma_{w_w}) = P_i p_1(\sigma_{w_w}) \tag{4.7}$$

The turbulence is assumed to be isotropic, so

$$\sigma_{u_w} = \sigma_{w_w} \tag{4.8}$$

Assuming that u and w turbulence velocities are uncorrelated, the standard deviations of the height response due to the $\bar{u}_w$ and $\bar{w}_w$ velocities, are

$$\sigma^2_{\Delta h(u_w)} = \int_0^\infty p(\sigma_{w_w}) \int_0^\infty \left| \frac{\Delta h}{u_w}(j\omega) \right|^2 \Phi_{u_w}(\omega, \sigma_{w_w})\, d\omega\, d\sigma_{w_w}$$

$$\sigma^2_{\Delta h(w_w)} = \int_0^\infty p(\sigma_{w_w}) \int_0^\infty \left| \frac{\Delta h}{w_w}(j\omega) \right|^2 \Phi_{w_w}(\omega, \sigma_w)\, d\omega\, d\sigma_w \tag{4.9}$$

The combined deviation of the vertical displacement of the aircraft due to turbulence is

$$\sigma_{\Delta h} = [\sigma^2_{\Delta h(u_w)} + \sigma^2_{\Delta h(w_w)}]^{1/2} \tag{4.10}$$

From an examination of turbulence data measured in the Air Force HICAT program[27], a scale of turbulence, L, of 2,000 ft was selected as a representative large value. The data for b_1 and P_1 presented by Pritchard[26] are shown in Fig. 4.2 and 4.3 The values of b_1 selected by Pritchard for 70 and 80 kilofeet appear to be realistic, but the values of P_1 may rely too

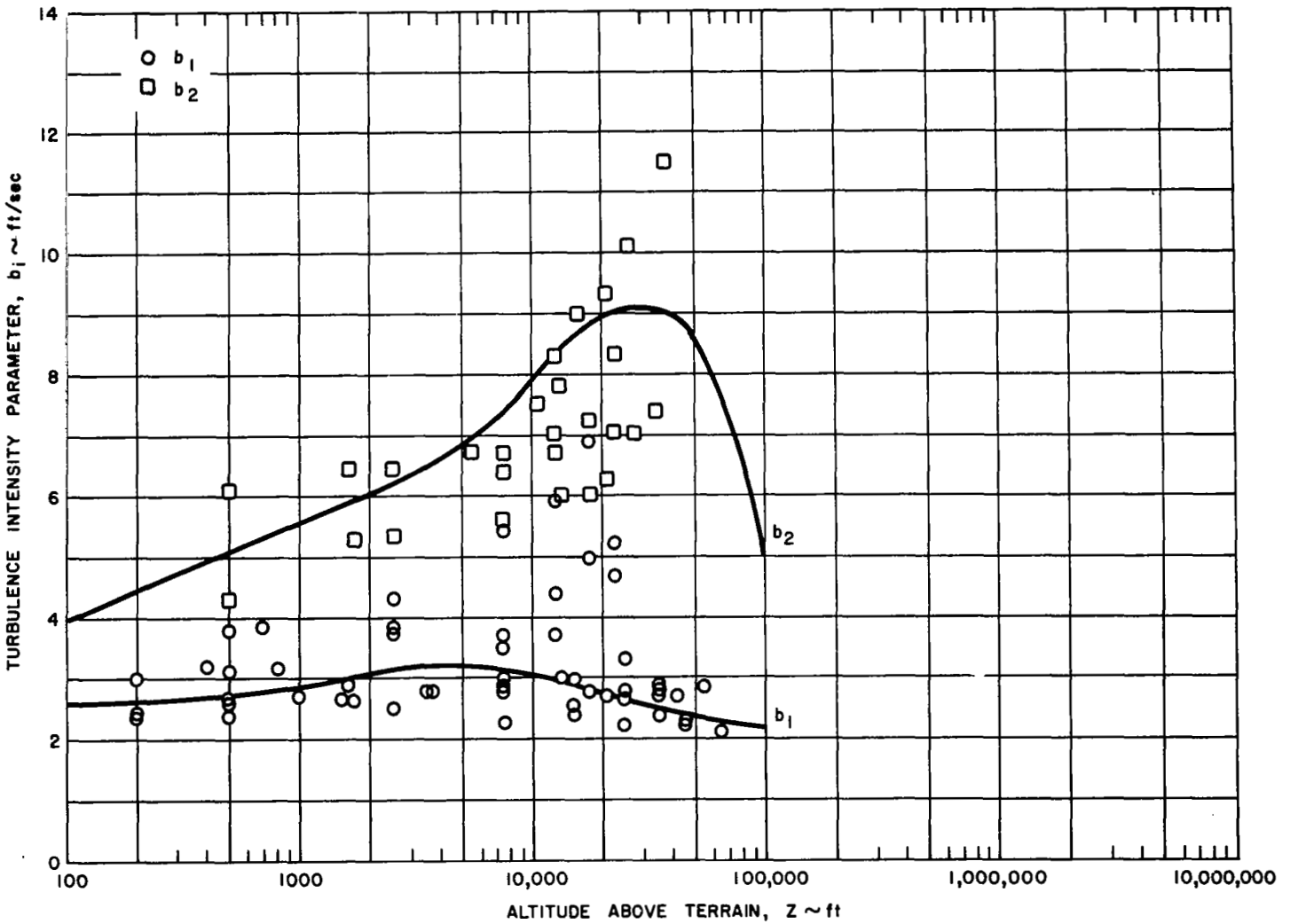

Fig. 4.2. The Intensity Parameters of Atmospheric Turbulence as Functions of Altitude-Data Points (From Reference 26)

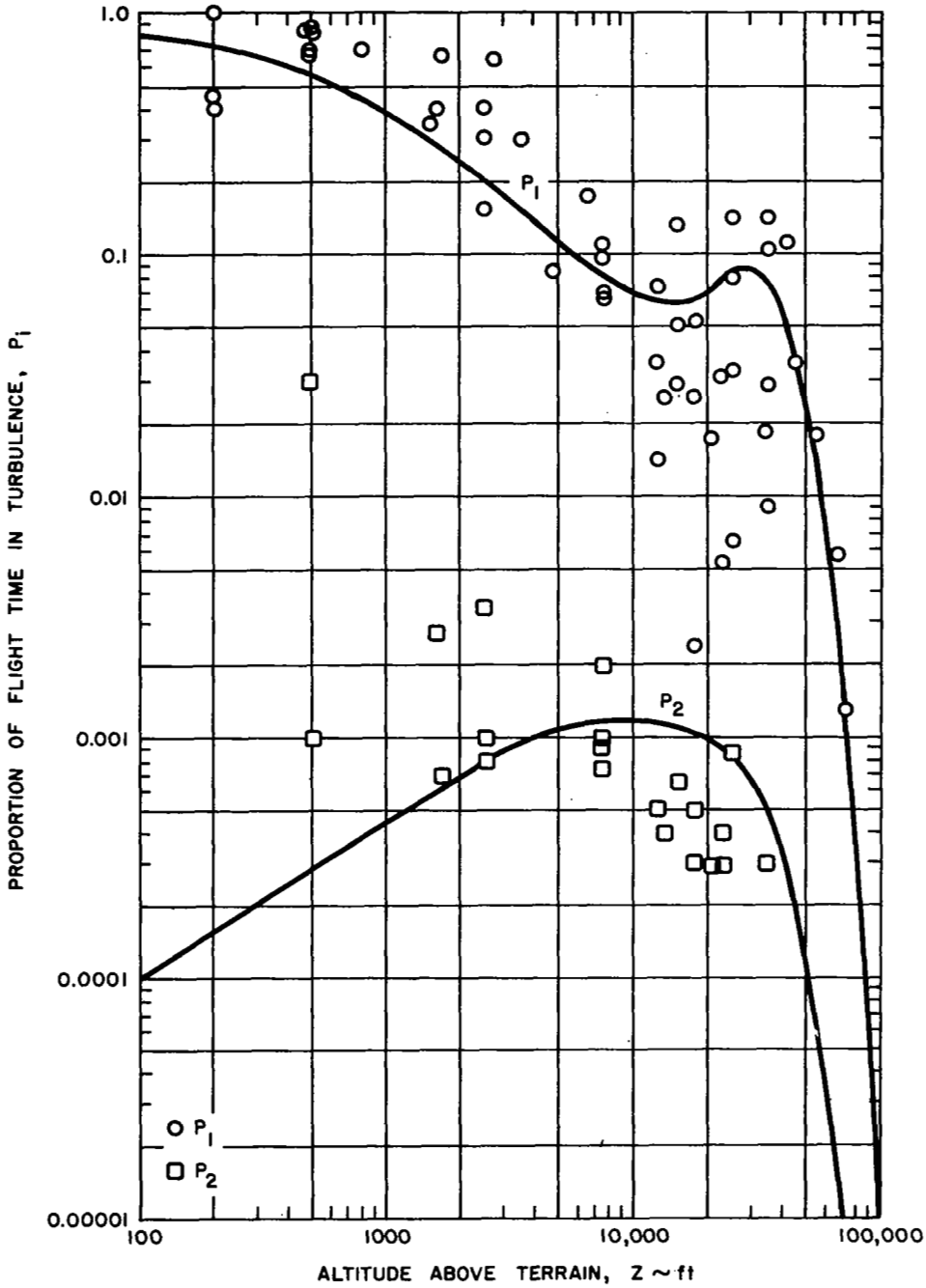

Fig. 4.3. The Proportion of Flight Distance in Atmospheric Turbulence as Functions of Altitude-Data Points (From Reference 26)

heavily on the few high-altitude data available. Therefore, to be conservative, larger values of P_1 have been selected (overestimates the vertical motion). The values selected are tabulated in Table 4.1.

Table 4.1

Turbulence Characteristics

Parameter	Pritchard Value		Value Used (Conservative)	
	70,000 ft	80,000 ft	70,000 ft	80,000 ft
L, ft	2000	2000	2000	2000
b, ft/sec	2.30	2.25	2.30	2.25
P_1	.002	.0003	.08	.08

4.3 ATMOSPHERIC TEMPERATURE

Pilots of high-speed aircraft have reported unusual experiences in which outside air temperatures suddenly increased to some much hotter value. Such temperature experiences have not been fully explained. They typically occur without warning and are not reflected in upper air data provided by the weather information system.

The temperature data reported in the Air Force HICAT program at altitudes up to 70,000 ft indicate the maximum temperature change to be about 10°C. Generally, it is only a few degrees in normal turbulence.

Because of this lack of statistical data on temperature variations, the response per degree will be computed, and the effect of the extreme variations will be examined.

4.4 ISOBARIC SURFACE

Weather circulations cause the true height of flight level altitudes to vary from one location to another so that an aircraft, following the pressure contours, may be actually climbing or descending although flight level altitudes are held constant. This behavior was noted most strikingly in early flights of the XB-70 where radar tracking indicated the aircraft to be climbing or descending while the pilot was flying a constant pressure altitude.

A review of upper air data by Thompson[28] for the 50 millibar (67,507 ft) flight level indicates that the maximum change in altitude due to these effects is about 5,000 ft per 1000 nautical miles, or 130 ft/min for an SST. These differences might be encountered in connection with the polar vortex, according to Thompson.

Again, statistical data are not available here, so this extreme case will be used to study the response. The model will assume that the pressure surface is fixed and that the contour is sinusoidal with a half-amplitude of 2500 ft and a length corresponding to one cycle per 2000 nmi.

5. ANALYSIS OF ALTIMETRY ERROR

In this section we will study the effect of altimeter system parameters on the altimetry error. We will consider as an objective, reducing the altimetry errors so vertical separations of 1000 or 2000 ft could be achievable at Mach 3.5 to about 80,000 ft. Separations of 2000 ft are now standard at subsonic jet altitudes. Providing technology for 1000-ft separations could be a research goal to meet future air traffic requirements.

Our aim here is to identify research requirements for meeting the technology requirements, not to perform detailed analyses of separation standards. Therefore, we will consider the order of magnitude of errors, not the details needed to set standards.

Calculations presented by Gracey[9] show that the collision probability for an aircraft on a vertical line to be 10^{-5} for a 3σ altimetry error of 500 ft at an assigned separation of 1000 ft, Fig. 5.1. We will interpret this result as indicating the altimetry error should be less than one-half of the vertical separation standard for standards of 1000 ft or more. We will reduce the altimetry error objective by an additional factor of two to allow for degradation of equipment during operation. Therefore the allowable altimetry error would be 250 or 500 ft for 1000 ft or 2000 ft separations, respectively.

The 3σ altimetry errors, Table 2.1, estimated by Boeing, of 365 ft for current subsonic transports and of 440-605 ft for

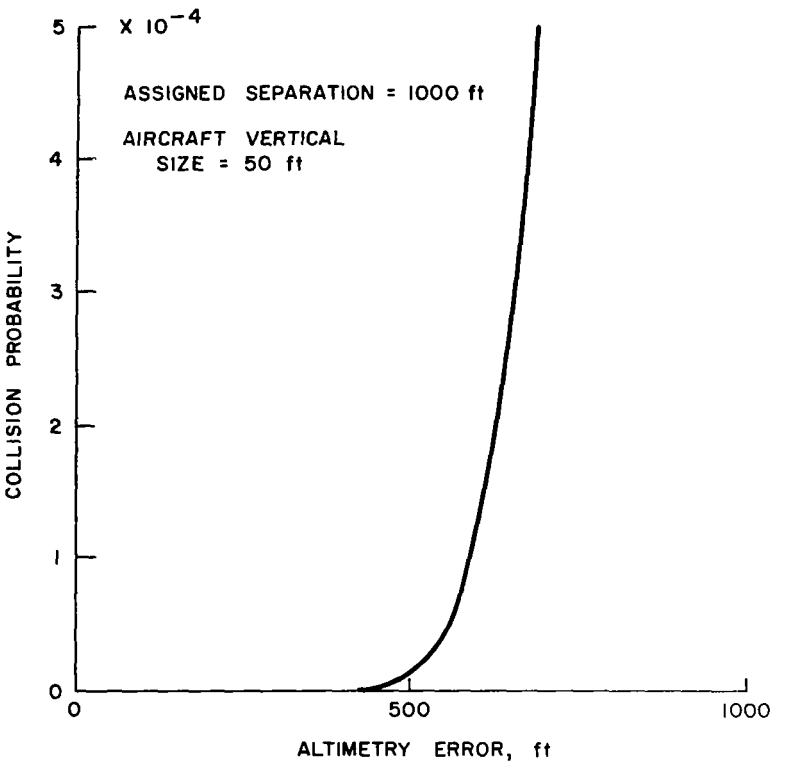

Fig. 5.1. Collision Probability Versus Altimetry Error (From Reference 9)

the Mach-2.7 SST are commensurable on this basis with the present 2000-ft standard. The Mach-2.7 aircraft error, scaled to Mach 3.5, Table 2.1 is 705-960 ft, which would require, on this basis, a 3000-4000 ft separation standard.

We consider the Mach-3.5 supersonic transport with characteristics listed in Tables 5.1, 5.2, and 5.3. It is cruising in altitude-hold at 77,800 ft at the end of the cruise leg. The aerodynamic properties have been scaled from properties of a representative Mach-2.7 transport to give a maximum lift-drag ratio.

The elevator-fixed characteristics for response to vertical turbulence are listed in Table 5.4, under $S_{\dot{\theta}} = 0$. In the presence of the atmospheric pressure gradient, the phugoid mode has a slight negative damping coefficient (-0.005) and a period of 164 seconds. The short-period mode has a 9.3 sec period. The corresponding magnitude plot of the $\Delta h/w_w$ transfer function for a sinusoidal vertical gust is shown in Fig. 5.2.

The data in Table 5.4 show that the phugoid mode is easily stabilized by the elevator servo gain, $S_{\dot{\theta}}$. The short-period mode disappears at a gain of 20, and reappears at a higher frequency for higher gain. Figure 5.2 shows the effect of the servo gain on the response. By increasing the servo gain, the response near the phugoid frequency is reduced. But, because of noise problems at high gain, the servo gain is fixed at $S_{\dot{\theta}} = 40$ sec for the remaining calculations.

TABLE 5.1

END OF CRUISE FLIGHT CONDITIONS

Flight Condition	Symbol	Units	Value
Mach number	M	–	3.5
Altitude	h_o	ft	77,800
Velocity	U_o	ft/sec	3,388
Dynamic pressure	q	psf	554
Lift/drag ratio	L/D	–	6.85

TABLE 5.2

END OF CRUISE PHYSICAL CHARACTERISTICS

Characteristics	Symbol	Units	Value
Aircraft weight	W	lb	388,200
Wing sweep	Λ	deg	76
Moment of inertia	I_y	slug-ft^2	6.25×10^7
Reference area	S	ft^2	9000
Reference chord	c	ft	192.5
Thrust offset	ϵ	deg	0.75
Thrust moment arm	ℓ_ϵ	ft	3.24
Tail moment arm	ℓ_t	ft	55

TABLE 5.3

END OF CRUISE AERODYNAMIC PROPERTIES
$M = 3.5$, $h_o = 77{,}800$ ft

C_D	0.0115	C_{z_u}	0.0595
C_{D_α}	0.0836	C_{z_α}	-0.938
C_L	0.0779	$C_{z_{\dot{\alpha}}}$	0
C_{L_α}	0.926	C_{z_q}	-0.623
$C_{L_{\delta_e}}$	0.0118	$C_{z_{\delta_e}}$	-0.0118
C_{L_M}	-0.017	C_{m_u}	-0.0035
C_{x_u}	-0.0213	C_{m_α}	-0.029
C_{x_α}	-0.0057	$C_{m_{\dot{\alpha}}}$	0.0
$C_{x_{\delta_e}}$	0.0	C_{m_q}	-0.178
		$C_{m_{\delta_e}}$	-0.00596
		C_{m_M}	-0.001

TABLE 5.4

CHARACTERISTICS OF RESPONSE TO w_w-GUST

FOR VARIOUS ELEVATOR GAINS $S_{\dot{\theta}}$

$M = 3.5$, $h_o = 77{,}800$ ft

Elevator Servo Gain, $S_{\dot{\theta}}$ Sec	Response Mode			
	Phugoid		Short-Period	
	Frequency Rad/Sec	Damping Coef.	Frequency Rad/Sec	Damping Coef.
0	0.038	-0.005	0.67	0.14
10	0.035	0.008	0.78	0.78
20	0.032	0.025	—	—
40	0.028	0.062	6.1	0.82
100	0.022	0.17	9.7	0.52
200	0.018	0.31	13.6	0.37

$$\left[\frac{\delta_e}{\theta}(s)\right] = \frac{S_{\dot{\theta}} s}{0.1s + 1}$$

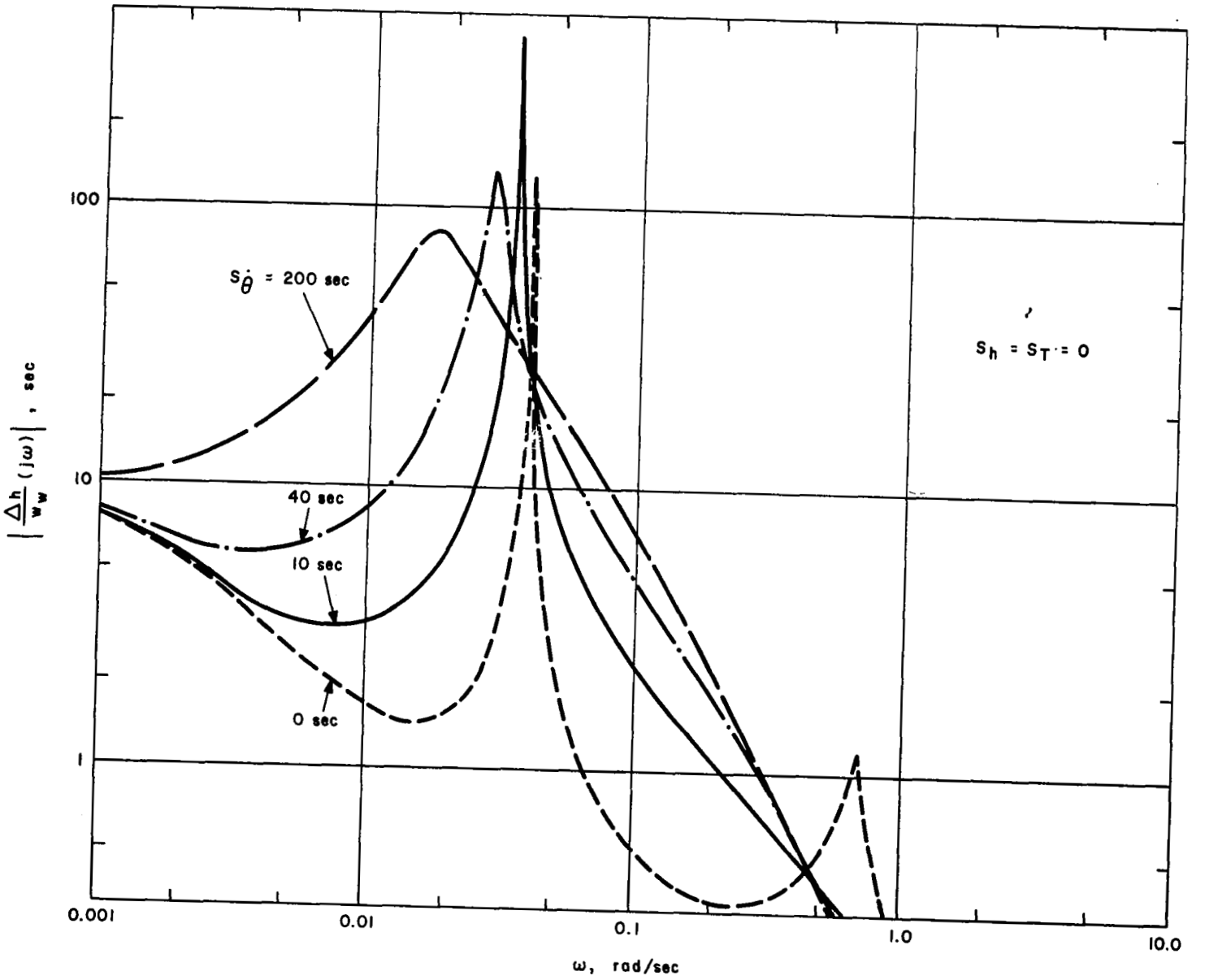

Fig. 5.2. Magnitude of $\Delta h/w_w$ Transfer Function Versus ω for $s = j\omega$ With Elevator Control Only

The magnitude of the $\Delta h/u_w$ transfer function for a longitudinal gust is shown in Fig. 5.3, with $S_{\dot{\theta}} = 40$. The 3σ height error is only 1.5 ft due to longitudinal turbulence compared to 8.5 ft due to vertical turbulence, so only the response to vertical turbulence is presented from here on.

With an uncompensated system, $K_{\delta_e} = \frac{1}{0.25s + 1}$, the damping coefficient for the phugoid mode is driven negative by extremely small values of the altimeter gain S_h. Therefore, the lead-lag compensation term

$$\frac{2s + 1}{0.25s + 1}$$

was selected from a root-locus study with a perfect altimeter in order to stabilize the phugoid mode. Additional lead compensation ($\tau_{h_2} s + 1$) is introduced in order to stabilize the short-period mode. Lead compensation of 60 sec had been used by Piggott.[8] Unfortunately, using large values of lead compensation confounds the analysis of probe lag effects, as first-order probe lag can be identically compensated by equal magnitude lead compensation.

Calculations were made to determine how far τ_{h_2} could be reduced. The results are presented in Table 5.5 for, what is called, the "nominal" hybrid system: $\tau = 10$ sec, $S_{\dot{\theta}} = 40$ sec, $\tau_e = 0.1$ sec, $\tau_{h_1} = 0.25$ sec, $\tau_{h_3} = 2.0$ sec, $\omega_n = 0.015$ rad/sec,

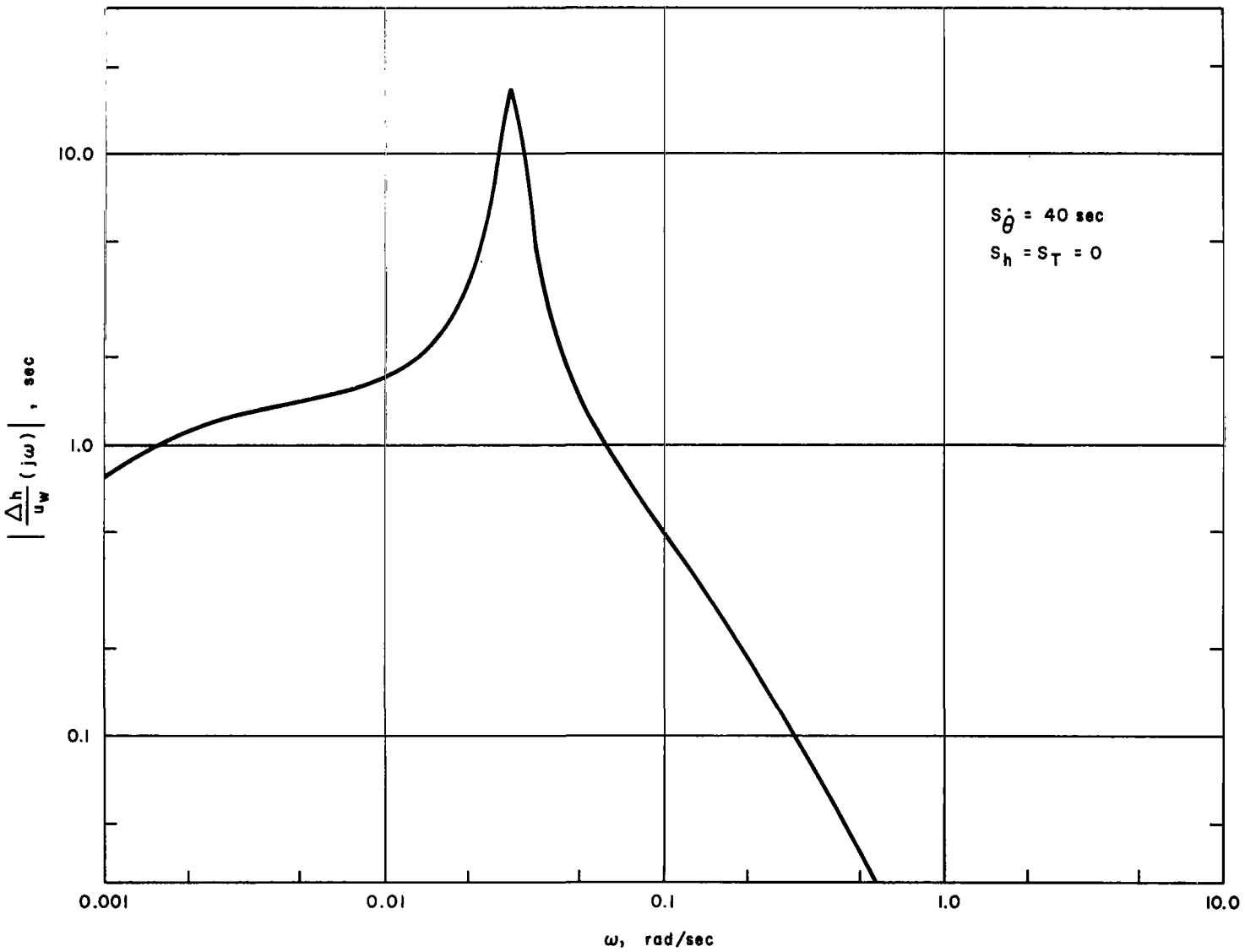

Fig. 5.3. Magnitude of $\Delta h/u_w$ Transfer Function Versus ω for $s = j\omega$ With Elevator Control Only

TABLE 5.5

CHARACTERISTICS OF RESPONSE TO w_w-GUST FOR VARIOUS VALUES OF COMPENSATION LEAD τ_{h_2}

$M = 3.5$, $h_o = 77{,}800$ ft

$\tau = 10$ sec, $S_{\dot{\theta}}^{\cdot} = 40$ sec, $\tau_c = 0.1$ sec

$\tau_{h_1} = 0.25$ sec, $\tau_{h_3} = 2.0$

$\omega_n = 0.015$, $\zeta = 0.6$

Variables		Response Mode					
Lead τ_{h_2} (Sec)	Gain S_h (Rad/ft)	Phugoid		Short Period		Mod-Short Period	
		Frequency (Rad/Sec)	Damping Coef.	Frequency (Rad/Sec)	Damping Coef.	Frequency (Rad/Sec)	Damping Coef.
0		Could not be stabilized.					
1.9	0.02	0.017	0.56	0.88	0.28	3.3	0.75
5.0	0.005	0.017	0.56	0.54	0.46	3.9	0.79
9.5	0.002	0.017	0.56	0.44	0.54	4.2	0.82

$$\left[\frac{\delta e(s)}{\Delta h(s)}\right] = S_h K_{\delta_e}(s)\, H_{\Delta h}(s)$$

$$K_{\delta_e}(s) = \frac{(\tau_{h_2} s + 1)(2s + 1)}{(0.1s + 1)(0.25s + 1)}$$

$$H_{\Delta h}(s) = \frac{0.15\bar{s}^3 + \bar{s}^2 + 1.2\bar{s} + 1}{(\bar{s}^2 + 1.2\bar{s} + 1)(10s + 1)}$$

and $\zeta = 0.6$. The gain S_h is varied to keep the damping of the phugoid and modified-short period modes essentially constant. The result is the short-period mode is divergent for $\tau_{h_2} = 0$ sec. For $\tau_{h_2} = 1.9$ sec, the short-period mode is damped to 0.28, so the value 1.9 sec is used hereon for this compensation, giving

$$K_{\delta_e}(s) = \frac{(1.9s + 1)(2s + 1)}{(0.1s + 1)(0.25s + 1)}$$

for all further calculations. The magnitude of the $\Delta h/w_w$ transfer function for a perfect altimeter ($\tau = 0$, $\omega_n = \infty$) with this compensation is shown in Fig. 5.4. Two modes remain, at 0.89 and 3.3 rad/sec, having damping coefficients of 0.27 and 0.75, respectively. The 3σ height deviation for vertical turbulence is tabulated in Table 5.6, and for a perfect altimeter it is only 0.26 ft.

The response with a barometric system is computed by setting $\omega_n = \infty$. It turns out that the barometric system is stable only for very small values of S_h. Presumably, the compensation could be altered to admit larger values of S_h, but this would add another variable to the study. The magnitude of the $\Delta h/w_w$ transfer function is shown in Fig. 5.5. The response here differs only slightly from the response with the rate gyro alone. The height deviation due to vertical turbulence, Table 5.6, is 9.6 and 8.9 ft. This is negligible.

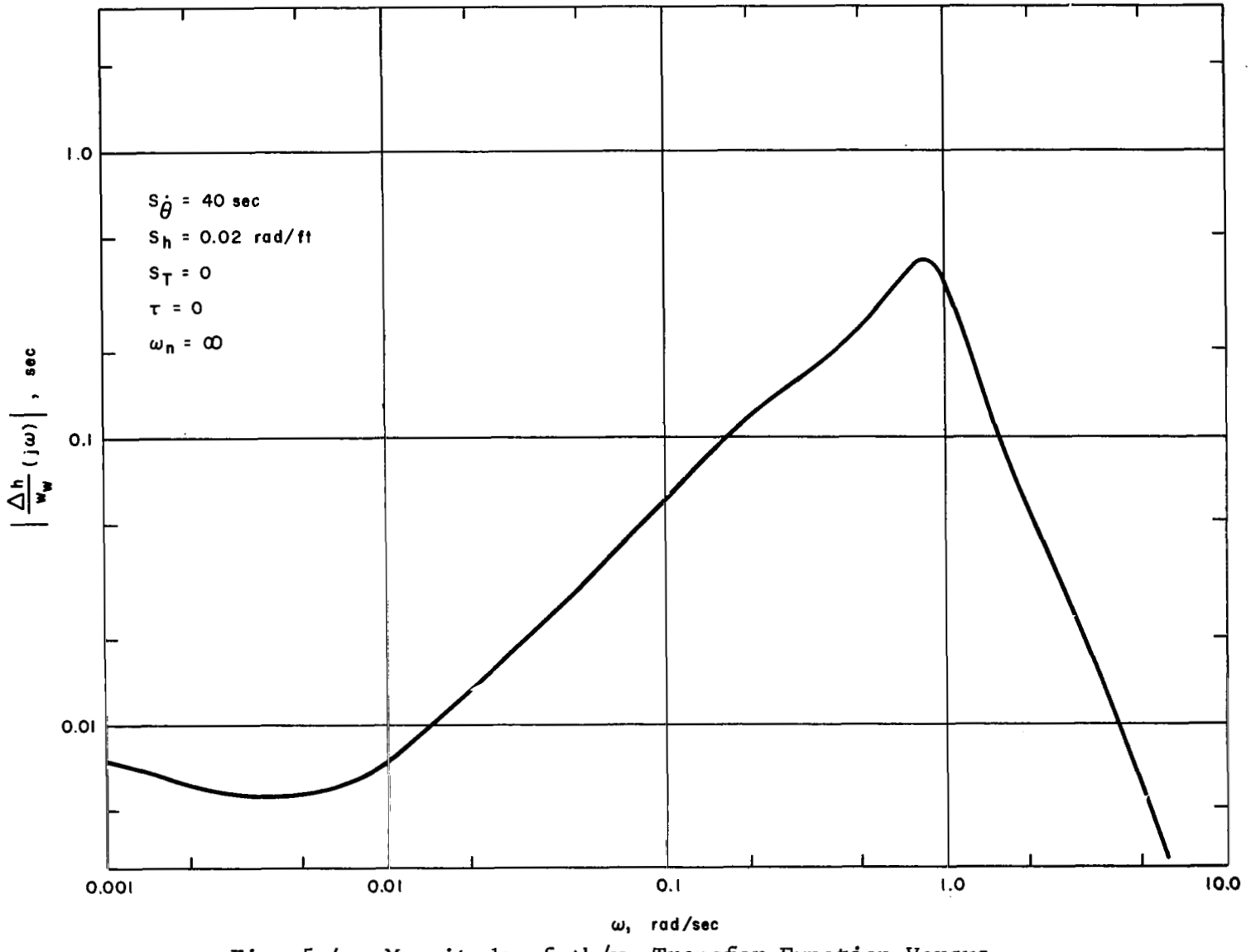

Fig. 5.4. Magnitude of $\Delta h/w_w$ Transfer Function Versus ω for $s = j\omega$ With Perfect Altimeter

TABLE 5.6

ALTIMETRY ERRORS

$M = 3.5$, $h_o = 77{,}800$ ft

τ (Sec)	$S_{\dot{\theta}}$ (Sec)	S_h (Rad/ft)	ω_n (Rad/sec)	ζ	$3\sigma_{\Delta h(w_w)}$ (ft)	$\frac{\sigma_{\Delta h(\theta)}}{\sigma_\theta}$ (ft/°C)	$\Delta h(\Delta h_I)$ (ft) $\Delta h_I = 2500$ ft
Elevator Control Only							
–	40	0	–	–	8.5	10.0	32
Perfect Altimeter							
0	40	0.02	∞	–	0.26	0.24	0.03
Barometric Altimeter							
1	40	10^{-5}	∞	–	9.6	10.5	21
10	40	10^{-6}	∞	–	8.9	10.2	30
Hybrid Altimeter							
0	40	0.02	0.015	0.6	0.25	0.24	63
3	40	0.02	0.05	0.6	0.24	0.24	5.7
10	40	0.02	0.015	0.6	0.25	0.24	63
10	40	0.02	0.05	0.6	0.24	0.24	5.7
30	40	0.02	0.005	0.6	0.25	0.24	580
30	40	0.02	0.015	0.6	0.25	0.24	63

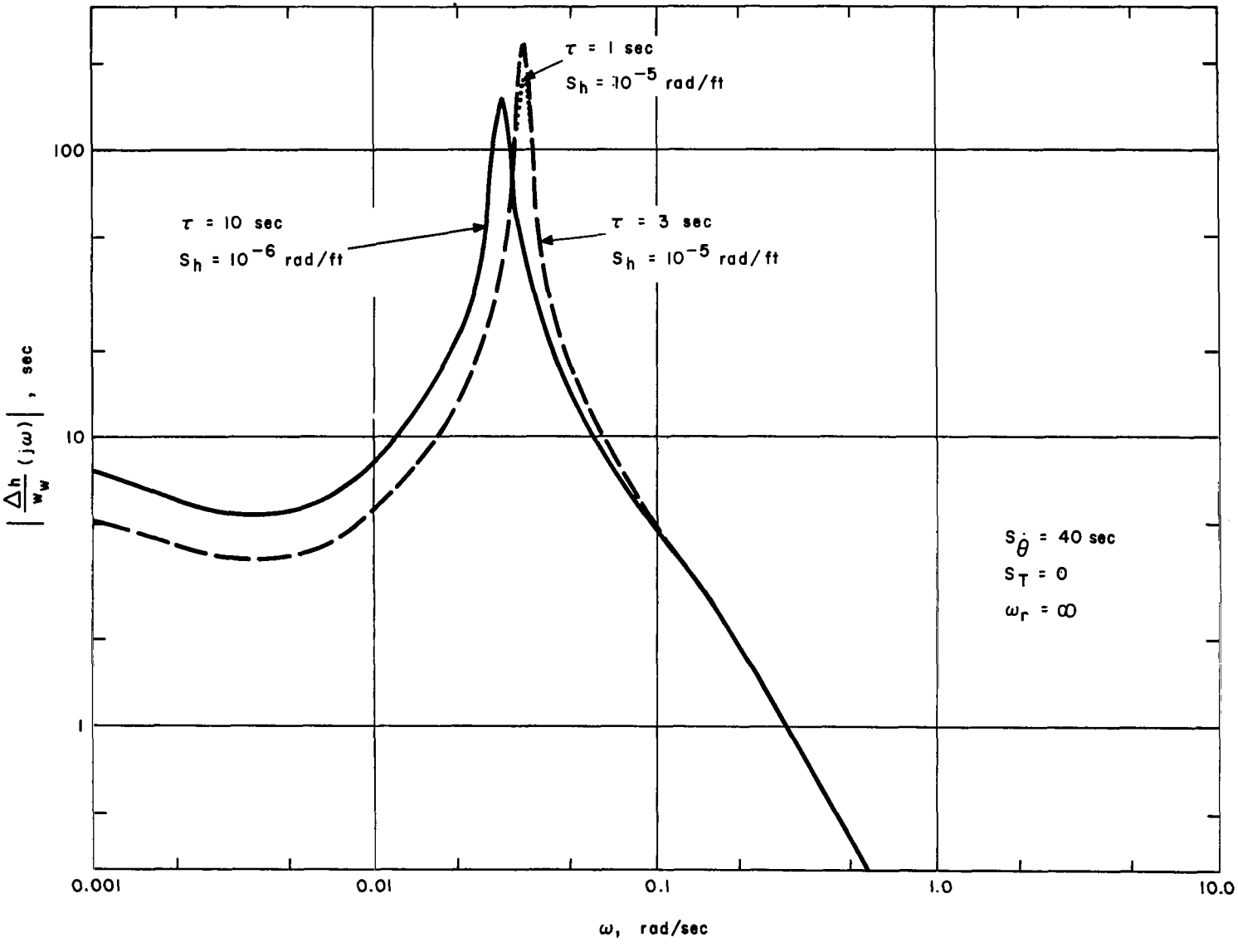

Fig. 5.5. Magnitude of $\Delta h/w_w$ Transfer Function Versus ω for $s = j\omega$ With Barometric Altimeter

Because the response with the barometric system is essentially the same as for the rate gyro alone, the barometric system is not fully utilized. Calculations have shown that the barometer can be used with higher gain if the lead compensation is increased. Increased lead compensation increases the error due to noise in the system. So, the fact that it is necessary to increase the lead compensation for the barometric system beyond the values for the hybrid system, indicates that the hybrid system has value in reducing noise problems. However, a thorough analysis of noise effects on a barometric system is beyond the scope of this study.

An extensive series of calculations have been performed to select a desirable combination of servo gain and altimeter gain. The stability boundaries for the gains are presented in Fig. 5.6 for τ = 10 sec, ω_n = 0.015 rad/sec, and ζ = 0.6. At a fixed value of the servo gain, the short-period mode is divergent for low altimeter gains, and the modified-short period mode is divergent for high altimeter gains. At $S_{\dot{\theta}}$ = 40 sec, a gain of S_h = 0.02 rad/ft provides a good compromise between the values of the damping coefficients of the short-period mode and the modified-short period mode.

The effect of the filter gain, ω_n, on the response is shown in Table 5.7, for τ = 10 sec. The filter gain governs the weighting of the signals from the inertial and barometric systems — increasing the gain weights the barometric signal more heavily,

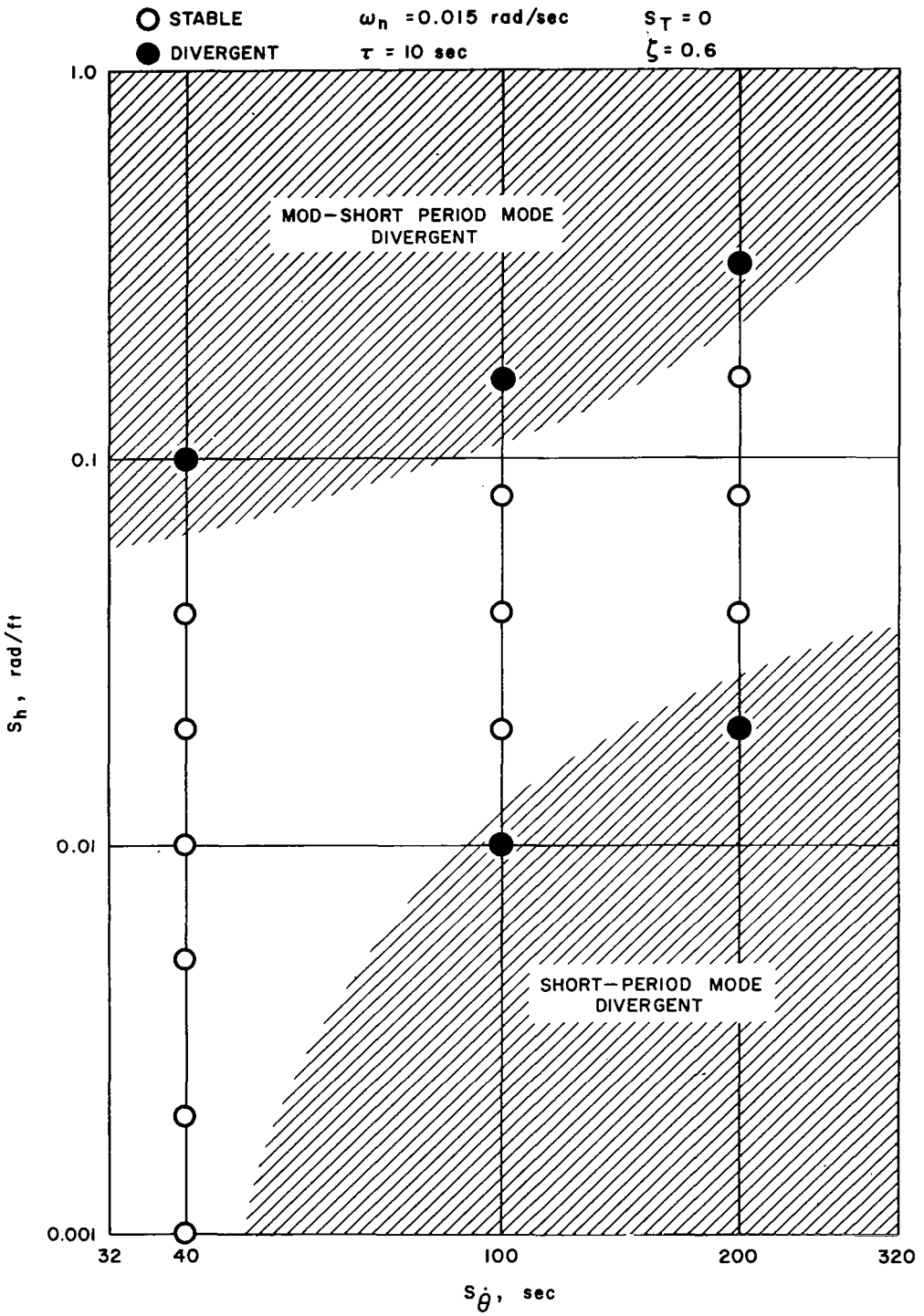

Fig. 5.6. Stability Boundaries for Gains of Hybrid Altimeter

TABLE 5.7

CHARACTERISTICS OF RESPONSE TO w_w-GUST FOR VARIOUS HYBRID SYSTEM FILTER GAINS ω_n

$M = 3.5$, $h_o = 77{,}800$ ft

$\tau = 10$ sec, $S_{\dot{\theta}} = 40$ sec, $S_h = 0.02$ rad/ft, $\zeta = 0.6$

$\tau_{h_1} = 0.25$ sec, $\tau_{h_2} = 1.9$ sec, $\tau_{h_3} = 2.0$ sec

Filter Gain ω_n	Response Mode					
	Phugoid		Short Period		Mod-Short Period	
	Frequency (Rad/Sec)	Damping Coef.	Frequency (Rad/Sec)	Damping Coef.	Frequency (Rad/Sec)	Damping Coef.
0	–	–	0.88	0.27	3.3	0.75
0.015	0.017	0.56	0.88	0.28	3.3	0.75
0.050	0.061	0.27	0.88	0.32	3.3	0.74
0.150	0.140	-0.07	0.87	0.44	3.3	0.73

$$\left[\frac{\delta_e(s)}{\Delta h(s)}\right] = S_h K_{\delta_e}(s)\, H_{\Delta h}(s)$$

$$K_{\delta_e}(s) = \frac{(1.9s + 1)(2s + 1)}{(0.1s + 1)(0.25s + 1)}$$

$$H_{\Delta h}(s) = \frac{10\bar{s}^3 + \bar{s}^2 + (1.2 - \frac{0.00003}{\omega_n})\bar{s} + 1}{(\bar{s}^2 + 1.2\bar{s} + 1)(10s + 1)}$$

$$\bar{s} = \frac{s}{\omega_n}$$

and reducing the gain weights the inertial signal more. For $\omega_n = 0$, the phugoid mode is completely eliminated; but, it will be seen, there are other problems at low values of ω_n. The inertial signal is needed to damp the phugoid. At $\omega_n = 0.15$ rad/sec, the phugoid is divergent. The other two modes are relatively unaffected by the filter gain.

The occurrence of oscillatory divergence of the phugoid mode depends essentially upon the value of the product $\tau\omega_n$. The approximate location of the stability boundary in τ, ω_n coordinates is shown in Fig. 5.7. For the 6 examples plotted in these coordinates, 5 are stable and 1 is divergent. At $\tau = 10$ sec, the boundary of the stable region lies somewhere between the point at $\omega_n = 0.05$, for which the phugoid oscillation is stable, and $\omega_n = 0.15$, for which it is divergent. The stability boundary has been taken as the line $\tau\omega_n = 1.0$. To provide phugoid oscillatory stability, ω_n should be made small enough to be well below the divergent zone.

On the other hand, it was shown in Section 2.4 that small values of ω_n can produce large altimetry errors (the barometric system signal would be too small). For example, to allow 1000-ft separations, it is desirable to keep the error due to the vertical acceleration measurement to the order of 100 ft. The relationship between the altitude error and ω_n is indicated by the hatched areas in Fig. 5.7, as a function of $(u)\ddot{h}_i$. Representative values of $(u)\ddot{h}_i$ are tabulated in Table 2.4. The location of

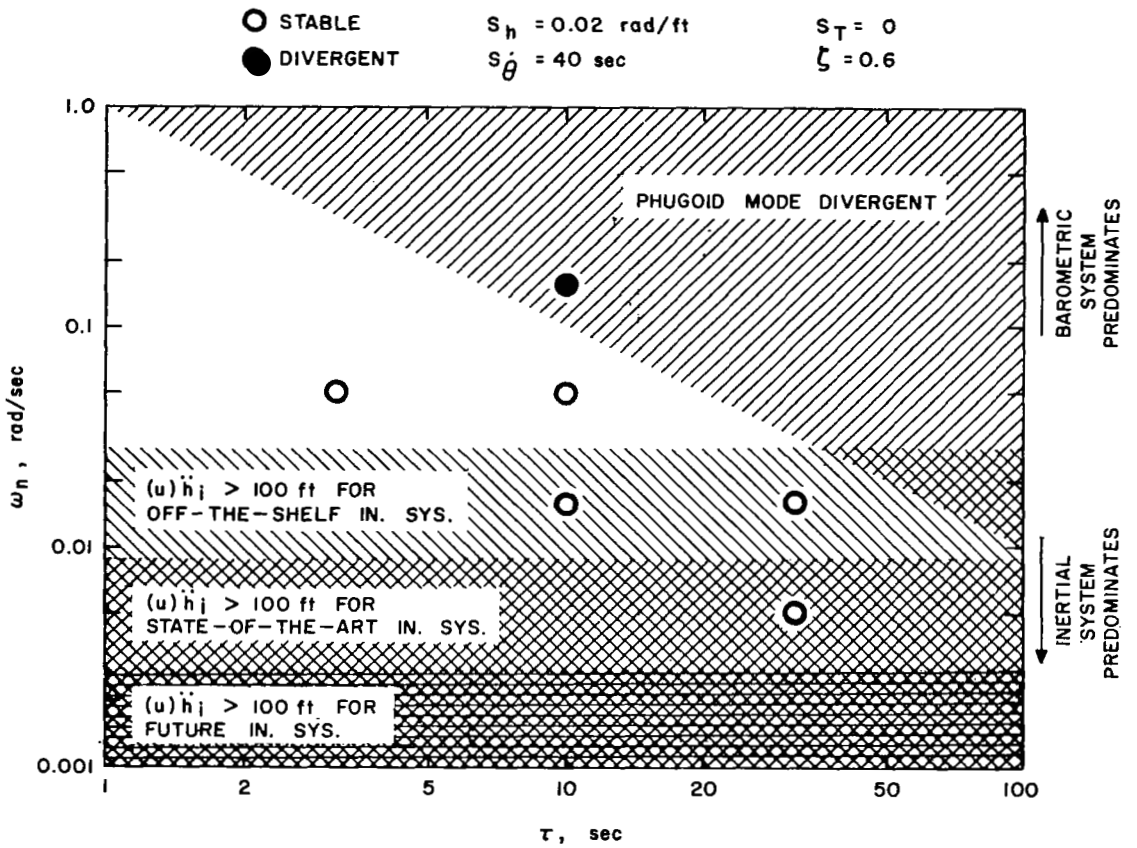

Fig. 5.7. Stability Boundary for Filter Gain of Hybrid Altimeter

the boundary for various accuracies of an inertial system is also shown in Fig. 5.7.

Figure 5.7 shows that the gain ω_n must be kept within a triangular zone bounded on the high side by phugoid mode divergence and on the low side by vertical accelerometer error. For τ = 30 sec and an off-the-shelf inertial system, there is no latitude in the selection of ω_n; in fact, for τ = 30 sec, it would be impractical to keep the vertical error to 100 ft without going to a state of the art system. For τ = 10 sec, there is some latitude in the selection of ω_n with an off-the-shelf system, but with the vertical error so sensitive to ω_n, Fig. 2.4-3, a state of the art system might prove more satisfactory. For τ less than 10 seconds, it appears that an off-the-shelf inertial system would admit obtaining a reasonably small vertical error.

The magnitude of the $\Delta h/w_w$ transfer function for the hybrid inertial-barometric altimeter is shown in Fig. 5.8. Four values of the probe lag are used: τ = 0, 3, 10, and 30 sec. The filter gain is varied from ω_n = 0.005 to 0.05 rad/sec, depending upon τ. The elevator servo gain $S_{\dot{\theta}}$ and altimeter gain S_h are 40 sec and 0.02 rad/ft, respectively. The magnitude of the vertical deviation due to vertical turbulence is tabulated in Table 5.6.

The striking result is that the response with the hybrid altimeter is essentially independent of the probe lag for the whole range of probe lag from 0 to 30 seconds. The gain ω_n must be reduced for large values of τ, to preserve phugoid mode stability, but otherwise the effect of probe lag is negligible.

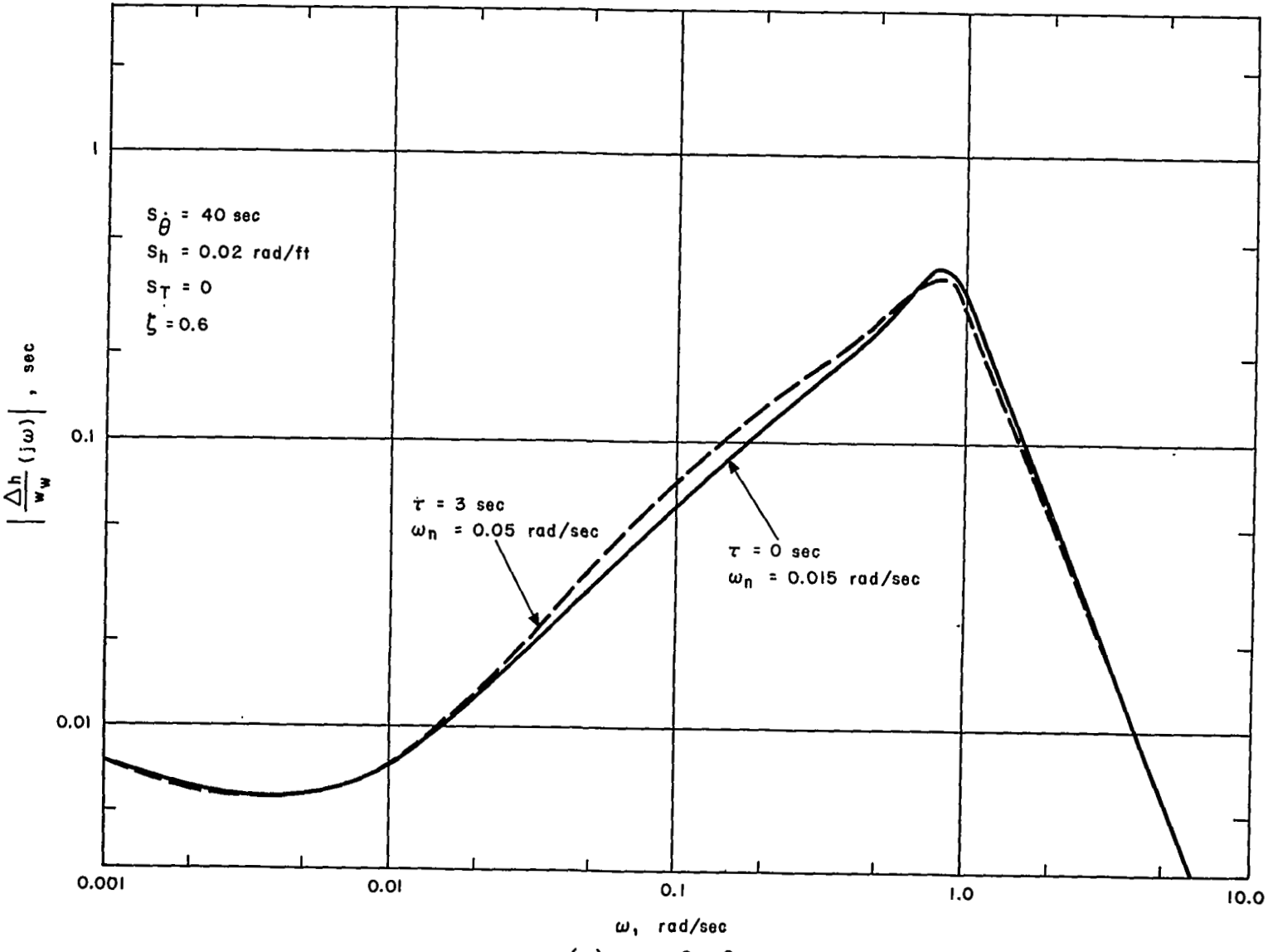

(a) τ = 0, 3 sec

Fig. 5.8. Magnitude of $\Delta h/w_W$ Transfer Function Versus ω for $s = j\omega$ With Hybrid Altimeter

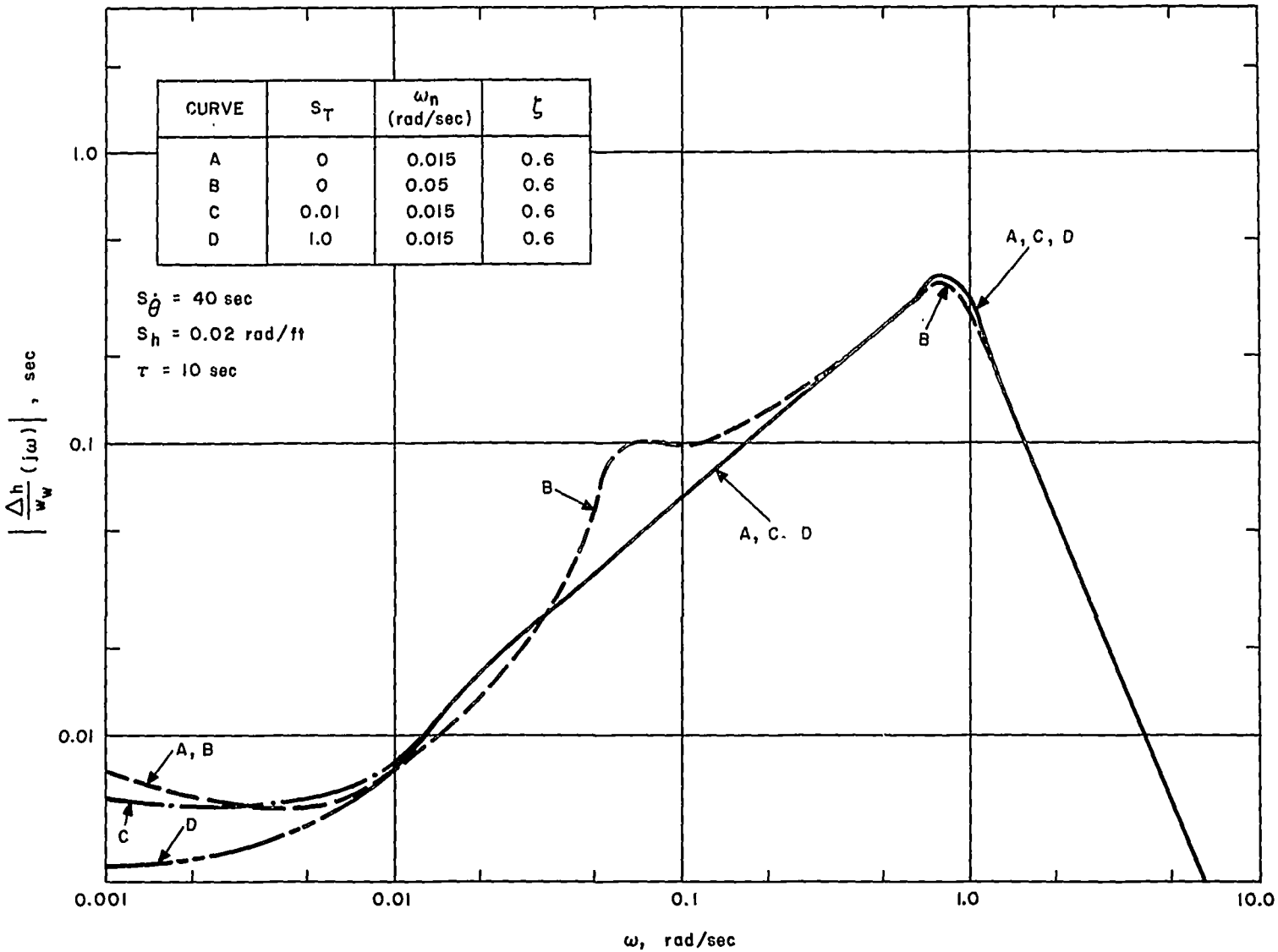

(b) τ = 10 sec

Fig. 5.8. Magnitude of $\Delta h/w_w$ Transfer Function Versus ω for $s = j\omega$ With Hybrid Altimeter (Cont.)

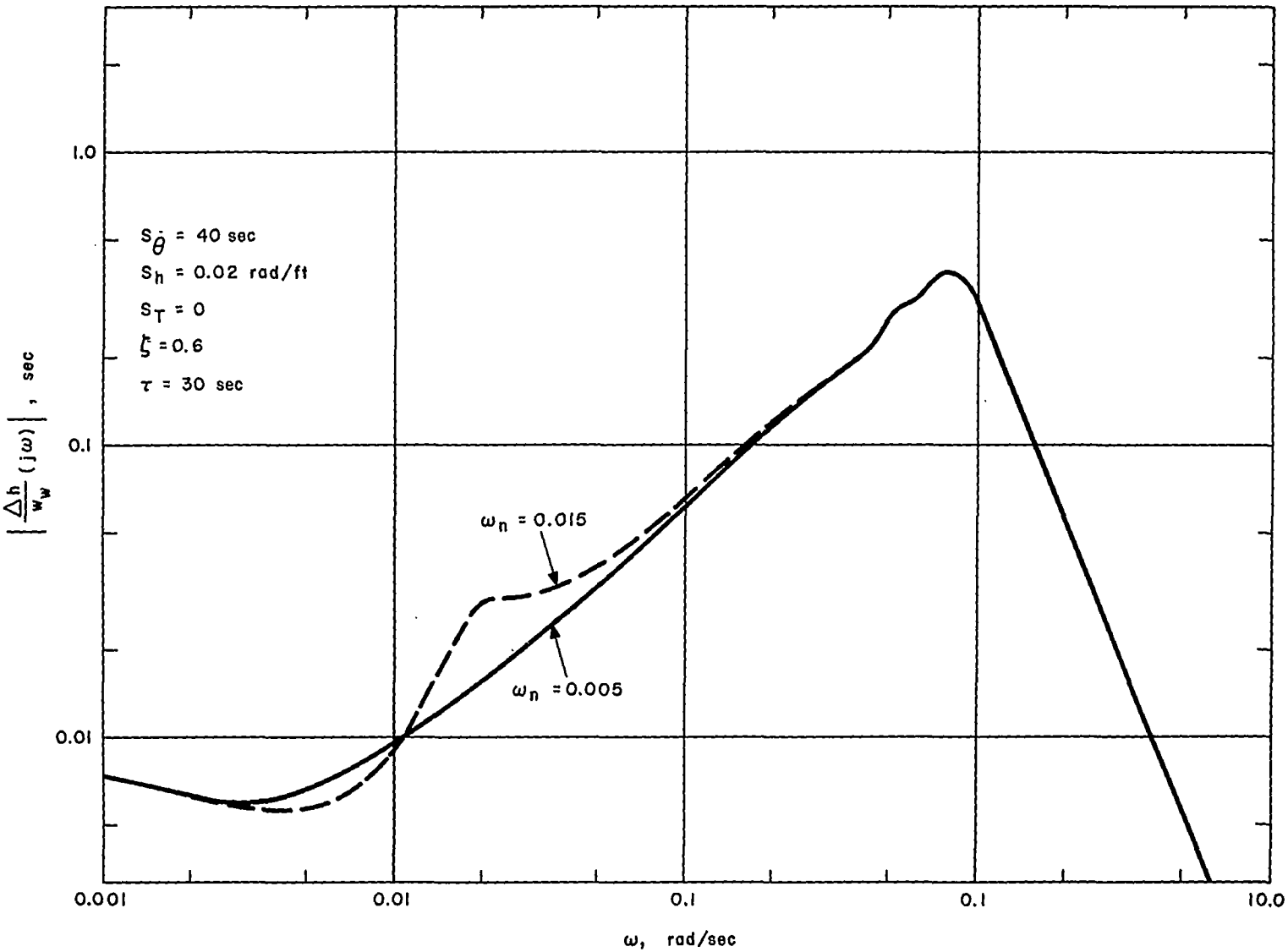

(c) τ = 30 sec

Fig. 5.8. Magnitude of $\Delta h/w_w$ Transfer Function Versus ω for $s = j\omega$ With Hybrid Altimeter (Cont.)

The effect of the engine thrust control is shown in Fig. 5.8b. Three values of engine thrust are studied: $S_T = 0$, 0.01, and 1.0; the response is divergent for larger values of S_T. One set of thrust compensation parameters was employed: $\tau_{T_1} = 50$ sec, $\tau_{T_2} = 10$ sec, and an engine lag $\tau_E = 8$ sec, and a throttle lag $\tau_t = 0.15$ seconds, giving

$$K_T(s) = \frac{(50s + 1)(10s + 1)}{(8s + 1)(0.15s + 1)}$$

The engine thrust control only affects the response at the extremely low frequencies, where it reduces the response. But the response is so small at these frequencies, that thrust control was not employed in the calculations of response to vertical wind.

The effect of filter gain ω_n on the response with the hybrid altimeter is shown in Fig. 5.8b and c. The response of the phugoid mode increases with increasing ω_n. In other words, the inertial system reduces the amplitude of the phugoid mode. For $\tau = 10$ sec, $\omega_n = 0.15$ rad/sec, and for $\tau = 30$ sec, $\omega_n = 0.05$ rad/sec, the phugoid mode is divergent.

The 3σ altitude deviation, Table 5.6, is about 0.24 ft for non-divergent cases with the hybrid altimeter, which is negligible. The altitude deviation has been reduced by a factor of about 40 using the hybrid altimeter, nearly two orders of magnitude, from the deviation for the barometric system. Furthermore, there are no sharp peaks in the response curve as a function of frequency.

To facilitate further comparison, representative curves of vertical gust response from Figures 5.2, 5.4, 5.5 and 5.8 are combined into Figure 5.9. The effect of the hybrid altimeter in the control system is to reduce the gust response of the system below about 0.5 rad/sec almost to the same low curve as achieved by a perfect altimeter. The effect of adding thrust control to the hybrid system is virtually negligible and is not included here.

The magnitude of the transfer function $\Delta h/\Theta$ due to atmospheric temperature variations is presented in Fig. 5.10 - 5.13, and the altitude deviation due to "white" temperature variations (equal amplitude at all frequencies) is tabulated in Table 5.6. The speed of sound of air has been computed from temperature assuming air to be a perfect gas. Figure 5.10 shows that the height deviation can be quite large at the slow variations of the phugoid frequency, ranging from about 10 to 1000 ft/^{o}C. During B70 and U2 flights at these high altitudes, temperature variations of 5-10^{o}C have been experienced, and difficulty was experienced in maintaining altitude.[1] Figure 5.10 shows the large magnitude of response that can occur for a system with elevator control only.

With the perfect altimeter, Fig. 5.11, the altitude variations due to temperature are reduced significantly. The altitude deviation is reduced to 0.24 ft/^{o}C. But the deviation with the barometric system, Fig. 5.12, is greater than 100 ft/^{o}C at the phugoid frequency; it is 10.2 to 10.5 ft/^{o}C for "white" temperature variations.

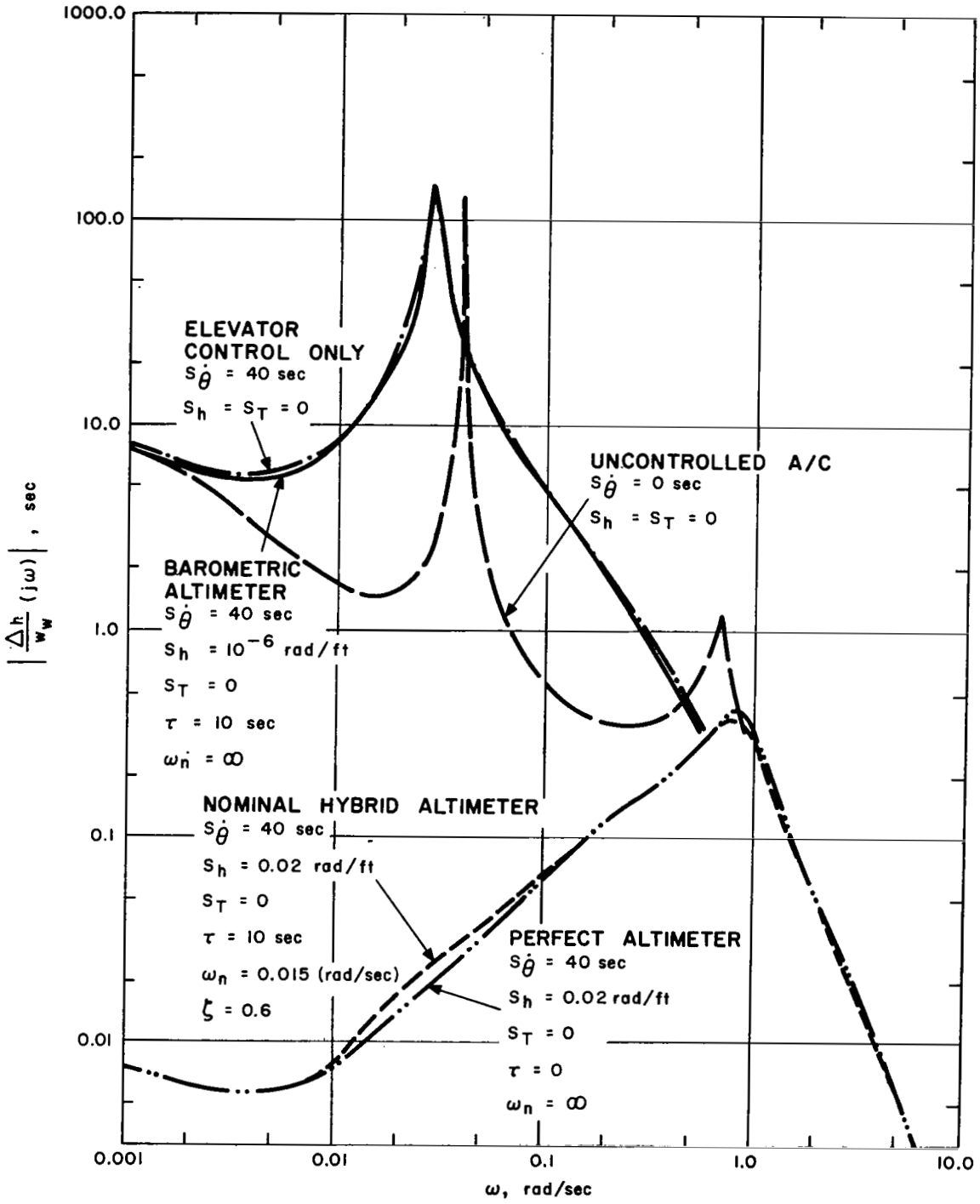

Fig. 5.9. Combination of Vertical Gust Response Bode Plots for Several Altitude Control Systems

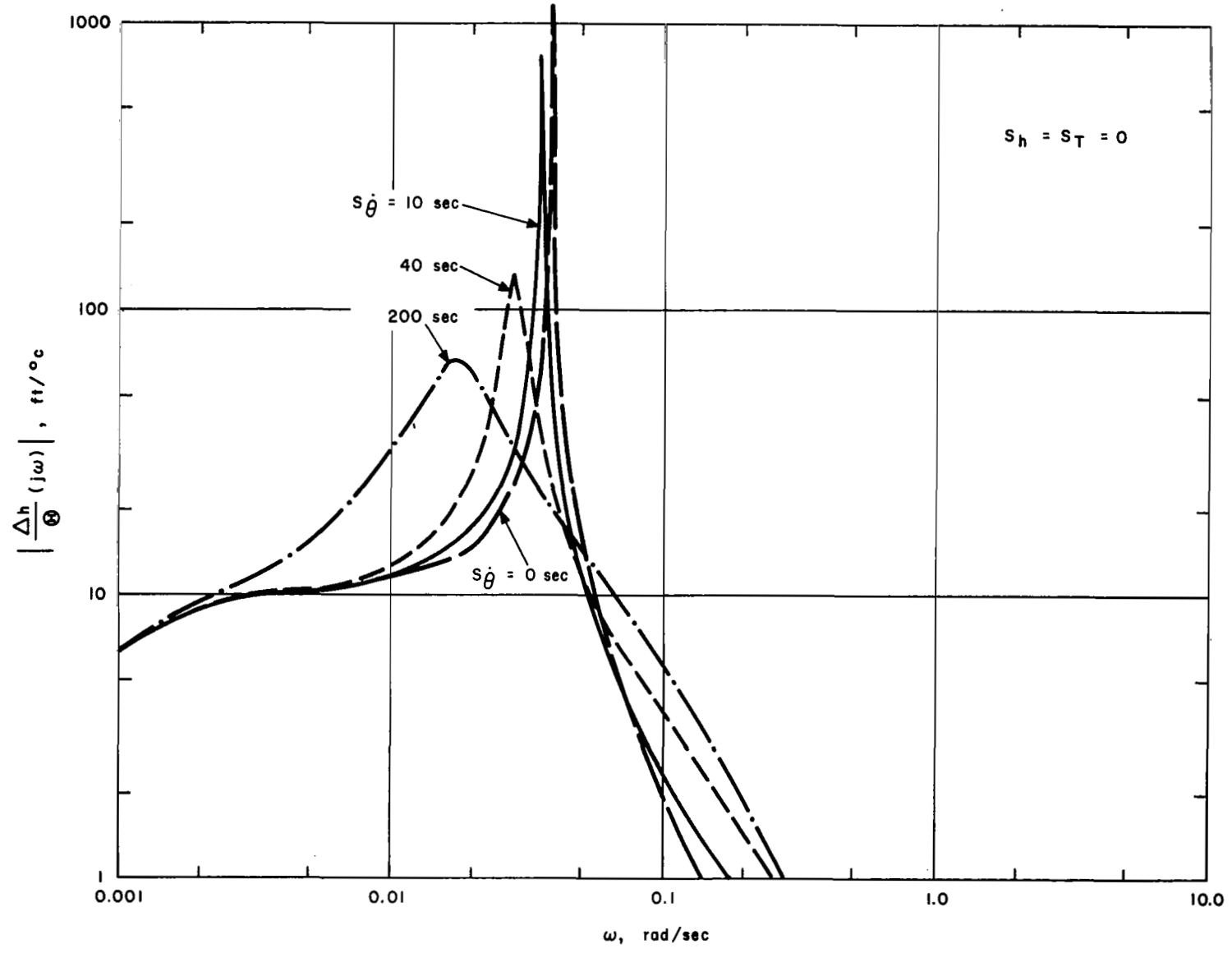

Fig. 5.10. Magnitude of $\Delta h/\theta$ Transfer Function Versus ω for $s = j\omega$ With Elevator Control Only

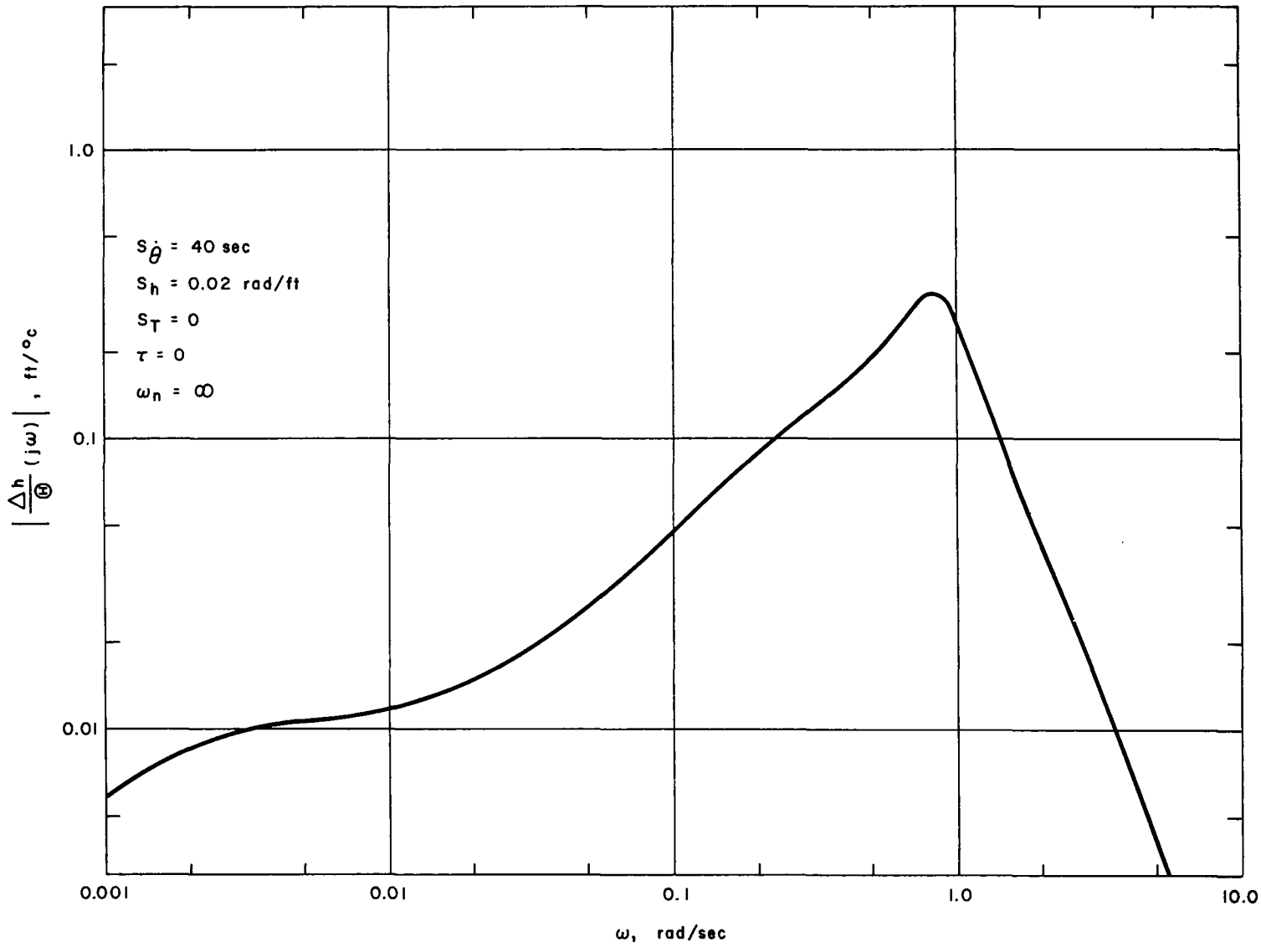

Fig. 5.11. Magnitude of $\Delta h/\theta$ Transfer Function Versus ω for $s = j\omega$ With Perfect Altimeter

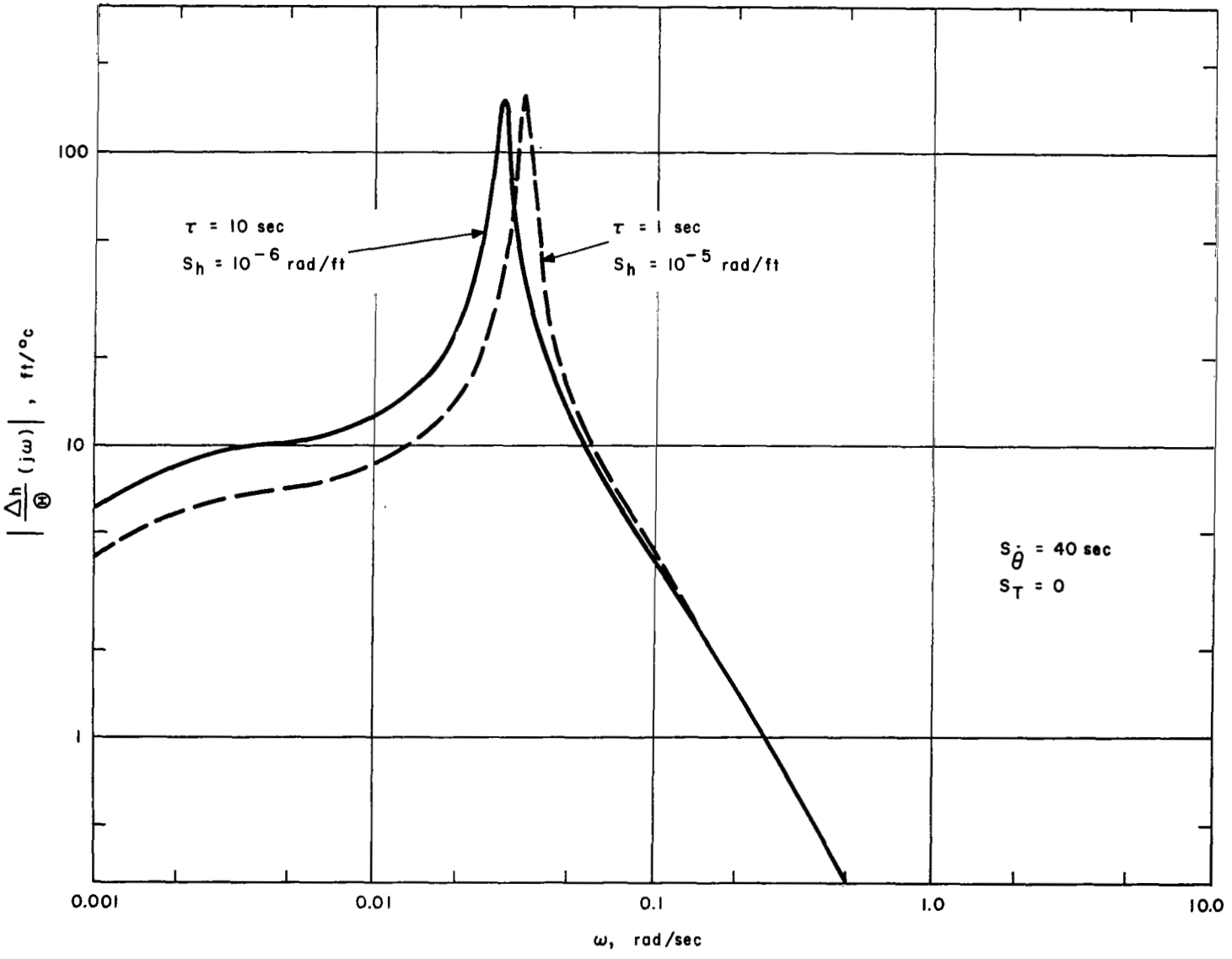

Fig. 5.12. Magnitude of $\Delta h/\theta$ Transfer Function Versus ω for $s = j\omega$ With Barometric Altimeter

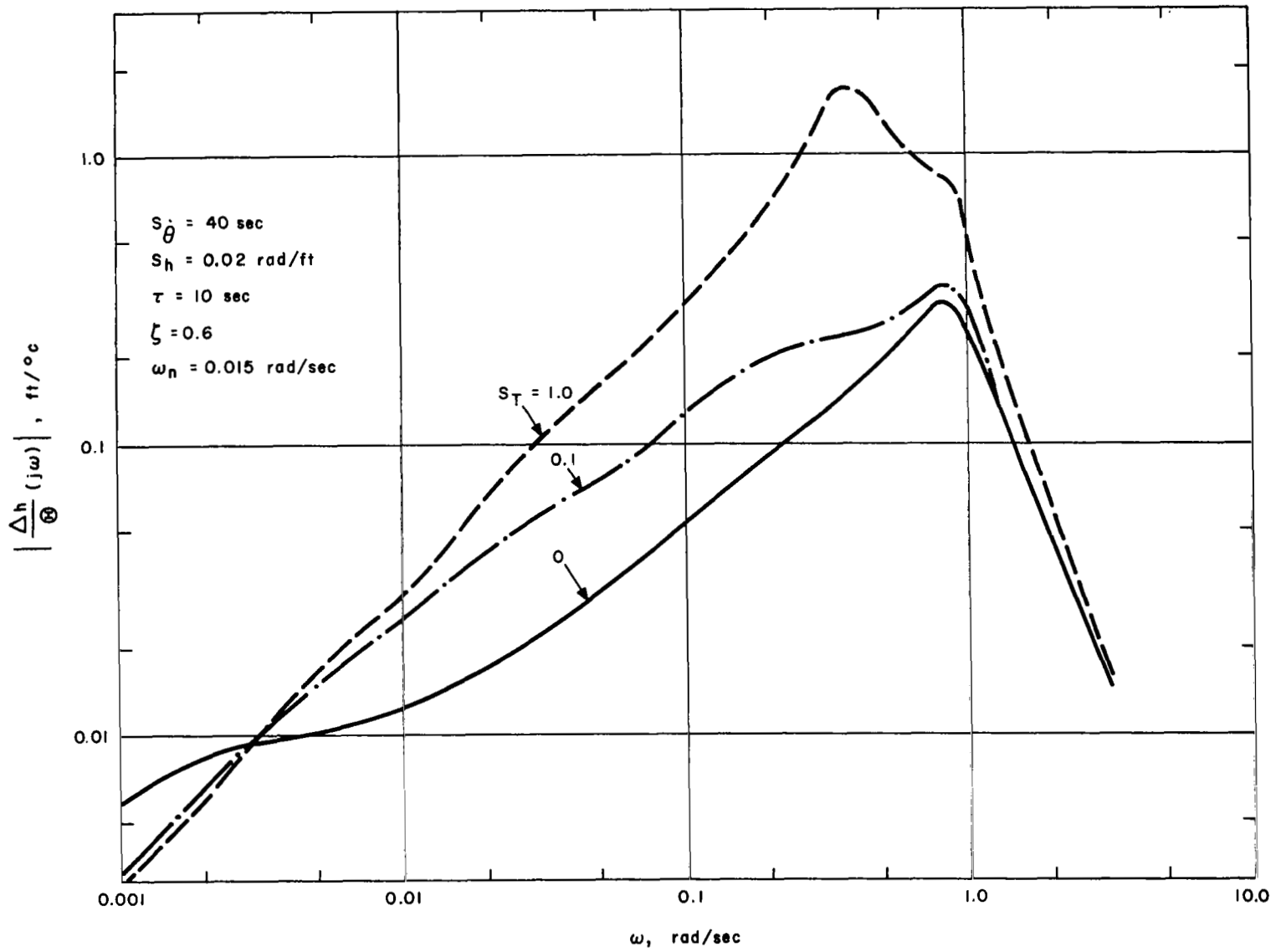

Fig. 5.13. Magnitude of $\Delta h/\theta$ Transfer Function Versus ω for $s = j\omega$ With Hybrid Altimeter

The response due to temperature variations with the hybrid system is shown in Fig. 5.13. The response is reduced orders of magnitude in the phugoid range, the sensitive range, from the response with the barometric system. The response to "white" temperature variations is essentially the same as for the perfect altimeter, 0.24 ft/^{o}C, which is negligible.

Adding thrust control to the hybrid altimeter system increases the altimetry errors for temperature variations of frequencies greater than about 0.003 rad/sec, Fig. 5.13. For a thrust gain S_T = 1.0, the largest magnitude of the transfer function $\Delta h/\theta$ is only 3 ft/^{o}C, which is not large. But the frequency is so high, that Mach number control would not be a concern. At the low frequencies where Mach number control might be desired, such as for $\omega_n < 0.01$ rad/sec, the response is negligible.

Representative temperature response curves from Figures 5.10-5.13 are combined into Figure 5.14 for ease of comparison. The effect of the hybrid control system is to reduce remarkably the temperature response of the system below about 0.5 rad/sec to virtually the same as achieved by a perfect altimeter. The effect of adding thrust control to the hybrid system is to increase temperature response throughout most of the range of interest; the resulting temperature response below about 0.2 rad/sec is, however, still superior to that for the systems not having the hybrid altimeter.

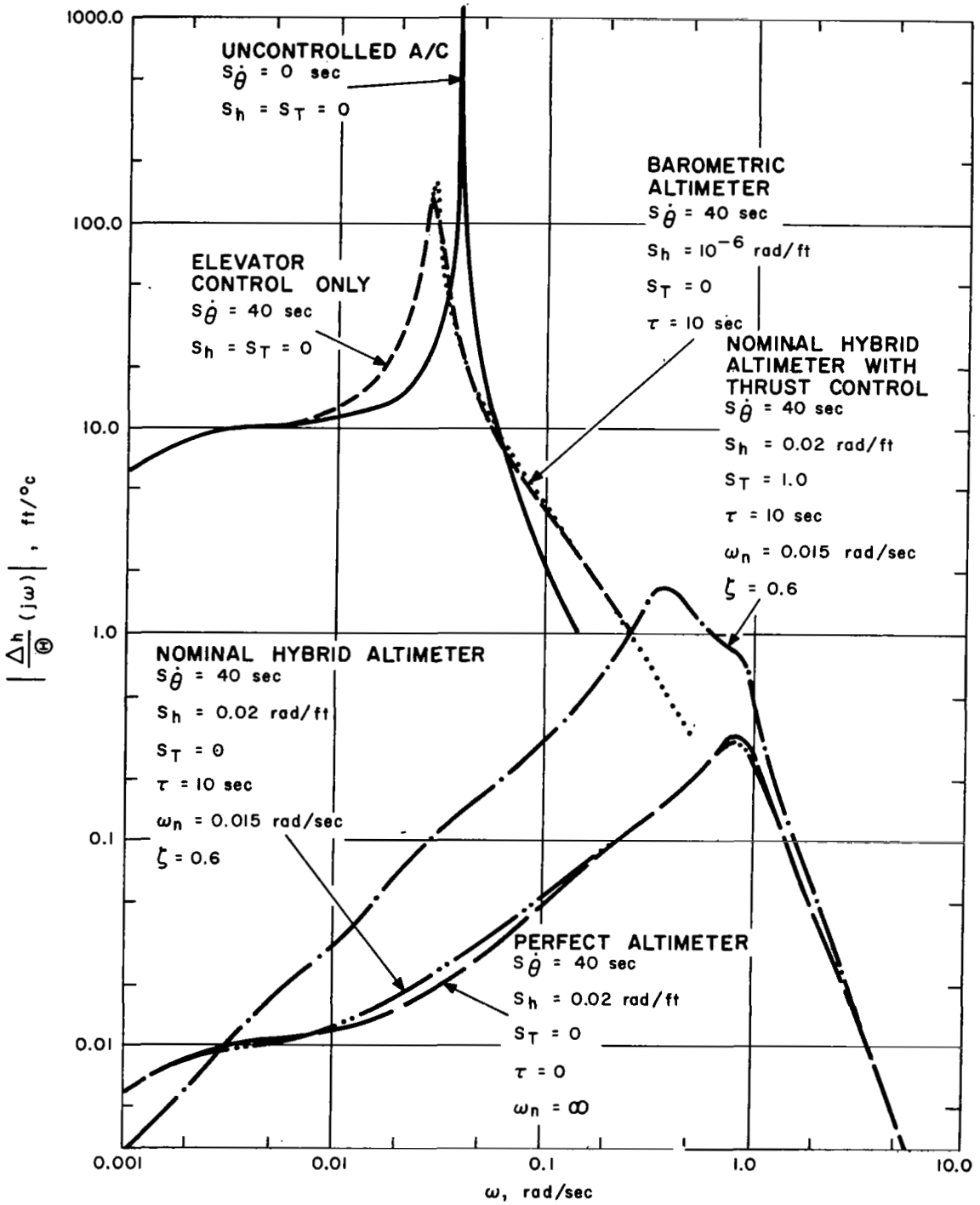

Fig. 5.14. Combination of Temperature Change Response Bode Plots for Several Altitude Control Systems

The maximum height errors due to variations in the height of the isobaric surface Δh_I are tabulated in Table 5.6. The extreme example given in Sec. 4.4 is used - a sinusoidal variation of ±2500 ft amplitude and a 2000 nmi wavelength. With the barometric altimeter, the maximum deviation from the isobaric surface is 21 to 30 ft. For the hybrid altimeter, the error depends upon the filter gain ω_n, being inversely proportional to the square of ω_n. With ω_n = 0.015 rad/sec, the maximum deviation is only 62.5 ft, but with 0.005 rad/sec it is 580 ft. This is due to the large amount of inertial system signal – the inertial system tends to hold a constant tape-line altitude instead of following the isobaric surface.

We will now examine the effect of errors in the altimeter system components. For the barometric system only static errors, not frequency dependent, are known. The errors are tabulated in Table 2.2. The instrument and static pressure errors for current systems are both too large. The instrument error of 240 ft projected for future systems is probably acceptable for 2000-ft separations, but it would need to be halved for 1000-ft separations. The static-pressure error of 800 ft projected for future systems would have to be cut to one-third for 2000-ft separations, an order of magnitude improvement over current operational equipment. The error would need to be halved again for 1000-ft separations.

The accuracy requirements of the inertial system are discussed relative to Fig. 5.15, which shows the effect of inertial system error on altimetry error at low frequencies. A "low cost" system, having a 3σ error of 0.02 g's is limited to a filter gain ω_n of 0.06 or more for a 200-ft height error. This means τ must be 10 sec or less for phugoid stability, Fig. 5.7. An off-the-shelf system, having 0.002-g accuracy, with $\omega_n = 0.03$ would allow 1000-ft separations for τ up to about 10 sec. However, due to practical problems, it may be advantageous to use a state-of-the-art inertial system if τ is as large as 10 see Fig. 5.7.

If the probe response time τ is 30 sec, phugoid stability requires $\omega_n = 0.015$ or more. A state-of-the-art system, 0.00025-g accuracy, would be required. A system of this accuracy should meet 1000-ft separation requirements satisfactorily.

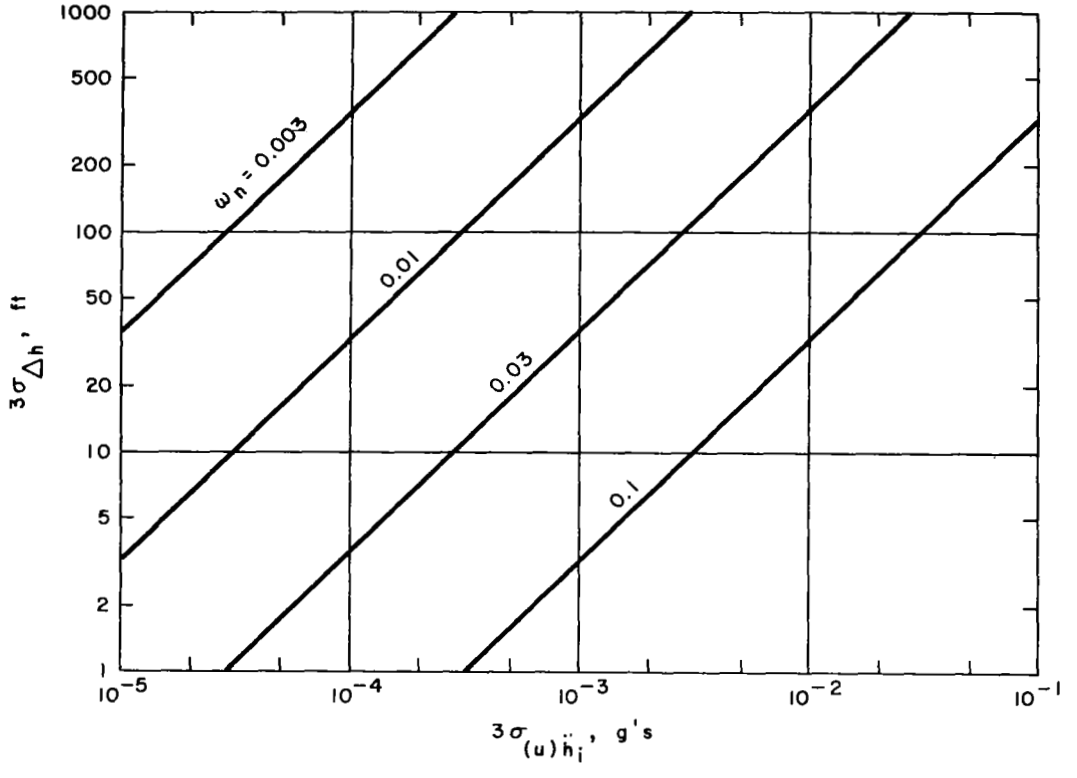

Fig. 5.15. Effect of Inertial System Error on Altimetry Error

6. CONCLUSIONS

We have represented a Mach-3.5 supersonic transport flying in altitude hold at 77,800 ft as a linear system subjected to atmospheric effects of turbulence, temperature variation, and variation of isobaric surface height. A hybrid inertial-barometric altimeter with a second-order filter is represented as a linear system providing control input to the autopilot for elevator rate control. The effects of barometric system errors and inertial system errors are modeled on a steady-state basis. Simple rate-gyro control and barometric altimeter control become limiting cases.

The static-pressure error of the barometric system must be reduced nearly an order of magnitude from the estimated 2000-ft (3σ) error of present operational systems in order to meet 2000-ft vertical separation requirements, and halved again for 1000-ft separations. Accuracies projected for barometric altimeters for next-generation supersonic transports would allow 3000-4000 ft vertical separations for a Mach-3.5 transport. The static pressure error appears to be much greater than the other errors of the hybrid system.

With a probe lag of 10 sec. or less, an off-the-shelf inertial system, having 3σ accuracy of 0.002 g's, would provide ample accuracy for a hybrid altimeter.

The computed height deviations due to turbulence or "white" temperature variations are acceptably small for all the altimeters. The deviations for the hybrid altimeter are smaller than for the barometric system by a factor of about 40. However, the barometric system could experience large deviations in flying through oscillatory gust or temperature variations near the phugoid frequency, such as waves in the atmosphere, whereas the hybrid altimeter has negligible deviations at all frequencies.

The autopilot plays an important role in the study. The lead and lag compensation gains of the altimeter system were restricted to 2 sec or less to enable the effects of probe lag greater than 2 sec to be studied. The hybrid altimeter performed very well under this restriction. However, for the barometric altimeter, the phugoid mode became unstable for relatively small amounts of control gain. The response was as good with the hybrid altimeter as with the perfect altimeter. The response was limited only by the compensation employed.

Further analysis of the barometric altimeter would be worthwhile. The barometric system appears to need more compensation to remove the large response near the phugoid frequency. But this requires an analysis of noise effects associated with increasing the lead gain. Therefore, although the response of the barometric system was not nearly as good as for the hybrid system, it cannot be said that the response of the barometric system is necessarily poor. This requires further study.

There appears to be no problem in following the height variations of the isobaric surface with the hybrid altimeter, except, perhaps, if the probe lag is as large as 30 seconds. In this case, additional deviations of 500 ft or more might be experienced due to inertial system accelerometer uncertainty.

Improved data on long wavelength turbulence, updrafts, waves, atmospheric temperature variation, and isobaric surface variations could be useful in evaluating altimetry at extremely high altitudes. However, the lack of atmospheric data does not appear to be critical to an evaluation of the inertial barometric system.

Data on the lag of pressure systems at supersonic speeds is needed. At such high stagnation temperatures ($860^{o}F$ at Mach 3.5), it may be difficult to meet pressure measurement accuracy requirements without compromising probe lag.

The encouraging results given by this analysis for a hybrid altimetry system require verification by flight tests. For example, Piggott[8] analyzed height keeping errors of aircraft due to atmospheric turbulence for a perfect altimeter, and he found that the measured altitude errors for subsonic jets in cruise are greater than the predicted errors by about two orders of magnitude. In the present analysis, the additional effects of barometric system static errors and lag and inertial system errors have been included in the analysis, as well as atmospheric temperature and pressure effects. But it remains to be demonstrated that all of the principal factors involved in altimetry at supersonic speeds and extremely high altitudes have been accounted for adequately.

Appendix A

NATURE OF VERTICAL SEPARATION PROBLEM

Based on SST fleet projections for the 1990 time period (Ref. 28), the traffic congestion on North Atlantic routes at SST altitudes would be similar to the congestion currently experienced by jet aircraft.

Present-day jet aircraft experience performance penalties with 2000-ft vertical separations. Various values have been discussed for vertical separation requirements at SST altitudes, of which 5000 feet is representative.

Projecting the current enroute congestion to the SST air traffic, let us examine the performance problem for typical SST flight. Figure A-1 presents the specific range (nmi/lb fuel) for an SST on intercontinental missions, as a function of altitude and total aircraft weight. These curves were obtained from information prepared by Boeing for the B2707-100 design and presented in Reference 29. The specific range characteristics will change as the design of the Boeing SST is modified. But the effect of the vertical separation standards on the performance should be typified by the effects illustrated here.

In Figures A-1a and b, the specific-range history is shown for two hypothetical missions operating under either 2,000-ft or 5,000-ft separation standards. We will consider

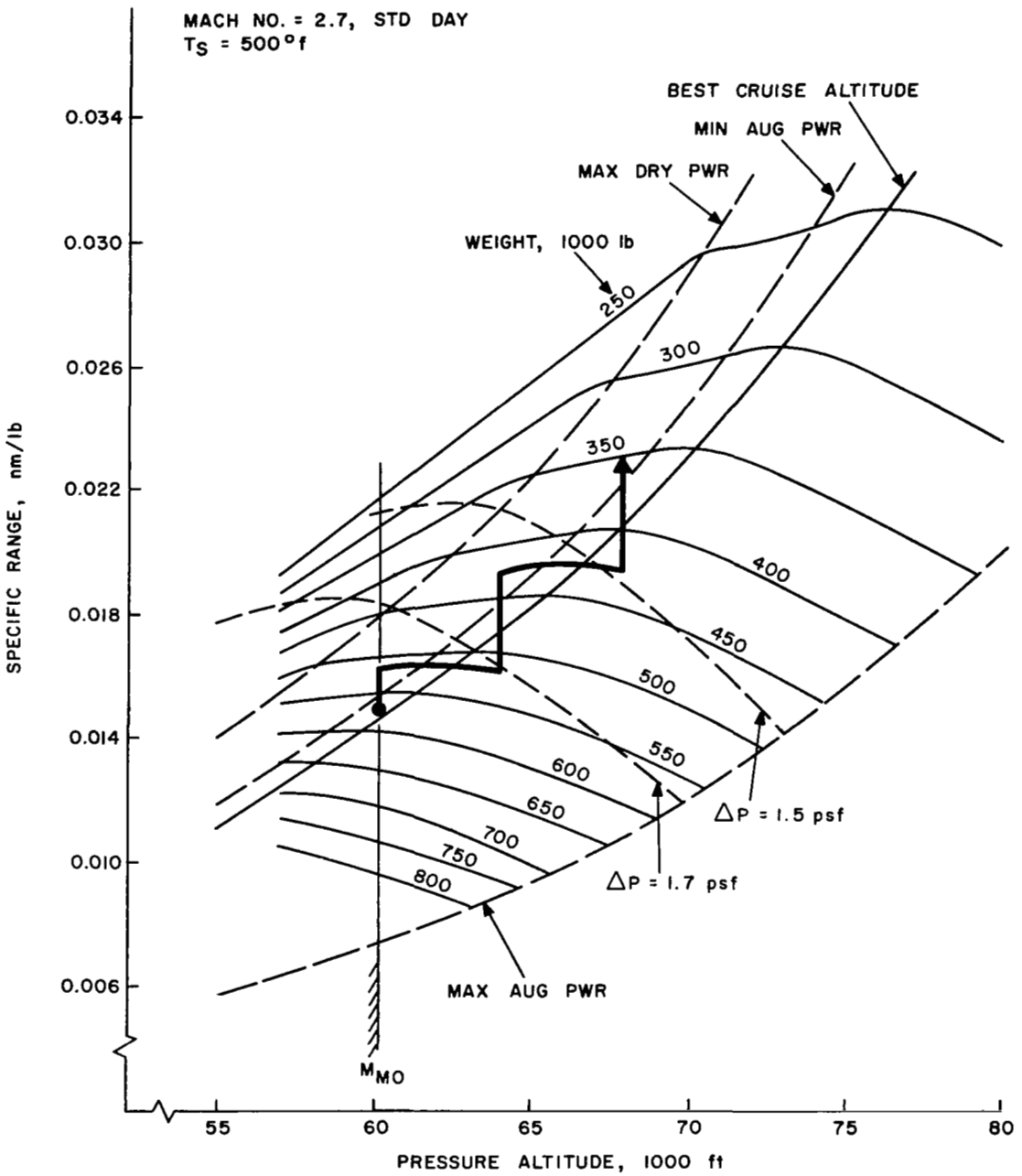

(a) 2000-ft Separation Standard With No Boom Restriction

Fig. A.1. Supersonic Aircraft Specific Range Profiles for Two Vertical Separation Standards

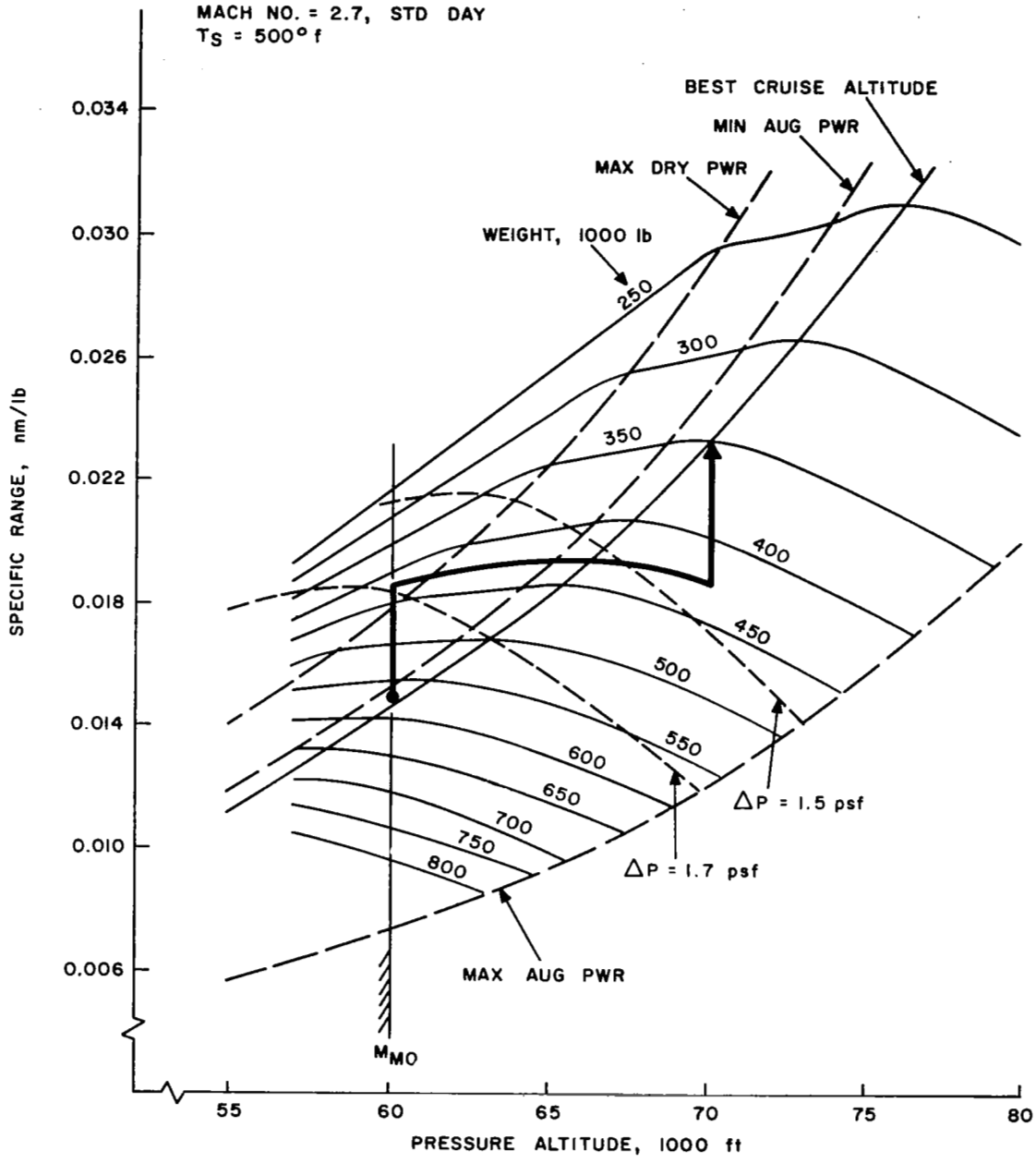

(b) 5000-ft Separation Standard With No Boom Restriction

Fig. A.1. Supersonic Aircraft Specific Range Profiles for Two Vertical Separation Standards (Cont.)

alternate flight levels starting at 60,000 ft, which, for argument sake, will be designated as "eastbound." Between alternate eastbound flight levels would be interspersed alternate "westbound" flight levels. The problems would be similar for aircraft using westbound flight levels, differing only in details, so we will restrict our attention to the eastbound aircraft. The aircraft is assumed to have a taxi weight of 675,000 lbs. It reaches the cruise altitude with a weight of about 570,000 lbs. To simplify the performance analysis, only the fuel consumed in level flight will be computed, and not the fuel consumed in climbing between flight levels.

Figures A-1a and b show the specific range history for aircraft initially cleared for supersonic cruise at 60,000 ft and having no cruise restriction on sonic boom. The sonic boom at sea level would be 1.88 psf. Initially at cruise, the aircraft are at the best cruise altitude. As the fuel is consumed the specific range decreases. The aircraft would continue at 60,000 ft until the specific range at the next higher eastbound altitude would be as favorable. At this time, the aircraft operating under the 2,000-ft separation standard, Figure A-1a, would, hopefully, be cleared for 64,000 ft, etc. The aircraft operating under the 5,000-ft separation standard would continue further at 60,000-ft flight level until the specific range matches the value at 70,000 ft, at which time it would, desirably, be cleared to 70,000 ft.

The cruise performance for the 2,000-ft and 5,000-ft separations is compared in Figure A-2. Here the fuel consumed in best-cruise-altitude flight is taken as a standard, and the additional fuel required for the layered flight levels is plotted. It is seen here that considerably more fuel is burned with the 5,000-ft separation standard than with the 2,000-ft standard. If, in addition, a sonic boom restriction of 1.7 psf is placed on intercontinental cruise conditions, the fuel penalty can become extremely high for the 5,000-ft separation standard. The penalty on the 2,000-ft separation standard with 1.7 psf boom restriction is much less severe.

The improvement in the specific range with the reduced separation is quite clear. And, of course, the assumption has been made that air space is available when desired. If it is not available, as often happens at present for jet aircraft, then the additional fuel required goes up much faster with 5,000-ft separations.

This brief exercise illustrates the penalties that might be expected with 5000-ft separation standards at SST altitudes. The penalties could become higher if aircraft are forced by congestion to fly even further off optimum altitude.

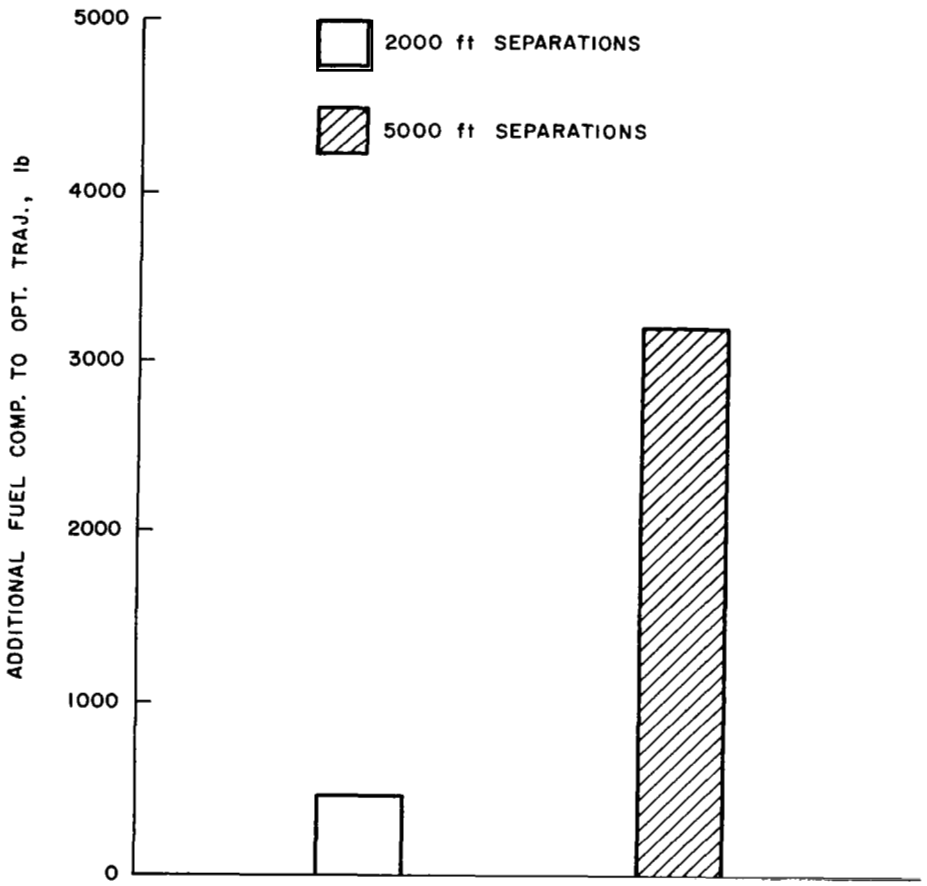

Fig. A.2. Effect of Vertical Separation Standard on Fuel Requirements for Representative Transport During Supersonic Cruise in Layered Flight Levels (No Boom Restrictions)

Appendix B

GRAVITATIONAL FIELD COMPENSATION

As was mentioned in Section 2.3, the measurement of the vertical acceleration of the aircraft requires an independent calculation of the vertical component of the Earth's gravitational field (see Eq. 2.29). This calculation requires an estimate of altitude, which will be called $\tilde{h}$. There are three choices of quantities that can be used for $\tilde{h}$: the inertially derived altitude, h_i; the barometrically derived value, h_b; or the hybrid system indication, $\hat{h}_b$. We will now examine the selection.

The use of inertially derived altitude is unsatisfactory because of the exponential growth of error shown in Section 2.3 (Eq. 2.33). The use of $\hat{h}_b$ introduces altimeter system instability for choices of the filter natural frequency that allow $\omega_n \leq 2\omega_s^2$. The use of h_b for gravity compensation allows any choice of ω_n as far as the altimeter system stability is concerned. Based on altimeter system stability considerations alone, h_b appears to be the logical choice for gravity compensation calculations.

On the other hand, since $\hat{h}_b$ combines the low frequency characteristics of the barometric system with the high frequency characteristics of the inertial system, it might be expected

that the use of $\tilde{h} = \hat{h}_b$ could result in a better determination of vertical acceleration than using only $\tilde{h} = h_b$, at least in a limited frequency range. An investigation of this possibility, summarized in the paragraphs which follow, shows that the use of $h = h_b$ is superior at any frequency.

The response equation for the case where $\tilde{h} = h_b$ was developed in Section 2.4, giving the error equation, Eq. (2.40). The case where $\tilde{h} = \hat{h}_b$ can be developed in a similar manner as Eq. (2.40) by using

$$\ddot{h}_i = \ddot{h} + 2\omega_s^2(\hat{h}_b - h) + (u)\ddot{h}_i \tag{B.1}$$

where $\hat{h}_b - h$ replaces $h_b - h$ in Eq. (2.37). The error equations for $\tilde{h} = h_b$ and $\tilde{h} = \hat{h}_b$ can be written in the general form, using Laplace transform notation

$$\left(\frac{s^2}{\omega_n^2} + \frac{2\zeta}{\omega_n} s + 1 - A\right) \delta(\Delta\hat{h}_b) = -\tau s \frac{\frac{2\zeta}{\omega_n} s + 1 + B}{\tau s + 1} \Delta h$$

$$+ \left(\frac{s^2}{\omega_n^2} - 2\frac{\omega_s^2}{\omega_n^2}\right) \Delta h_I$$

$$+ \frac{\frac{2\zeta}{\omega_n} s + 1 + B}{\tau s + 1} (u) h_b$$

$$+ \frac{(u)\ddot{h}_i}{\omega_n^2} \tag{B.2}$$

where the values of the parameters A and B are given in the following table.

$\tilde{h}$	A	B
h_b	0	$2\frac{\omega_s^2}{\omega_n^2}$
$\hat{h}_b$	$2\frac{\omega_s^2}{\omega_n^2}$	0

A term by term comparison between the two cases $\tilde{h} = h_b$ and $\tilde{h} = \hat{h}_b$ shows that for all frequencies the individual error components of Eq. (B.2) are always larger for the $\tilde{h} = \hat{h}_b$ case. Therefore, the conclusion is reached that in the design of a linear second-order hybrid altimeter which uses both barometrically and inertially derived information, the use of the barometrically derived altitude h_b in the gravitational field compensation calculation is best.

Appendix C

DERIVATION OF AIRPLANE EQUATIONS OF MOTION

The derivation of the linearized longitudinal perturbation equations of motion for a supersonic airplane in quasi-steady level cruise is obtained by an extension of the procedure used by Etkin in Section 4.14 of Reference 30. Elevator displacement and thrust control are employed to control aircraft motion. Atmospheric disturbances considered are horizontal gust, vertical gust, ambient pressure variations, and ambient speed of sound variations. The usual stability derivative conventions are used as found in NASA and recent literature. However, it has been necessary to derive effects of pressure and speed of sound variations. An example of the derivation of these effects is given below for forces in the z-direction. (See Fig. C.1 for stability axes conventions).

Consider the incremental force ΔZ in the z-direction for small perturbations of the variables

$$\Delta Z = Z_u u + Z_w w + Z_{\dot{w}}\dot{w} + Z_q q + Z_{\delta_e}\delta_e + Z_T T + Z_p p + Z_a a \tag{C.1}$$

The force balance for initial steady state with zero initial pitch angle ($\theta_o = 0$) is

$$Z_o + mg = 0 \tag{C.2}$$

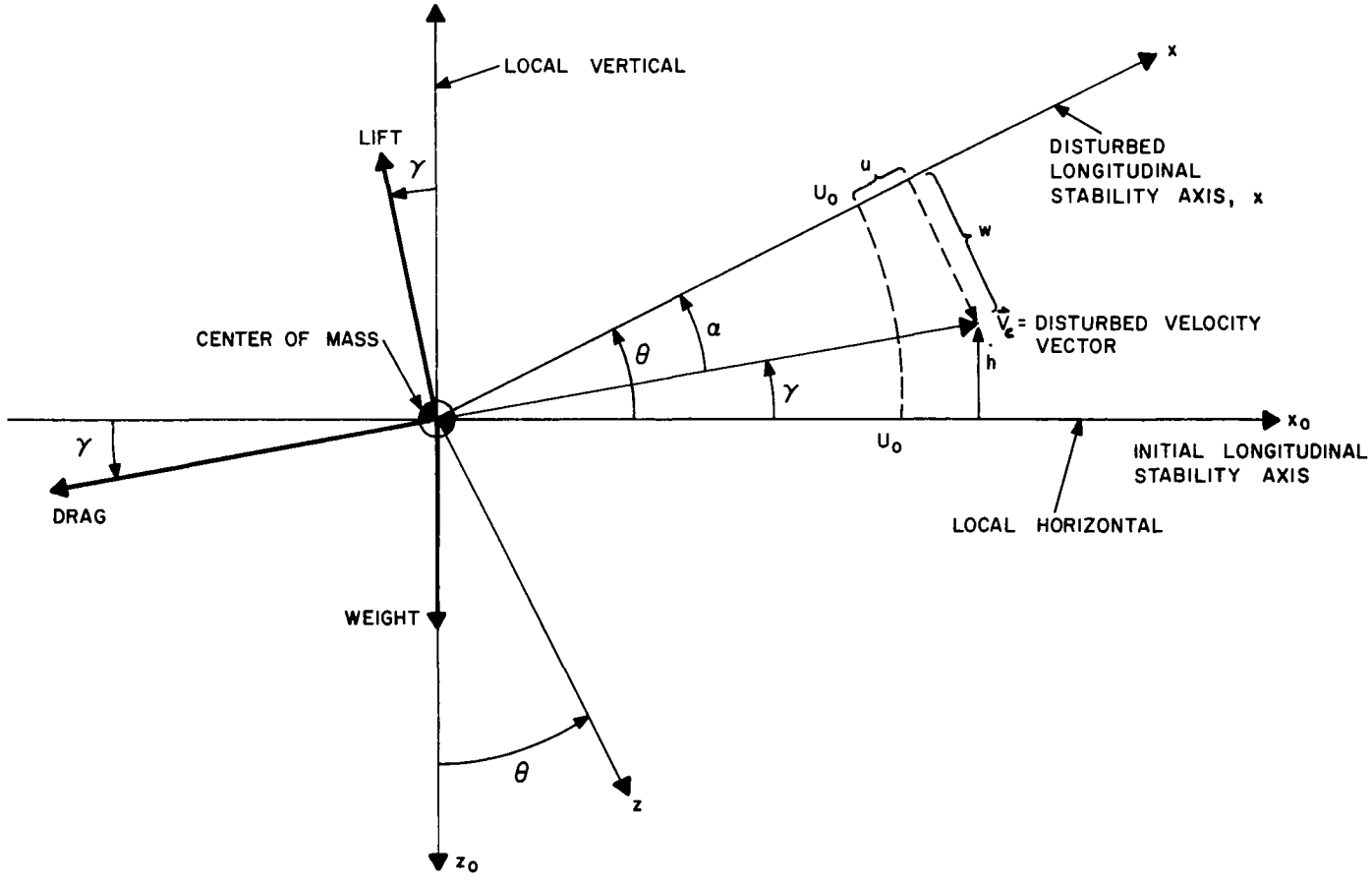

Fig. C.1. Stability Axes and Definition of Terms

The equation of motion in the z-direction is

$$Z_o + \Delta Z + mg = m(\dot{w} - U_o q) \tag{C.3}$$

Now define the nondimensional force coefficient in the z-direction, $C_z(\alpha, M)$, so that

$$Z = C_z \frac{1}{2} \rho_\infty V^2 S \tag{C.4}$$

It is assumed the coefficients are only functions of angle of attack and Mach number. Using the perfect gas relations, one can write

$$Z = C_z \frac{\gamma}{2} \frac{p_\infty}{a_\infty^2} V^2 S \tag{C.5}$$

The partial of Z with respect to p_∞ then becomes

$$Z_p = C_z \frac{1}{2} \rho_\infty \frac{V^2}{p_\infty} S = C_z q_\infty \frac{S}{p_\infty} = -C_L \, q_\infty \frac{S}{p_\infty} \tag{C.6}$$

The partial of Z with respect to a becomes

$$Z_a = -\frac{\gamma}{2} \frac{p_\infty}{a_\infty^2} V^2 S \, C_{z_M} \frac{M}{a} - C_z \frac{\gamma}{2} \frac{p_\infty}{a_\infty^3} 2V^2 S$$

$$= \left(2C_L + M \, C_{L_M}\right) \frac{q_\infty S}{a_\infty} \tag{C.7}$$

The other partials in Eq. (C.1) are similarly developed following Etkin.

The x-direction equation and moment equation are derived in a similar manner. The system of these three equations can be written in matrix form using Laplace transform notation with the Laplace variable s

$$[a(s)] \begin{Bmatrix} \bar{u}(s) \\ \bar{w}(s) \\ \theta(s) \end{Bmatrix} = [b(s)] \begin{Bmatrix} \delta_e(s) \\ \bar{T}(s) \\ \bar{u}_w(s) \\ \bar{w}_w(s) \\ \bar{p}(s) \\ \bar{a}(s) \end{Bmatrix} \tag{C.8}$$

where $\bar{u}$, $\bar{w}$ = reduced airplane velocity perturbations
θ = pitch-angle perturbation, rad
δ_e = elevator angle perturbation, rad
$\bar{T}$ = reduced thrust perturbation
$\bar{u}_w$, $\bar{w}_w$ = reduced wind velocity perturbations
$\bar{p}$ = reduced ambient pressure perturbation
$\bar{a}$ = reduced ambient sound speed perturbation

Coefficients a(s) and b(s) are listed below together with necessary auxiliary equations.

$$a_{11} = \frac{mU_o}{Sq_\infty} s - C_{x_u}$$

$$a_{12} = -C_{x_\alpha}$$

$$a_{13} = C_L$$

$$a_{21} = 2C_L - C_{z_u}$$

$$a_{22} = \left(\frac{mU_o}{Sq_\infty} - \frac{c}{2U_o} C_{z_{\dot{\alpha}}}\right)s - C_{z_\alpha} + C_L \frac{U_o}{p}\left(\frac{\partial p}{\partial z}\right) \frac{1}{s}$$

$$a_{23} = -\left(\frac{mU_o}{Sq_\infty} + \frac{c}{2U_o} C_{z_q}\right) s - C_L \frac{U_o}{p}\left(\frac{\partial p}{\partial z}\right) \frac{1}{s}$$

$$a_{31} = -C_{m_u}$$

$$a_{32} = -\frac{c}{2U_e} C_{m_{\dot{\alpha}}} s - C_{m_\alpha}$$

$$a_{33} = \frac{I_y}{Sq_\infty c} s^2 - \frac{c}{2U_o} C_{m_q} s$$

$$b_{11} = 0$$

$$b_{12} = \cos \epsilon$$

$$b_{13} = C_{x_u}$$

$$b_{14} = C_{x_\alpha}$$

$$b_{15} = 0$$

$$b_{16} = -C_{x_u}$$

$$b_{21} = C_{z_{\delta_e}}$$

$$b_{22} = -\sin \epsilon$$

$$b_{23} = C_{z_u} - 2C_L$$

Appendix D

PRESENTATION OF FINAL EQUATIONS

To complete the system of equations necessary to calculate flight technical error, it is necessary to specify an altitude relationship to the equations of motion and a set of control equations.

The altitude rate of the airplane is given by the linearized, small-angle approximation

$$sh = U_o\theta(s) - w(s) \tag{D.1}$$

The altitude of the airplane is related to the displacement Δh_I of the isobaric surface from its standard-atmosphere altitude h_o and the airplane displacement Δh from the isobaric surface by Eq. (2.8)

$$h = h_o + \Delta h_I + \Delta h \tag{D.2}$$

For most of the calculations, the displacement of the isobaric surface is not included, so in these cases $\Delta h_I = 0$.

The objective of the control system is to minimize the displacement of the airplane from the isobaric surface, that is reduce Δh. The control system has already been discussed in Chapter 3, so only the equations will be presented here, in their Laplace transform form.

The elevator control equation, Eq. (3.1), is written

$$(\tau_e s + 1)\delta_e(s) = S_{\dot{\theta}} s[\theta(s) - \theta_c(s)] \tag{D.3}$$

The form of the compensation, Eq. (3-2), is

$$s\theta_c(s) = -\frac{S_h}{S_{\dot{\theta}}}(\tau_e s + 1)\, K_{\delta_e}(s)\, \Delta\hat{h}_b \tag{D.4}$$

where

$$K_{\delta_e}(s) = \frac{(\tau_{h_2} s + 1)(\tau_{h_3} s + 1)}{(\tau_e s + 1)(\tau_{h_1} s + 1)} \tag{D.5}$$

The hybrid altimeter equation, Eq. (2.39), is

$$\left(\frac{s^2}{\omega_n^2} + \frac{2\zeta}{\omega_n} s + 1\right)\Delta\hat{h}_b(s) = \left[\frac{\tau}{\omega_n^2} s^3 + \frac{s^2}{\omega_n^2} + \frac{2}{\omega_n}\left(\zeta - \frac{\tau\omega_s^2}{\omega_n}\right)s + 1\right]\frac{\Delta h(s)}{\tau s + 1}$$

$$+ \left(\frac{s^2 - 2\omega_s^2}{\omega_n^2}\right)\Delta h_I(s) + \left(\frac{2\zeta}{\omega_n} s + 1 + \frac{2\omega_s^2}{\omega_n^2}\right)(u)h_b(s)$$

$$+ \frac{(u)\ddot{h}_i(s)}{\omega_n^2} \tag{D.6}$$

Combining the above four equations gives the elevator control equation, Eq. (3.3)

$$\delta_e(s) = S_{\dot{\theta}} G_\theta(s)\theta(s) + S_h K_{\delta_e}(s)[H_{\Delta h}(s)\, \Delta h(s) + H_{\Delta h_I}(s)\, \Delta h_I(s)$$

$$+ H_{(u)h_b}(s)\, (u)h_b(s) + H_{(u)\ddot{h}_i}(s)\, (u)\ddot{h}_i(s)] \tag{D.7}$$

where the expressions for $G_\theta(s)$, $H_{\Delta h}(s)$, etc., are given by

$$G_\theta(s) = \frac{s}{\tau_e s + 1} \tag{D.8}$$

$$H_{\Delta h}(s) = \frac{\bar{\tau}\bar{s}^3 + \bar{s}^2 + 2\left(\zeta - \bar{\tau}\bar{\omega}_s^2\right)\bar{s} + 1}{(\bar{s}^2 + 2\zeta\bar{s} + 1)(\tau s + 1)} \tag{D.9}$$

$$H_{\Delta h_I}(s) = \frac{\bar{s}^2 - 2\,\bar{\omega}_s^2}{(\bar{s}^2 + 2\zeta\bar{s} + 1)(\tau s + 1)} \tag{D.10}$$

$$H_{(u)h_b}(s) = \frac{2\zeta\bar{s} + 1 + 2\bar{\omega}_s^2}{(\bar{s}^2 + 2\zeta\bar{s} + 1)(\tau s + 1)} \tag{D.11}$$

$$H_{(u)\ddot{h}_i}(s) = \frac{1}{(\bar{s}^2 + 2\zeta\bar{s} + 1)\omega_n^2} \tag{D.12}$$

where $\bar{s} = \frac{s}{\omega_n}$, $\bar{\omega}_s = \frac{\omega_s}{\omega_n}$, $\bar{\tau} = \tau\omega_n$

The thrust control equation, Eq. (3.4), is

$$\bar{T}(s) = S_T K_T(s)[\bar{u}(s) + \bar{u}_w(s) - \bar{a}(s)] \tag{D.13}$$

where the expression for $K_T(s)$ is

$$K_T(s) = \frac{(\tau_{T_1} s + 1)(\tau_{T_2} s + 1)}{(\tau_E s + 1)(\tau_t s + 1)} \tag{D.14}$$

and $K_T(s)$ represents the engine and throttle lag and engine control compensation.

The effects of two types of atmospheric pressure variations are studied: (1) the vertical variation due to the vertical pressure gradient $(\partial p/\partial z)_{atm}$, and (2) horizontal variations due to the vertical displacement of the isobaric surfaces. These are both studied using Eq. (2.8) and Eq. (2.10) giving

$$(p - p_o) = \left(\frac{\partial p}{\partial h}\right)_{atmos} (h - h_o - \Delta h_I) \tag{D.15}$$

Noting that p_o and h_o are constant for cruise in the altitude-hold mode, and using the trajectory equation, Eq. (D.1), one obtains

$$\bar{p}(s) = \frac{1}{s}\left(\frac{1}{p}\frac{\partial p}{\partial h}\right)_{atmos} \{U_o[\theta(s) - \bar{w}(s)] - s\Delta h_I(s)\} \tag{D.16}$$

Equations (D.7), (D.13) and (D.16) are substituted in the system of Eq. (C.8), and terms are rearranged giving

$$[A(s)]\begin{Bmatrix}\bar{u}(s)\\ \bar{w}(s)\\ \theta(s)\\ \Delta h(s)\end{Bmatrix} = [B(s)]\begin{Bmatrix}\bar{u}_w(s)\\ \bar{w}_w(s)\\ \Delta h_I(s)\\ \bar{a}(s)\\ (u)h_b\\ (u)\ddot{h}_i\end{Bmatrix} \tag{D.17}$$

The elements of the A(s) and B(s) matrices are listed below.

$$A_{11} = a_{11} - S_T b_{12} K_T$$

$$A_{12} = a_{12}$$

$$A_{13} = a_{13}$$

$$A_{14} = 0$$

$$A_{21} = a_{21} - S_T b_{22} K_T$$

$$A_{22} = a_{22}$$

$$A_{23} = a_{23} - S_{\dot{\theta}} b_{21} G_{\theta}$$

$$A_{24} = S_h b_{21} K_{\delta_e} H_{\Delta h}$$

$$A_{31} = a_{31} - S_T b_{32} K_T$$

$$A_{32} = a_{32}$$

$$A_{33} = a_{33} - S_{\dot{\theta}} b_{31} G_{\theta}$$

$$A_{34} = -S_h b_{31} K_{\delta_e} H_{\Delta h}$$

$$A_{41} = 0$$

$$A_{42} = U_o$$

$$A_{43} = -U_o$$

$$A_{44} = s$$

$$B_{11} = b_{13} + S_T b_{12} K_T$$

$$B_{12} = b_{14}$$

$$B_{13} = 0$$

$$B_{14} = b_{16} - S_T b_{12} K_T$$

$$B_{15} = 0$$

$$B_{16} = 0$$

$$B_{21} = b_{23} + S_T b_{22} K_T$$

$$B_{22} = b_{24}$$

$$B_{23} = S_h b_{21} K_{\delta_e} H_{\Delta h_I} + b_{25}$$

$$B_{24} = b_{26} - S_T b_{22} K_T$$

$$B_{25} = S_h b_{21} K_{\delta_e} H_{(u)h_b}$$

$$B_{26} = S_h b_{21} K_{\delta_e} H_{(u)\ddot{h}_i}$$

$$B_{31} = b_{33} + S_T b_{32} K_T$$

$$B_{32} = b_{34}$$

$$B_{33} = S_h b_{31} K_{\delta e} H_{\Delta h_I}$$

$$B_{34} = b_{36} - S_T b_{32} K_T$$

$$B_{35} = S_h b_{31} K_{\delta e} H_{(u)h_b}$$

$$B_{36} = S_h b_{31} K_{\delta e} H_{(u)\ddot{h}_i}$$

$$B_{41} = 0$$

$B_{42} = 0$

$B_{43} = -\dot{s}$

$B_{44} = 0$

$B_{45} = 0$

$B_{46} = 0$

REFERENCES

1. Ruetenik, J. R., Barry, J. M., Ives, D. C., Survey of Avionics Instrumentation Needs for Advanced Supersonic Transports, Kaman AviDyne TR-43, April 1967.

2. "How Serious Are the Atmospheric Problems of the SST," Panel at the AIAA 6th Aerospace Sciences Meeting, New York, January 26, 1968.

3. Gracey, W., Survey of Altitude-Measuring Methods for the Vertical Separation of Aircraft, NASA TN D-738 (1961).

4. Davies, W. P., et al., "Height Measurement in Supersonic Aircraft," Institute of Navigation Journal, January 1966.

5. Staff of the Instrumentation Laboratory M.I.T., Inertial Navigation Study for Civil Air Transport, M.I.T. Instrumentation Laboratory Report 484, March 1965.

6. Ryan, T., "Two Inertial Techniques in Height Measurement," M.I.T. 16.41 Term Paper, 1966.

7. Thompson, J. H., Design Considerations for Supersonic Transport Altimetry Systems, Kaman AviDyne TR-44, May 1967.

8. Piggott, B.A.M., Atmospheric Turbulence and Aircraft Height-Keeping Accuracy, Ministry of Technology, ARC CP No. 1009, August 1967.

9. Gracey, W., Recent Developments in Pressure Altimetry, Journal of Aircraft, pp. 161-165, May - June 1965.

10. Minzner, R. A., Champion, K. S. W., and Pond, H. L., The ARDC Model Atmosphere, 1959, Air Force Cambridge Research Laboratories, AFCRC-TR-59-267, August 1959.

11. Altimetry and the Vertical Separation of Aircraft, International Air Transport Association, Montreal, Canada (January 1960).

12. Loria, J., Correspondence with Boeing SST Office, November 15, 1968.

13. Summary of the Work of the Vertical Separation Panel, International Civil Aviation Organization, Montreal, Canada, Rept. VS P-WP/57 (February 15, 1961).

14. Silsby, N. S., and Stickle, J. W., Flight Calibrations of Fuselage Static-Pressure-Vent Installations of Three Types of Transports, NASA TN D-1356, 1962.

15. Chaffois, J., Pitot-Static Probes for Subsonic and Supersonic Aircraft, RAE Translation 1032, November 1963.

16. Noll, R., Correspondence with NASA Flight Research Center, April 9, 1968.

17. Britting, K. R., Analysis of Space Stabilized Inertial Navigation Systems, Massachusetts Institute of Technology, E.A.L. RE-35, 1968.

18. Proxmeyer, C., Inertial Navigation Systems, McGraw-Hill, 1964.

19. Britting, K. R., Airborne Gravimeter Specific Force Compensation, M.I.T., E.A.L. RE-25, July 1966.

20. Savant, C. J., Jr., Howard, R. C., Solloway, C. B., Savant, C. A., Principles of Inertial Navigation, McGraw-Hill Book Co., Inc., New York, 1961.

21. Britting, K. R., Strapdown Navigation Equations for Geographic and Tangent Coordinate Frames, M.I.T. M.S.L. RE-56, 1969.

22. Searcy, J. B., Determination of Geopotential Anomalies From Airborne Measurements, M.I.T., M.S.L. TE-15, 1966.

23. Britting, K. R., Error Analysis of Strapdown Local Level Inertial Systems Which Compute in Geographic Coordinates, M.I.T., M.S.L., RE-56, 1969.

24. Report of the National Committee for Clear Air Turbulence, U.S. Dept. of Commerce, December 1966.

25. Kordes, E. E., and Love, B. J., Preliminary Evaluation of XB-70 Airplane Encounters With High-Altitude Turbulence, NASA TN D-4209, October 1967.

26. Pritchard, F. E., Easterbrook, C. C., and McVehil, G. E., Spectral and Exceedance Probability Models of Atmospheric Turbulence for Use in Aircraft Design and Operation, Cornell Aeronautical Laboratory, Inc., Air Force Flight Dynamics Laboratory, AFFDL-TR-65-122, November 1965.

27. Crooks, W. M., Hoblit, F. M., Mitchell, F. A., et al, Project HICAT High Altitude Clear Air Turbulence Measurements and Meteorological Correlation. Lockheed-California Company, Air Force Flight Dynamics Laboratory, AFFDL-TR-68-127, November 1968.

28. Thompson, J. K., New Environments for SST?, AIAA 5th Annual Meeting, Paper No. 68-998, October 21-24, 1968.

29. Boeing Phase II Proposal, Airplane Performance (GE), V2-B2707-4, September 6, 1966.

30. Etkin, Bernard, Dynamics of Flight, John Wiley & Sons, Inc., New York, 1959.

SYMBOLS

$\underline{A}$	accelerometer scale factor uncertainty matrix
a, a_∞	ambient speed of sound, ft/sec
a'	speed of sound perturbation, ft/sec
$\overline{a}$	nondimensional perturbation $\frac{a'}{a}$
a_D	effective vertical component of the scale factor uncertainty
b_1, b_2	parameter in probability density equation of gust velocity in nonstorm and storm, respectively, ft/sec
c	wing reference chord, ft
c_p	pressure coefficient
D	differential operator d/dt
E	product of earth's mass and universal gravitational constant, ft^3/sec^2
$\underline{f}$	specific force, ft/sec^2
$\delta \underline{f}$	acceleration measurement error, ft/sec^2
$(u)\underline{f}$	accelerometer uncertainty, ft/sec^2
Δf_c	centrifugal acceleration compensation error, ft/sec^2
f_D	vertical specific force component, ft/sec^2
$(u)f_D$	uncertainty of the effective vertical acceleromter, ft/sec^2
f_H	horizontal specific force, ft/sec^2
G	vertical component of the elliptical earth gravitational field, ft/sec^2
g	acceleration due to gravity, 32.2 ft/sec^2
$\underline{G}$	gravitational field acceleration, ft/sec^2
ΔG	gravity anomoly, ft/sec^2
G_D	vertical component of the gravitational field, ft/sec^2

h	altitude of airplane mass center, ft
Δh	altitude deviation, $h - h_o$, ft
h_B	altitude determined by a perfect barometric system, ft
h_b	altitude determined by barometric system, ft
$(u)h_b$	uncertainty in altitude determined by the barometric system, ft
$\hat{h}_b$	altitude determined by hybrid system, ft
δh_b	$h_b - h$
$\delta \hat{h}_b$	$\hat{h}_b - h$
Δh_b	$h_b - h_o$
$\Delta \hat{h}_b$	$\hat{h}_b - h_o$
Δh_I	actual distance of isobaric surface (at pressure p_o) above h_o, ft
h_i	altitude determined by inertial system, ft
$(u)h_i$	uncertainty in altitude determined by inertial system, ft
h_o	desired altitude; this altitude corresponds to a nominal pressure of p_o for an atmosphere that exactly matches standard atmospheric tables, ft
$\underline{I}$	identity matrix

I_y	pitch plane moment of inertia, slug-ft^2
J	ellipticity constant
L	integral scale of turbulence, ft
L	geographic latitude, rad
δL	latitude estimation error, rad
l_t	tail moment arm, ft
l_ϵ	thrust moment arm about center of mass, positive pitch up, ft
L/D	lift/drag ratio
M	mach number, U_o/a
m	airplane mass, slugs
p, p_∞	ambient pressure, force-lb/ft^2
p_o	nominal pressure at altitude h_o from standard atmospheric tables, force-lb/ft^2
p'	pressure perturbation, force-lb/ft^2
$\overline{p}$	nondimensional perturbation $\frac{p'}{p}$
$p(\sigma)$	probability density of rms gust velocity σ
$p_1(\sigma), p_2(\sigma)$	probability density function $p(\sigma)$ during nonstorm and storm, respectively

p_0, p_1, p_2	probability of encountering, smooth air, nonstorm or storm, respectively
q	pitch rate, $\dot{\theta}$, rad/sec
q, q_∞	free stream dynamic pressure, $\frac{1}{2} \rho V^2$, force-lb/ft^2
r	distance from Earth center, ft
$\ddot{\underline{r}}$	inertially referenced acceleration, ft/sec^2
r_L	radius of curvature in meridian plane, ft
r_1	radius of curvature in co-meridian plane, ft
r_o	magnitude of the geocentric earth radius at the point below the aircraft, ft
S	wing plan area, ft^2
s	Laplace transform variable, sec^{-1}
S_h	altimeter control gain, rad/ft
S_T	throttle control gain
$S_{\dot{\theta}}$	elevator servo gain, sec
T	thrust perturbation, force-lb
$\bar{T}$	nondimensional perturbation $\frac{T}{qS}$
U_o	steady cruise velocity, ft/sec
U,W	scalar components of V_c, ft/sec

u,w	perturbations of U, W, ft/sec
$\bar{u},\bar{w}$	nondimensional perturbations $\frac{u}{U_o}$, $\frac{w}{U_o}$
U_w,W_w	x-component of wind velocity, positive toward aircraft, and z-component of wind velocity, positive upward, ft/sec
u_w,w_w	perturbations of U_w,W_w
$\bar{u}_w,\bar{w}_w$	nondimensional perturbations $\frac{u_w}{U_o}$, $\frac{w_w}{U_o}$
$\vec{V}_c$	velocity vector of airplane mass center relative to earth-fixed coordinates, ft/sec
V	scalar magnitude of V_c, ft/sec
W	airplane gross weight, lb
x,z	stability coordinates fixed on aircraft mass center; forward along fuselage axis and downward, respectively (see Fig. D-1), ft
α	angle of attack, rad
γ	ratio of specific heats of air, 1.4
δ_e	elevator angle from equilibrium, positive surface downward, rad
ϵ	thrust offset angle, positive thrust up, rad
ϵ	transformation error angle, rad
ζ	second-order filter damping ratio

$\ominus$	temperature, ^{o}C
Λ	wing sweep, deg
λ	celestial longitude, rad
$\delta\lambda$	longitude estimation error, rad
ρ, ρ_{∞}	ambient density, slugs/ft^2
$\sigma_{\Delta h}$	rms altitude deviation from isobaric surface, ft
σ_{u_w}, σ_{w_w}	rms longitudinal gust velocity, and rms vertical gust velocity, ft/sec
τ	time constant of barometric system, sec
Φ_{u_w}, Φ_{w_w}	turbulence spectra for longitudinal and transverse components, respectively, (ft/sec)^2/(rad/ft)
Ω	reduced frequency, $\frac{\omega}{U_o}$, rad/ft
ω	radial frequency, rad/sec
ω_n	second-order filter undamped natural frequency, rad/sec
ω_s	Schuler radial frequency, $(\frac{E}{r^3})^{1/2}$, rad/sec